

UNSTEADY MOMENTUM FLUXES IN TWO-PHASE FLOW AND
THE VIBRATION OF NUCLEAR REACTOR COMPONENTS

Tien Sieh Yih

Peter Griffith

Report No. 70318-58

Contract No. AT(30-1)-3496

November 1968

Department of Mechanical Engineering
Massachusetts Institute of Technology
Cambridge, Massachusetts

ABSTRACT

The steady and unsteady components of the momentum flux in a two-phase flow have been measured at the exit of a vertical pipe. Measured momentum flux data has been machine processed by standard random vibration techniques to obtain the power spectral density curves. From these curves, the predominant frequency and the rms value of the unsteady momentum flux have been obtained.

The effects of the average flow velocity, volumetric quality, system pressure, flow channel size and geometry on the unsteady momentum fluxes have been observed. It has been found that the fluctuation of momentum fluxes is important only in the low frequency range. The maximum values of unsteady momentum fluxes appeared in either the high void slug flow or the low void annular flow regime. The experimental results have been correlated and suggestions have been made for constructing the power spectral density curve of momentum fluxes under untested conditions.

In the sample problems, using the experimental results, the effect of the unsteady momentum fluxes on a steam generator U-tube and a reactor fuel rod has been studied. The amplitudes of the structural vibrations resulting from the two-phase excitation have been found. In addition, it has also been found that there is a possibility of unstable vibrations owing to a nonlinear restoring force on the mechanical system. This nonlinearity is due to the unsteady component of the momentum flux in the flow past the system. In both examples, the major vibrations occurred in a narrow frequency band around the natural frequency of the mechanical system.

ACKNOWLEDGEMENTS

The authors wish to thank Professors D. C. Karnopp and E. A. Mason for their helpful suggestions and comments.

Mr. R. S. Sidell was most helpful in the design of the electronic devices. Mr. J. A. Caloggero and his colleagues of the M.I.T. Engineering Projects Laboratory assisted with the construction of the set up for the experiments.

This work was sponsored by the U. S. Atomic Energy Commission.

TABLE OF CONTENTS

	Page
TITLE PAGE	i
ABSTRACT	ii
ACKNOWLEDGEMENTS	iii
TABLE OF CONTENTS	iv
LIST OF SYMBOLS	vi
1. INTRODUCTION	1-1
1.1 Fluctuation in Two-Phase Flow	1-1
1.2 Unsteady Momentum Fluxes	1-2
1.3 Flow-Induced Vibration	1-3
1.4 Exploratory Investigation	1-4
2. PHYSICAL BASIS OF THE FLUCTUATIONS	2-1
2.1 Flow Regimes	2-1
2.2 Variation of Flow Density	2-2
2.3 Variation and Distribution of Velocity	2-2
2.4 Momentum Flux Fluctuation	2-4
3. DESCRIPTION OF EXPERIMENTS	3-1
3.1 Measuring Techniques	3-1
3.2 Variables Used and Their Testing Ranges	3-4
3.3 Experimental Apparatus	3-7
3.3.1 Fluids Feed System	3-7
3.3.2 Tank and Internals	3-8
3.3.3 Recording System	3-11
3.4 Experimental Procedure	3-15
3.4.1 Pluck Test of Beam	3-15
3.4.2 Steady Momentum Flux Calibration	3-15
3.4.3 Checking the Function of the Turning Tee	3-18
3.4.4 Preliminary Tests	3-18
3.4.5 Systematic Tests	3-19
4. DATA PROCESSING	4-1
4.1 Random Vibration Techniques	4-1
4.2 Measurement of Spectral Density	4-2
4.3 Root Mean Square Value	4-5
4.4 Calibration of Power Spectral Density Curve	4-8

	Page
5. PRESENTATION AND DISCUSSION OF EXPERIMENTAL RESULTS	5-1
5.1 Some Particular Phenomena	5-1
5.2 General Trends	5-2
5.2.1 Effect of Average Flow Velocity	5-5
5.2.2 Effect of Pressure	5-10
5.2.3 Effect of Pipe Size	5-16
5.2.4 Effect of Pipe Geometry	5-16
5.3 Correlations	5-23
5.4 Reliability and Reproducibility	5-29
6. CONSTRUCTING A SPECTRAL DENSITY CURVE FOR UNTESTED CONDITIONS	6-1
7. APPLICATION SAMPLES	7-1
7.1 U-Tube Example	7-1
7.2 Fuel Rod Example	7-6
7.2.1 The Model	7-6
7.2.2 Stability	7-10
7.2.3 Prediction of the Vibration Amplitude	7-12
7.3 Discussion	7-13
8. CONCLUSIONS	8-1
9. SUGGESTIONS FOR FUTURE WORK	9-1
APPENDIX A Experimental Data	A-1
APPENDIX B Transfer Function of Beam-Tee Systems	B-1
APPENDIX C Calibration Coefficients of Steady Momentum Fluxes and Power Spectral Density Curves	C-1
APPENDIX D Numerical Examples for Predicting Vibration Amplitudes	D-1
APPENDIX E Equivalent Mass of Uniform Beams in Transverse Vibrations	E-1
APPENDIX F Accuracy of the Unsteady Momentum Flux Measurement Using the Turning Tee	F-1
APPENDIX G References	G-1

LIST OF SYMBOLS

A	Area under the spectral density curve of the force acting on the tee
A_p	Cross section area of pipe
A_{psd}	Area under the spectral density curve of momentum fluxes
A_r	Area under the spectral density curve of the sinusoidal "force"
A_t	Flow area of U-tube
C	Damping coefficient
C_c	Critical damping coefficient
C_y	Scale on the Y axis of the spectral density curve of the sinusoidal "force"
cps	Cycles per second
D	Diameter
E	Modulus of elasticity
F	Force
F_r	Froude number = Inertia force/Gravity force
F_s	rms value of the sinusoidal "force"
F_t	Total force
f	Frequency
f_c	Predominant frequency of unsteady momentum fluxes
f_o	Central frequency of the narrow band filter
Δf	Band width of the narrow band filter
$H(\omega)$	Transfer function
h	Height of the triangle in Fig. 6.1(a)
I	Moment of inertia of beam cross section area
I_Y	Moment of inertia of U-tube cross section area about Y axis, Fig. 7.1

K	Number of statistical degrees of freedom
K_{eq}	Equivalent number of statistical degrees of freedom
k	Spring constant
L	Length
L_b	Length of U-tube bend
L_f	Length, Fig. 6.1(a)
L_L	Length, Fig. 6.1(a)
l_f	Length of liquid slug
l_g	Length of gas bubble
M	Mass
M_e	Equivalent mass
N	Defined in equation (7.37)
n	Scale on the X axis of the spectral density curve
P	Momentum flux
P_{rms}	rms value of unsteady momentum fluxes
P_{st}	Steady momentum fluxes
P_{rms}/P_{st}	Unsteadiness of momentum fluxes
Q_f	Volume flow rate of water
Q_g	Volume flow rate of air
$R(\tau)$	Auto-correlation function, equation (4.1)
$R_F(\tau)$	Auto-correlation function of force, equation (7.9)
$R_p(\omega)$	Auto-correlation function of momentum fluxes
$S(\omega)$	Spectral density, equation (4.2)
$S_F(\omega)$	Spectral density of force
$S_p(\omega)$	Spectral density of momentum fluxes
$S_x(\omega)$	Spectral density of vibration amplitude

T	Averaging time
T_s	Period of liquid slug
t	time
V	Average flow velocity
W_e	Weber number = Inertia force/Surface tension force
$W(f)$	Experimental spectral density, equation (4.4)
$W_F(f)$	Experimental spectral density of force
$W_P(f)$	Experimental spectral density of momentum fluxes
$W_x(f)$	Experimental spectral density of vibration amplitude
α	Void fraction
β	Volumetric quality, flowing void fraction
δ	Total deflection of fuel rod
δ_o	Initial deflection of fuel rod
ρ	Density
ρ_a	Density of air under standard conditions
ρ_f	Density of liquid phase
ρ_g	Density of gas phase
ρ_m	Average density of a two-phase flow
τ	Time lag, variable
τ_o	Time lag, constant
ω	Circular frequency
ω_k	Frequency of density fluctuation

1. INTRODUCTION

In recent years the general area of two-phase gas-liquid flow has received intensive study because the technology of two-phase flow has wide applications in modern engineering processes. The basic equations in fluid mechanics, i.e., the continuity, momentum and energy equations, can be used to describe any two-phase flow. However, such equations are no longer so powerful in solving problems as they are in dealing with single-phase flow because the solutions are not known in general and appear experimentally to be very complex. In order to obtain approximate analytical solutions, several two-phase flow models have been established each characterized by a different phase distribution. However, in most cases useful analytical solutions are impossible. Associated with the flow regime or phase distribution one finds fluctuations in two-phase flows, the analytical treatment of these is even more difficult than that of turbulent fluctuations in single-phase flow.

1.1 Fluctuations in Two-Phase Flow

Depending on the flow regime one might find either gas bubbles, liquid slugs, or waves in a two-phase flow. These are all accompanied with severe pulsations in pressure, void fraction and momentum fluxes. The knowledge of these fluctuations is of considerable importance to the development of the two-phase flow technology and its application to engineering problems. In spite of this, little work relating to the unsteady nature of two-phase flow has been done. To date, Semenov (1) is the only investigator known to have made a systematic investigation of the unsteadiness in the wall pressure of an air-water mixture

flowing in horizontal pipes. His method of data reduction was not specified. Therefore, the use of his results is limited. Hubbard and Dukler (2) also made pressure-time measurements of an air-water flow in a horizontal pipe. Random vibration techniques were applied in their data processing. Because they primarily aimed at the characterization of flow regimes, complete data of fluctuating wall pressure was not presented. Their results are closely related to those found in this work but are not the same because the quantity measured here, momentum flux, is not the same as pressure drop.

1.2 Unsteady Momentum Fluxes

Since the three time varying quantities, void fraction, pressure, and momentum flux, are all interrelated, measurements of the fluctuation in either one of them would lead to the understanding of the others. However, the momentum flux variations are the best to work with because they are defined experimentally at a surface while the void fraction and the pressure drop are defined over a volume and a length, respectively. Furthermore, the momentum flux is a more fundamental quantity than the pressure because the pressure difference between two sections includes friction and momentum terms. In comparison with the void fraction, the continuous measurement of the momentum flux is easier and more accurate.

Our knowledge of unsteady momentum fluxes may be very useful in solving some important engineering problems. For example, the fluctuation of momentum flux in a two-phase flow is a possible source of the structural vibrations of heat exchanger U-tubes and reactor fuel rods. In addition, the unsteady momentum flux measurements may be able to

provide better means for characterizing flow regimes than the wall pressure measurements.

1.3 Flow-Induced Vibration

Fluid induced vibration may take place in several ways. In the case of single-phase flow the structural vibration in cross flow is excited by the well-known vortex shedding; in parallel flow, either internal or external, the turbulence in the flow stream may be the excitation source. In the case of two-phase flow, the unsteady component of the momentum fluxes is probably the primary cause of both cross and parallel flow-induced vibrations.

Flow induced vibrations may cause such undesirable effects of engineering systems as:

1. The vibration gives rise to significant stresses and strains within the structure. Fatigue failures of components may occur.
2. The vibration causes periodic relative motion between components or systems leading to wear.
3. The vibration disturbs the normal function of the system.

Recently, much attention has been devoted to the study of flow-induced vibrations, especially that of reactor fuel elements (3 - 8). In most publications on this subject investigations were restricted to single-phase flow. Quinn (4) is the first investigator known to have conducted tests on single rods and multirod assemblies in both single and two-phase flow. Paidoussis (5) made the attempt to deal with two-phase flow by introducing a time independent void fraction into the density term of his empirical expression. A fluctuating two-phase flow, however, can excite vibrations which no steady flow can, and such a

model will not show these vibrations.

1.4 Exploratory Investigation

The objectives of this investigation were twofold.

1. To obtain more knowledge of the unsteady nature of two-phase flow which is useful in the fundamental understanding of the two-phase phenomena.

2. To provide basic information that can be applied to various two-phase flow-induced vibration problems.

Since no previous work has been done on this subject, every aspect of the unsteady momentum fluxes needs to be studied. In this work, effort was made to explore the unsteady momentum fluxes in several different directions rather than concentrated in one particular aspect.

In the present investigation the measuring technique of unsteady momentum fluxes was developed. Measurements of both steady and unsteady components of the momentum fluxes in an air-water adiabatic upflow were made. The measured data were machine processed using standard random vibration techniques. The experimental results were applied to two sample problems to estimate the vibration amplitudes of a steam generator U-tube and a reactor fuel rod.

2. PHYSICAL BASIS OF FLUCTUATIONS

2.1 Flow Regimes

The unsteady information of a two-phase flow has been used to characterize flow regimes (2). This implies that there is a strong correlation between the flow regimes and the fluctuations of a two-phase flow.

The flow regimes commonly occurring in a vertical adiabatic upflow are the following:

1. Bubbly flow is characterized by the gas phase being dispersed in the liquid phase in the form of discrete small bubbles.

2. Slug flow consists of large bubbles comparable in size to the tube diameter, separated by slugs of liquid. There may or may not be small bubbles in the liquid slug following the large bubble. Increasing gas flow decreases the separation distance between large bubbles. The liquid slugs may then break up and pieces of long gas cores are present in the flow.

3. Annular flow exists when the liquid flows in an annulus around a core which is occupied by the gas. The interface between liquid and gas consists of surface waves. At low void fraction there exists an extremely rough film with waves of irregular shape moving along the interface. The velocity of the waves is far from constant, giving surges in the liquid velocity. As the void fraction increases, the wall film thickness becomes small, and the surface waves take the form of symmetrical rings which move slowly upward with constant velocity and more or less regular spacing.

4. Mist flow is a high velocity gas stream with minute liquid

drops entrained in it.

The geometries of these flow regimes are sketched in Fig. 2.1.

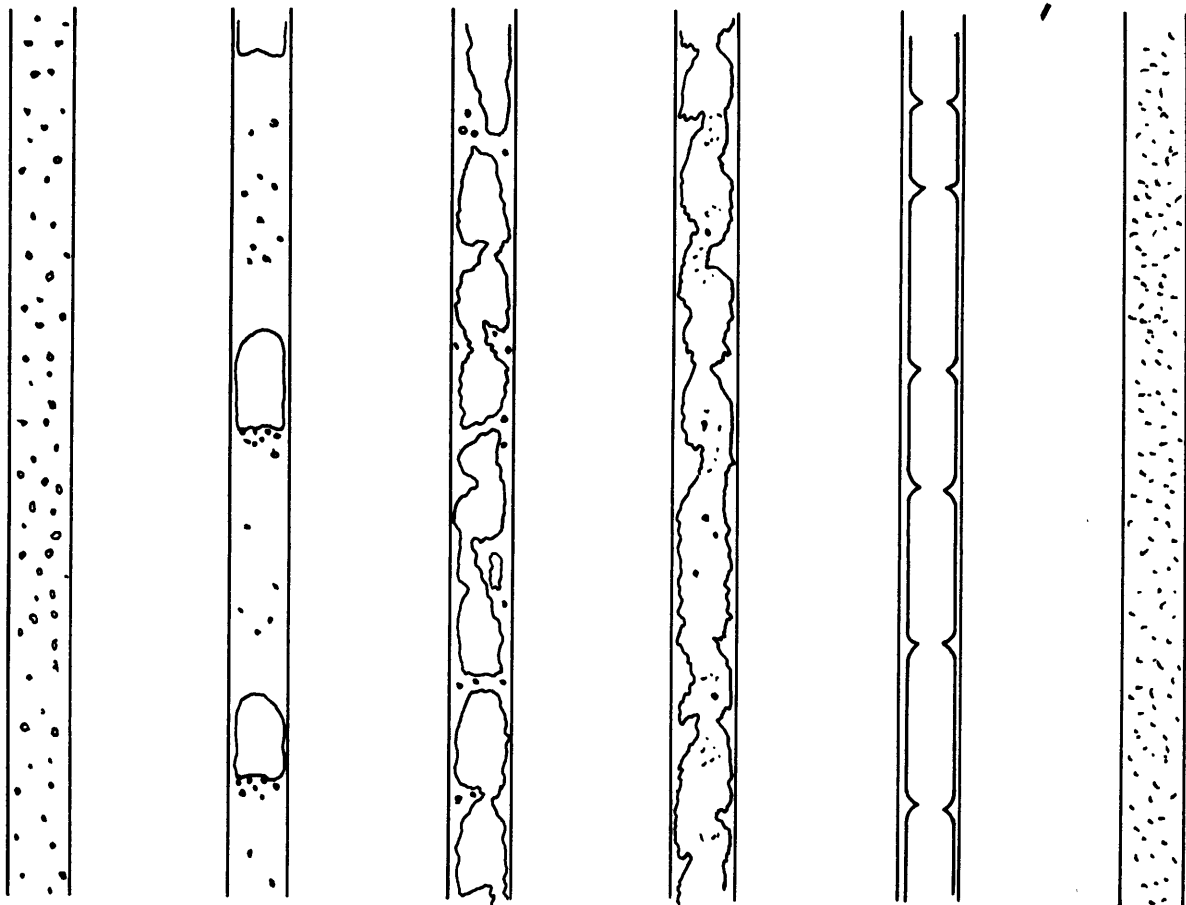
2.2 Variation of Flow Density

It is obvious, from the geometries of various flow regimes, that when a two-phase mixture flows through a pipe section there is the random variation of flow density with respect to time and position in the plane of that section. The flow density distributions of bubbly and mist flow are similar in the sense that there is the suspension of numerous discrete particles of one phase in the continuous flow of the other phase. The variation of the total mass flux across a section is very small in both cases. In high void annular flow one would expect a moderate variation of mass flow rate. In low void annular flow and slug flow violent fluctuations of mass flow rate take place.

2.3 Variation and Distribution of Velocity

In a two-phase flow there is the continuous flow of one or both phases. The velocity distribution and fluctuation in these continuous phases are, to some extent, similar to that in the single-phase turbulent flow in pipes. For a single-phase turbulent pipe flow the intensity of turbulence (a quantity defined as the ratio of the root mean square value of the fluctuation velocity to the average velocity) has values from zero to 10% (Ref. 9, p. 157). The turbulent velocity fluctuations in any continuous phase of a two-phase flow might be of the same order of magnitude.

The velocity distribution in a two-phase flow of one flow regime is quite different from that of other flow regimes. For the bubbly up-flow, the discrete gas bubbles move at higher speeds than the liquid phase. The rise velocity of bubbles has been studied in detail by



(a)

BUBBLY
FLOW

(b)

SLUG FLOW

(c)

(d)

ANNULAR FLOW

(e)

(f)

MIST
FLOW

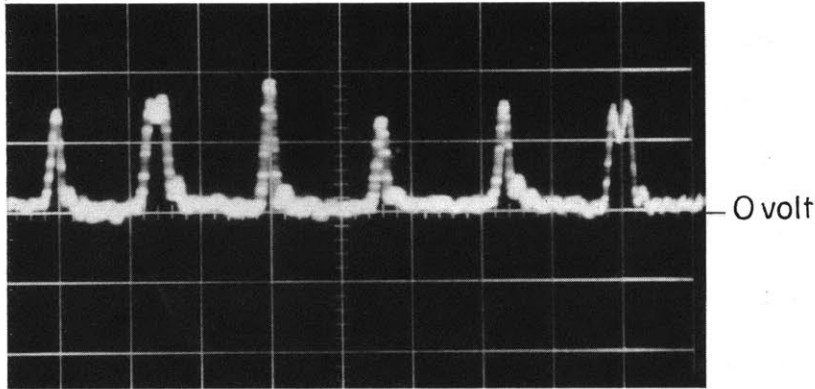
FIGURE 2.1 SKETCHES OF FLOW REGIME GEOMETRIES IN ADIABATIC TWO-PHASE VERTICAL UPFLOW

Peebles and Garber (10) and many other investigators. In a mist upflow the liquid drops move at much lower velocities than the gas phase. For the slug flow, the core of liquid in the center of a pipe moves at a velocity about 20% faster than the mean velocity in the pipe (11). The gas bubbles move even faster than the liquid slugs. The average velocity of the waves at the interface of an annular flow is on the order of one tenth of the gas core velocity (12). The waves may account for a large part of all of the liquid flow; under some conditions the thin film between waves is stationary or even downward-moving. Therefore, one would expect that the intensity of velocity fluctuation in a two-phase flow may be well above 10%.

2.4 Momentum Flux Fluctuation

In the bubbly and mist flow regimes, although the density and velocity are not uniform at a flow section, the total momentum efflux from a section is almost a constant with respect to time.

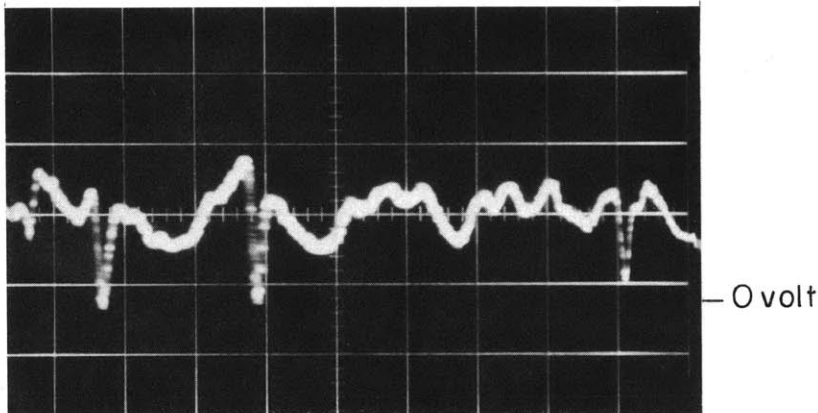
For slug and annular flow regimes, the flow density across a section varies rapidly with time. The velocity of the increased liquid portion, i.e., waves in annular flow or core of liquid slug in slug flow, is always higher than the average velocity of the liquid phase. Thus, one can expect the momentum flux fluctuation to be in phase with the flow density fluctuation but with somewhat larger amplitude than the latter. The pictures in Fig. 2.2 are samples of the momentum flux fluctuation in different flow regimes. The flow conditions in Fig. 2.2(a) are: $\beta = 89.8\%$, $V = 55$ ft/sec and the voltage reading representing the average momentum flux is 0.105 volts. This can be considered in the annular flow regimes as sketched in Fig. 2.1(e). When liquid waves



(a)

$$\beta = 89.8\%$$

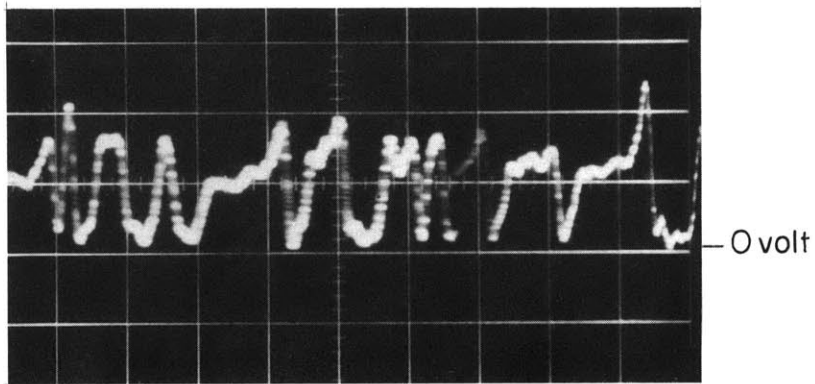
$$V = 55 \text{ ft/sec.}$$



(b)

$$\beta = 27\%$$

$$V = 38 \text{ ft/sec}$$



(c)

$$\beta = 70\%$$

$$V = 55 \text{ ft/sec.}$$

Horiz. Scale=0.05 sec/unit , Vert. Scale= 0.5 volts/unit

FIGURE 2.2 FLUCTUATIONS OF MOMENTUM FLUXES

passed through a flow section, the momentum flux sharply increased and appeared in the picture as separate upward peaks. Flow conditions in Fig. 2.2(b) are: $\beta = 27\%$, $V = 38$ ft/sec and the voltage reading of average momentum flux is 0.57 volts. This is probably in the slug flow regime corresponding to Fig. 2.1(b). As a large gas bubble moved across a section the momentum fluxes suddenly dropped to almost zero. The picture in Fig. 2.2(c) shows the fluctuation of momentum fluxes of a two-phase flow with $\beta = 70\%$, $V = 55$ ft/sec, which may be in the flow regime shown in Fig. 2.1(c) or (d).

3. DESCRIPTION OF EXPERIMENTS

The experimental apparatus is shown schematically in Figures 3.1 and 3.2. This is a modification of Andeen's apparatus which was used in the investigation of steady momentum fluxes (13). By means of a turning tee the momentum fluxes of the air-water flow at the exit plane of the vertical test pipe is converted into a force which acts upon the beam built inside the tank. The displacement of the beam is then picked up by a transducer. After being amplified and filtered the signals are recorded on the magnetic tape.

3.1 Measuring Techniques

Both the steady and the unsteady momentum fluxes are measured by the same beam-tee system. In the measurement of the steady momentum fluxes the voltage reading on the vacuum tube volt meter (VTVM) is proportional to the time average of the momentum fluxes, provided that the deflection of the beam is small and the transducer is working in its linear operating range. In the unsteady momentum flux measurement, the turning tee and beam combination is a dynamic system and can be treated as a linear time-invariant vibratory system of single degree of freedom. In the frequency domain, the response of a dynamic system is equal to the excitation times the transfer function of this system (see Appendix B). The momentum fluxes of the two-phase flow from the test pipe is the excitation to the beam-tee system while the beam deflection is the response. If the electric signals from the transducer are recorded after being rectified and amplified, then the record is the history of the beam displacement times a constant. To record the history of the momentum fluxes, a special filter set has been designed

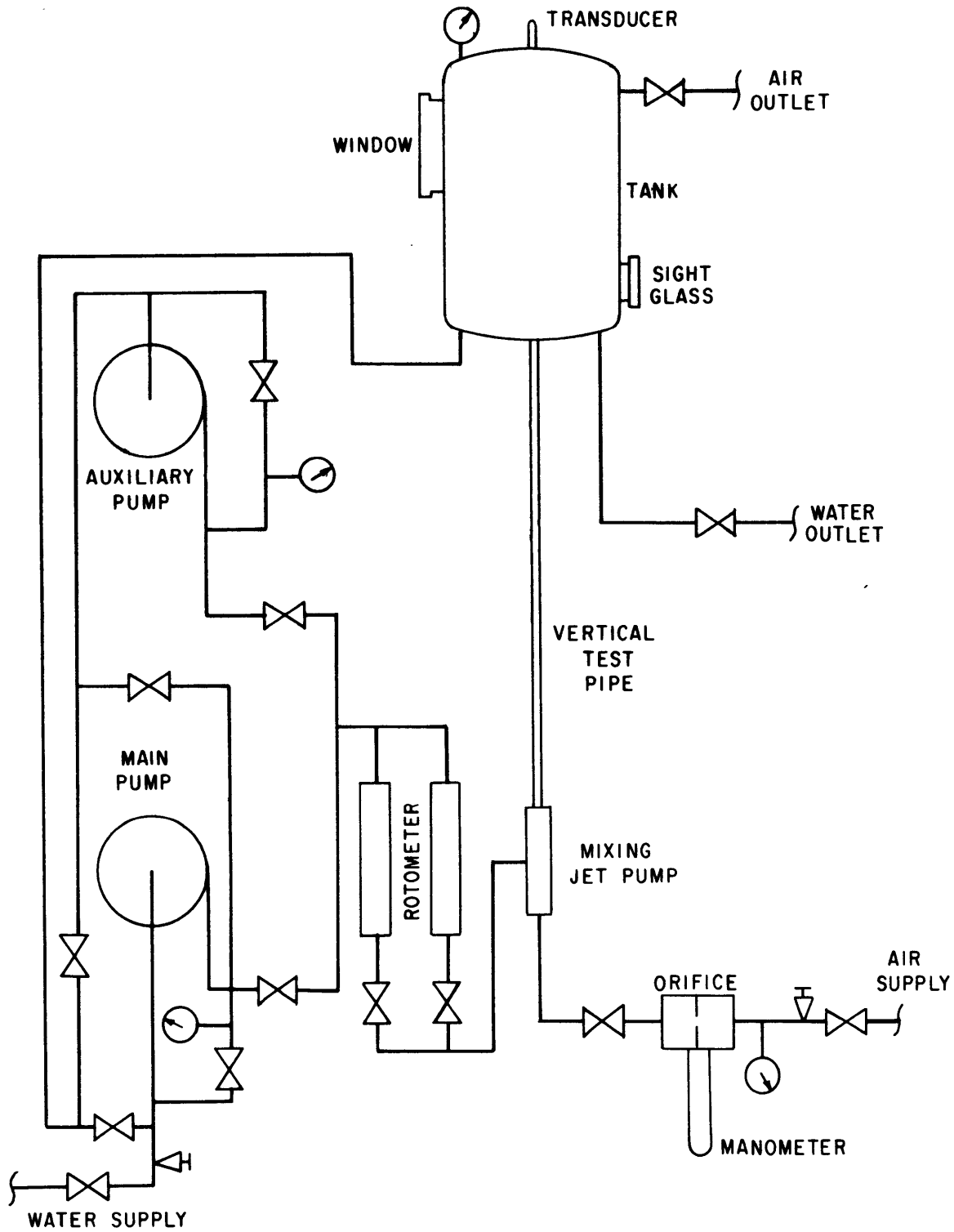


FIGURE 3.1 ARRANGEMENT OF APPARATUS (A)

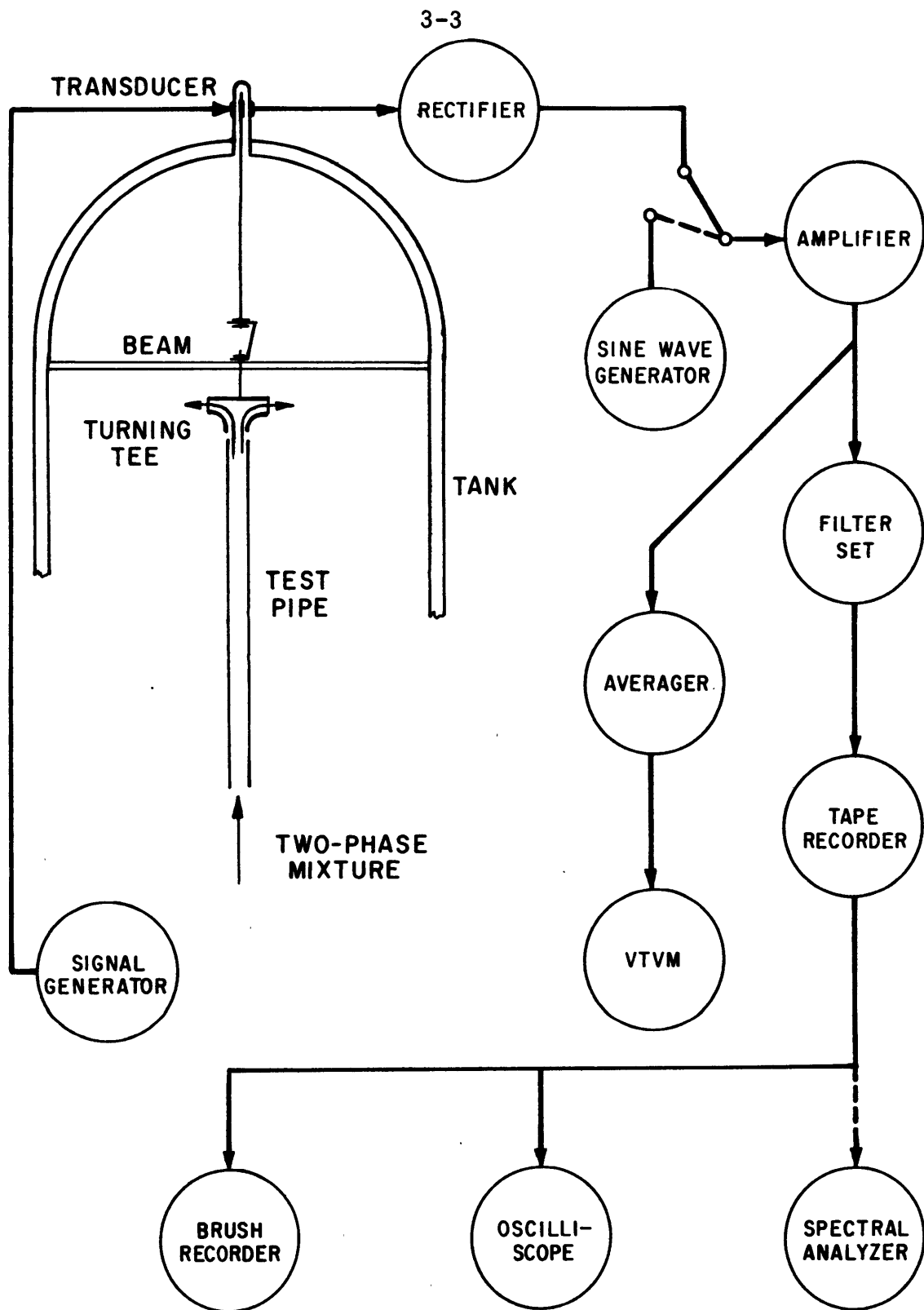


FIGURE 3.2 ARRANGEMENT OF APPARATUS (B)

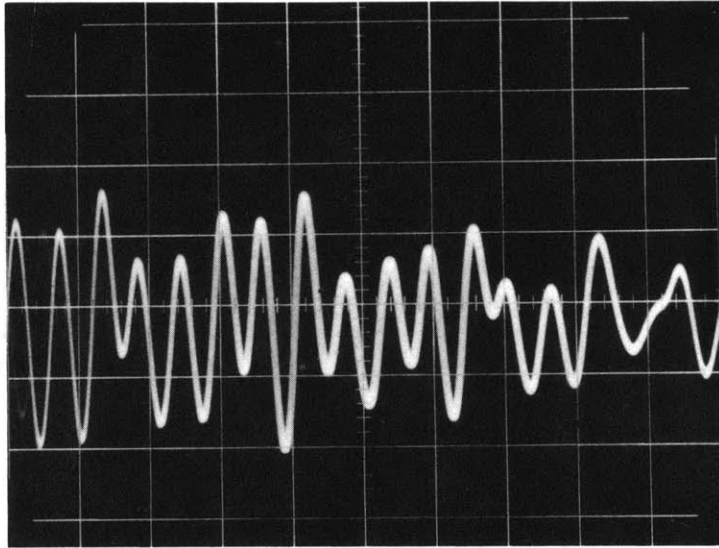
to convert the response signals to the excitation signals. The picture in Fig. 3.3(a) is an example of the response signal. The corresponding excitation signal is shown in Fig. 3.3(b). Due to the random nature of the excitation, the predominant response frequency of the beam-tee system is very close to its natural frequency which is about 84 cycles/sec.

3.2 Variables Used and Their Testing Ranges

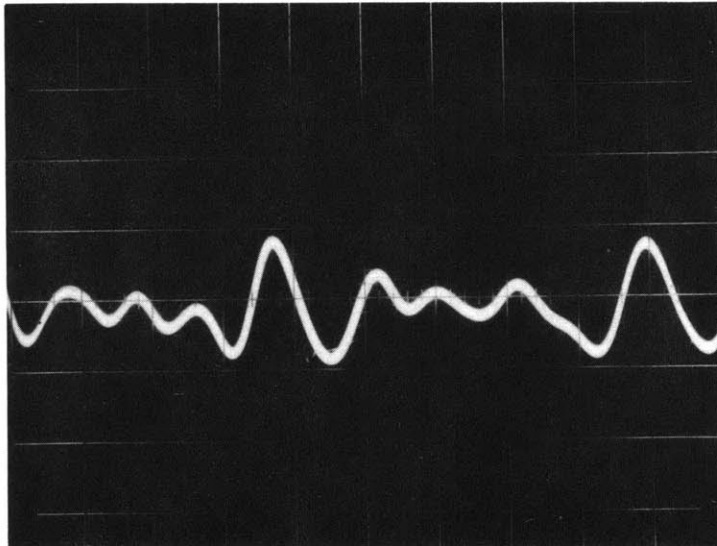
The fluctuation of momentum fluxes in a two-phase flow is closely related to the flow regimes which can be determined by the average flow velocity $V = \frac{Q_g + Q_f}{A_p}$ and the volumetric quality or flowing void fraction $\beta = \frac{Q_g}{Q_g + Q_f}$ (14,15). The air volume flow rate Q_g , the water volume flow rate Q_f as well as the pipe cross sectional area A_p can be easily measured to a good accuracy. Hence, the average flow velocity and the volumetric quality have been chosen as two major variables in this investigation.

Most of the experiments were conducted in the velocity range of 55 ft/sec to 250 ft/sec and volumetric quality range of 50% to 100%. The lower end of the velocity range was limited by the sensitivity of the measuring system while the lower values of β were restricted by the water supplying capacity.

Test pipes with different sizes and cross section geometries have been used in this investigation. The diameters of three round pipes are 1 inch, 5/8 inch and 1/4 inch. The different geometries are round, rectangular, triangular and annular. The cross-sectional areas of these pipes are shown in full size in Fig. 3.4. The flow areas in the four pipes shown in Fig. 3.4(a), (b), (c) and (d) are approximately equal. In the annular pipe three sets of spacers were soldered on the



(a) Response Horiz. Scale = 0.02sec/unit
Vert. Scale = 2 volts/unit



(b) Excitation Horiz. Scale = 0.02 sec/unit
Vert. Scale = 1 volt/unit

FIGURE 3.3 EXCITATION AND RESPONSE SIGNALS
OF THE BEAM - TEE SYSTEM

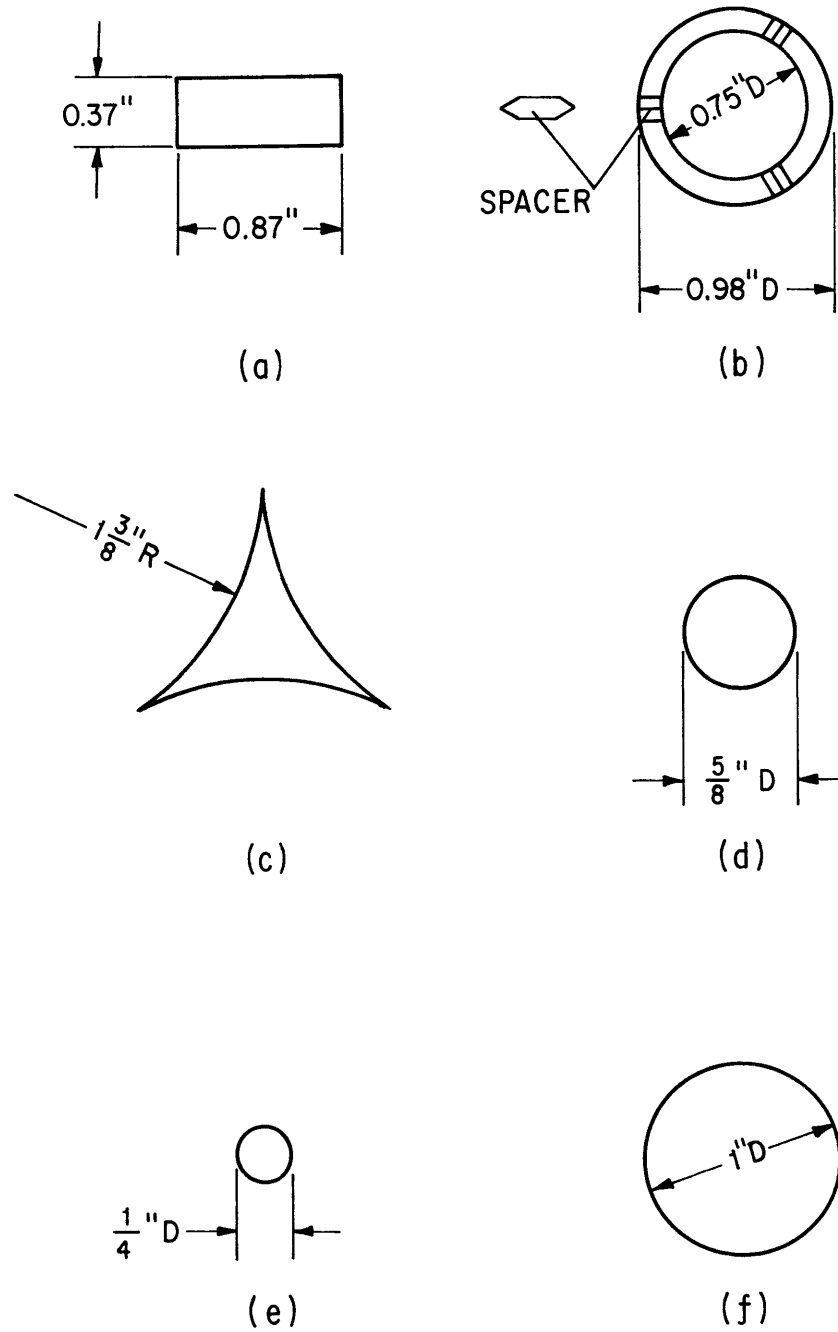


FIGURE 3.4 CROSS SECTIONS OF TEST PIPES

inner tube. The distances from the pipe inlet to these three sets of spacers are about 2, 4 and 6 ft, respectively. Each set consists of three spacers equally distributed in the horizontal plane.

The pressure at the exit of the test pipe was maintained at one atmospheric pressure for most of the experiments. To investigate the effect of pressure upon the unsteady momentum fluxes, a few tests were run with the exit pressure kept at two atmospheric pressure. Further increase in exit pressure was not successful because of the very high two-phase flow resistance and the limited air supply pressure.

3.3 Experimental Apparatus

The experimental apparatus consists of six test pipes and three other parts, namely, the fluid feed system, the tank and its internals and the recording system.

The length of the 1/4 inch diameter test pipe is 7 1/2 feet and the lengths of the other five pipes are all about 8 1/2 feet. When either one of the five larger pipes was used in the experiments there was no change in the apparatus. Since the flow area of the 1/4 inch round pipe is much smaller than the others, the force acting on the beam by the two-phase flow from this pipe would be proportionally smaller. Thus, another more sensitive beam-tee system was built in a second tank for experiments using this small test pipe. Corresponding changes were made in the fluids feed system and the recording circuit.

3.3.1 Fluids Feed System

The layout of air and water feed system is shown in Fig. 3.1.

City water was supplied to the system at room temperature. Two pumps were available to this project. To utilize the full capacity of

the existing equipment the piping connecting two pumps was so arranged that the main pump and the auxiliary pump could work either simultaneously or separately to feed or circulate water. Both pumps were bypassed so that they would not be overloaded. The water flow rate was measured by either one of the two Flowrator Meters with measuring capacities of 5.7 gal/min. and 19.3 gal/min. At low water flow rate the smaller Flowrator Meter was used to assure accurate measurements.

Air at about room temperature was supplied from the laboratory supply at 125 psi. When air was fed directly into the test pipe the fluctuation of supply pressure occurred. Sometimes the fluctuation amplitude was as high as 10% of the mean supply pressure. In the measurement of unsteady momentum fluxes this is a very undesirable situation. Hence a pressure regulator was installed in the air pipeline to eliminate this trouble. Air flow rate was measured by orifice meters. The orifice meter of an 0.100 inch diameter orifice plate in a 1 inch diameter pipe equipped with oil manometer was used in experiments using the 1/4 inch diameter test pipe. For experiments using other pipes, an orifice meter with a 0.413 inch diameter orifice plate in a 2 inch diameter pipe connected with mercury and oil manometers was employed.

3.3.2 Tank and Internals

The steel tank served as a container to provide an atmosphere at the testing pressure in which to surround the turning tee, beam and the exit of the test pipe. It was also the mounting frame for the test pipe, the beam and the transducer. The manhole located on the side wall of the tank was covered by a glass window during actual operation.

Actions inside the tank were viewed through this window.

The function of the turning tee was to turn the flow from the vertical test pipe into a horizontal plane so that the turning tee received the total axial momentum in the pipe flow. The upper part of the tee was a circular, flat plate deflector. Its lower part was a divergent nozzle-shaped piece which provided the inlet and the guide wall for the two-phase flow. The two-phase mixture flowed radially outward through the gap between the upper and lower parts of the tee. Shown in Fig. 3.5(a) is the turning tee used for experiments of the five larger pipes; and the one in Fig. 3.5(b) for experiments of 1/4 inch diameter test pipe.

It has been seen from some preliminary runs conducted with the 5/8 inch diameter test pipe that the momentum flux fluctuation of a two-phase flow is important only in the low frequency domain below 50 cycles/sec. The trend of some earlier investigations into the unsteady nature of two-phase flow also shows that the significant fluctuations of two-phase flow are of relatively low frequencies. In order to obtain the fluctuating behavior of the momentum fluxes from the beam displacement, it is desirable to have a beam-tee system with a higher natural frequency than the main frequency range of the momentum flux fluctuation. Therefore, the natural frequency of the beam-tee system should be well above 50 cycles/sec. If the natural frequency of the dynamic system were extremely high, for instance, 10 times as high as the excitation frequency, then in the low frequency range the response would be almost linearly proportional to the excitation and measurements of the excitation would be very simple. To increase the natural frequency of a vibration system one must either increase the stiffness or reduce

3-10

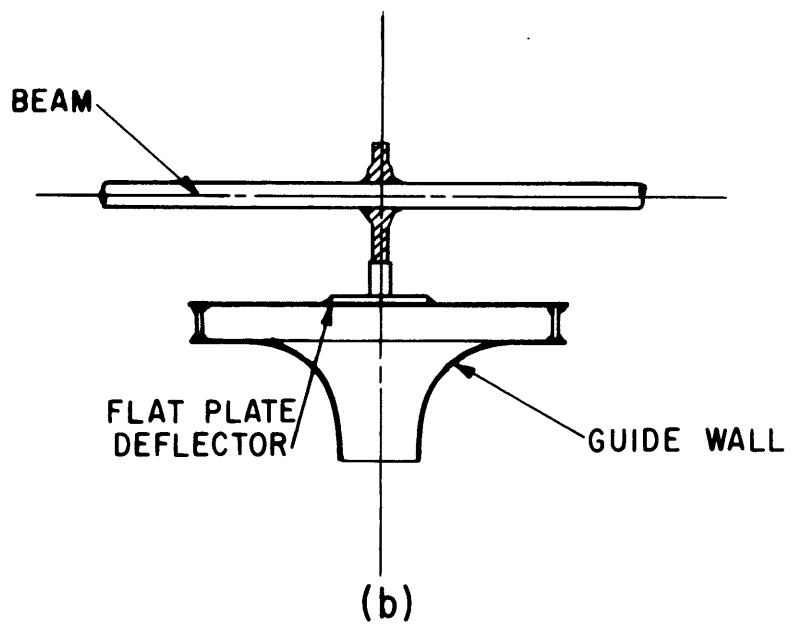
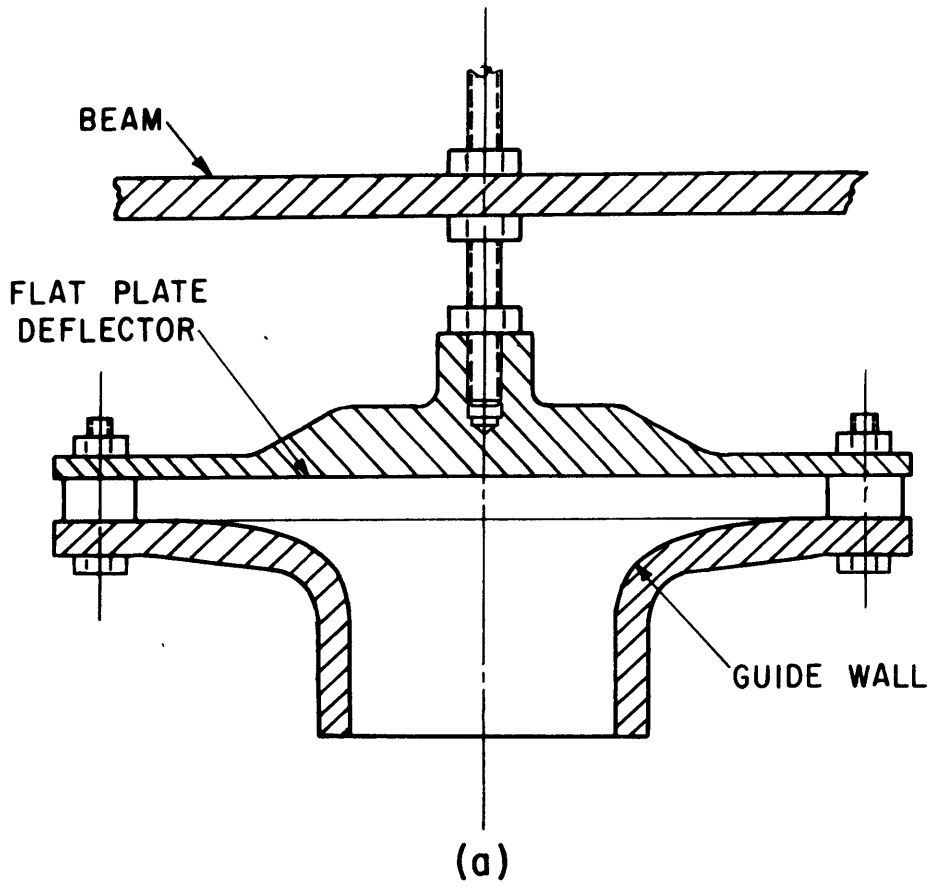


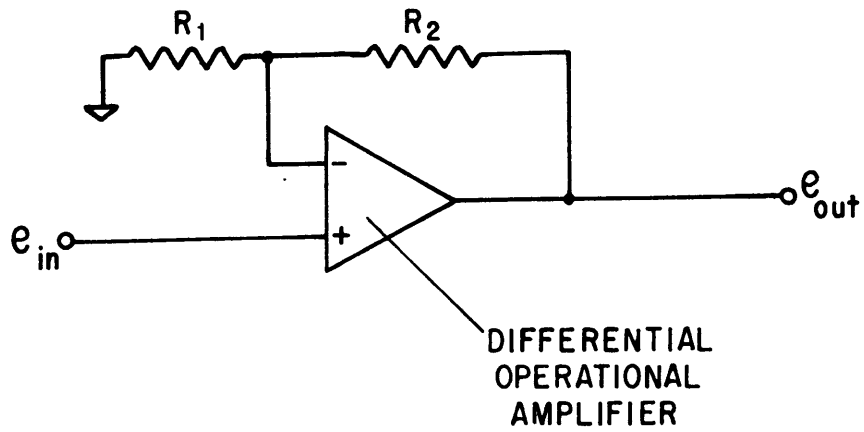
FIGURE 3.5 STRUCTURES OF TURNING TEE

the mass of the system. However, for the beam-tee system, the increase of stiffness is bounded by the necessary sensitivity; the reduction of mass is limited by the material property and the manufacturing technology. Thus the beam-tee systems used in this investigation were designed to have natural frequencies reasonably higher than the frequency range in which the momentum flux fluctuation is important. An inverse transfer technique was employed to obtain the fluctuating behavior of momentum fluxes in two-phase flow. The natural frequencies of the two beam-tee systems were designed to be 168 cycles/sec for the 1/4 inch diameter test pipe and 84 cycles/sec for other test pipes.

The Linear Variable Differential Transformers (LVDT) were selected as the transducers to transmit the information of the beam deflection. Two Sanborn Linearsyn Differential Transformers were used. The LVDT of Model 595DT-025 was used for experiments with 1/4 inch round test pipes and Model 590T-025 for other test pipes. The LVDT coil assembly was fixed on the tank and the core was attached on a push rod which was mounted upward from the beam. The relative position of the coil assembly to the core can be adjusted mechanically. The primary coil was fed a 5 KC signal with an amplitude of 12 volts.

3.3.3 Recording System

As shown in Fig. 3.2, the output from the LVDT goes to the amplifier after being rectified. The circuit diagram of this amplifier is shown in Fig. 3.6. One output from the amplifier is connected to the VTVM after being averaged by a resistor capacitor circuit with a 15 second time constant. Another output goes through the filter set and then to the magnetic tape recorder. The oscilloscope and Brush



$$e_{out} = \frac{R_2}{R_1} e_{in}$$

$$R_1 = 10 \text{ K } \Omega$$

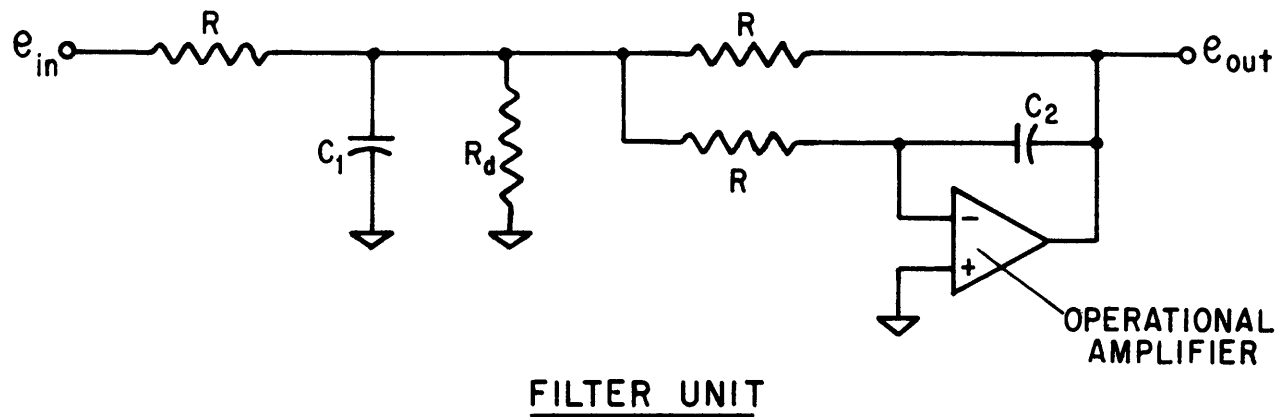
$$R_2 = 100 \text{ K } \Omega$$

FIGURE 3.6 AMPLIFIER IN RECORDING SYSTEM

recorder are connected to the playback of the tape recorder. While signals are being recorded on the tape they can be viewed on the oscilloscope to detect any irregularities. Signals were also recorded on the Brush recording chart which can be preserved for possible future reference. The input to the amplifier can be switched over to receive signals from the sine wave generator to check the electronic drift in the recording circuit and to calibrate the power spectral density curve of the unsteady momentum fluxes.

The filter set has two functions. (1) To simulate the inverse of the transfer function of the beam-tee system in the low frequency range where the significant fluctuations of momentum fluxes exist. (After passing through this filter set the signals are proportional to the excitation in this low frequency range.) (2) To decrease the energy level at the beam natural frequency before recording signals on the magnetic tape so that the recording capacity of the tape can be utilized more effectively.

Two filter sets have been used in the experiments. Filter set (A) is for the beam-tee system with natural frequency of 84 cycles/sec and set (B) for that of 168 cycles/sec. Each filter set consists of a tenth order low pass filter and a second order low pass filter. The tenth order filter is a series combination of five second order low pass filters. The R-C circuits of the five filter units are the same but the damping resistors, R_d , are different (16). The circuit diagram of a second order filter unit is shown in Fig. 3.7 where the values of the resistors and capacitors used in filter sets (A) and (B) are also listed. The performance curves of filters (A) and (B) are shown in



FILTER SET (A)

	C_1 (μf)	C_2 (μf)	R ($K\Omega$)	R_d ($K\Omega$)
2ND ORDER	0.18	.0018	100	7.7
10TH ORDER	0.3	.003	100	834 16.4 9 6.8 6

FILTER SET (B)

	C_1 (μf)	C_2 (μf)	R ($K\Omega$)	R_d ($K\Omega$)
2ND ORDER	0.1	.001	82	6.3
10TH ORDER	0.15	.0015	100	834 16.4 9 6.8 6

FIGURE 3.7 FILTER SET IN RECORDING SYSTEM

Figs. 3.8 and 3.9 respectively. There, the curves of the normalized reciprocal of the transfer function of the corresponding beam-tee systems are also presented for comparison. In Fig. 3.8 for frequencies below 50 cycles/sec, the maximum difference between two curves is 2% and the attenuation rate at 84 cycles/sec is 3%. In Fig. 3.9, below a frequency of 100 cycles/sec, the difference between two curves is less than 4% and the attenuation rate at 168 cycles/sec is about 4%.

3.4 Experimental Procedure

3.4.1 Pluck Test of Beam

After each beam-tee system was set up, Pluck tests of the beam were made. During these tests pictures of the beam free vibration curve were taken. From the free vibration curve the natural frequency of the beam-tee system was determined. Because the beam was fixed at both ends the equivalent mass of the system was equal to 40% of the mass of the beam (see Appendix E) plus all the masses attached at its center. Then the spring constant of the beam was computed and checked with the result of static load-deflection test. The decay rate of the free vibration curve was measured to obtain the damping coefficient. Knowing the spring constant, equivalent mass, and damping coefficient of the beam-tee system, its transfer function was calculated. Based on this information the filter set was designed.

3.4.2 Steady Momentum Flux Calibration

A static force of known magnitude was applied vertically upon the beam by a calibrated spring. The corresponding voltage reading on the VTVM was taken. The same procedure was repeated a few times with applied forces of different magnitudes. An averaging calibration

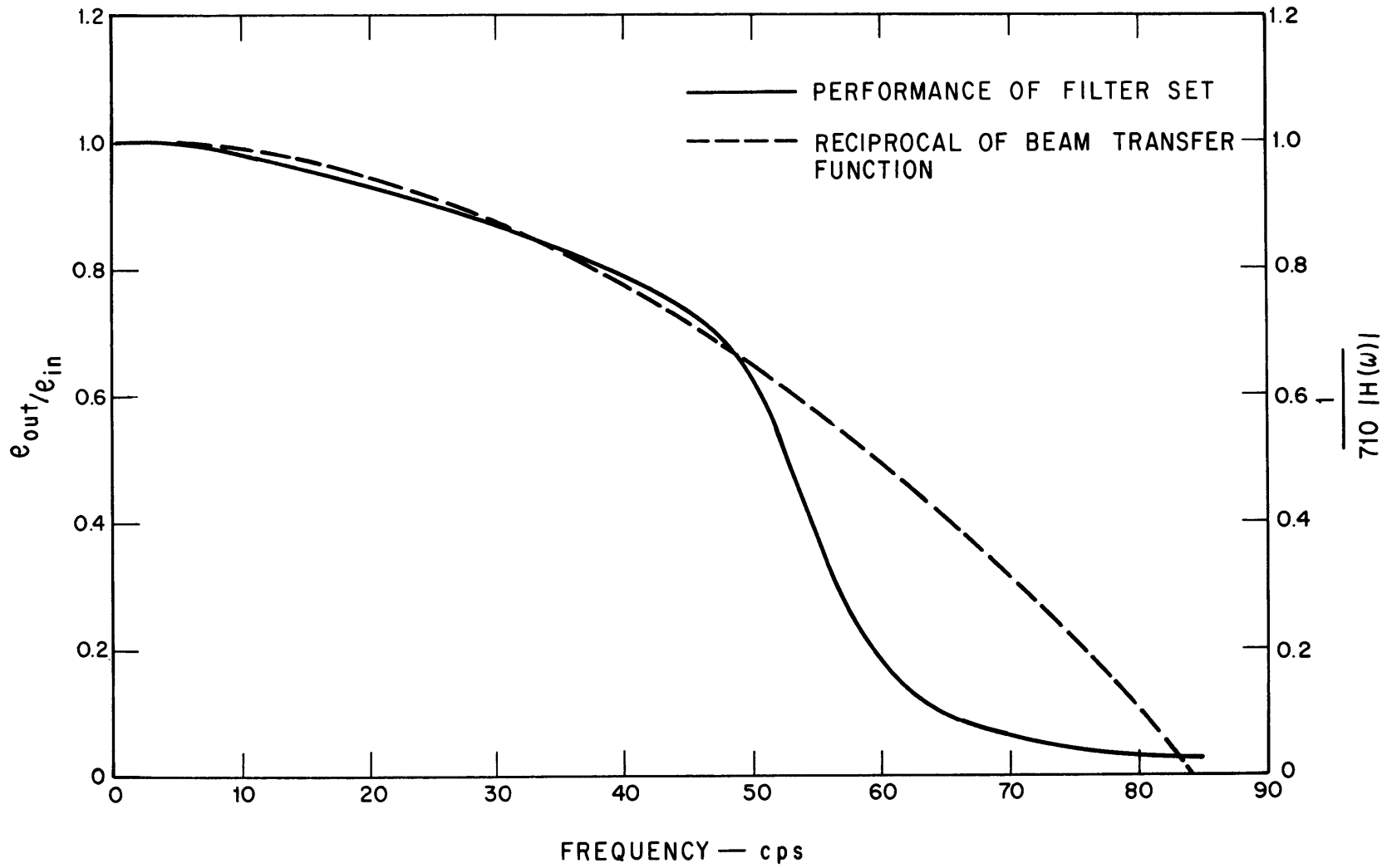


FIGURE 3.8 PERFORMANCE CURVE OF FILTER SET (A) AND RECIPROCAL OF BEAM-TEE TRANSFER FUNCTION

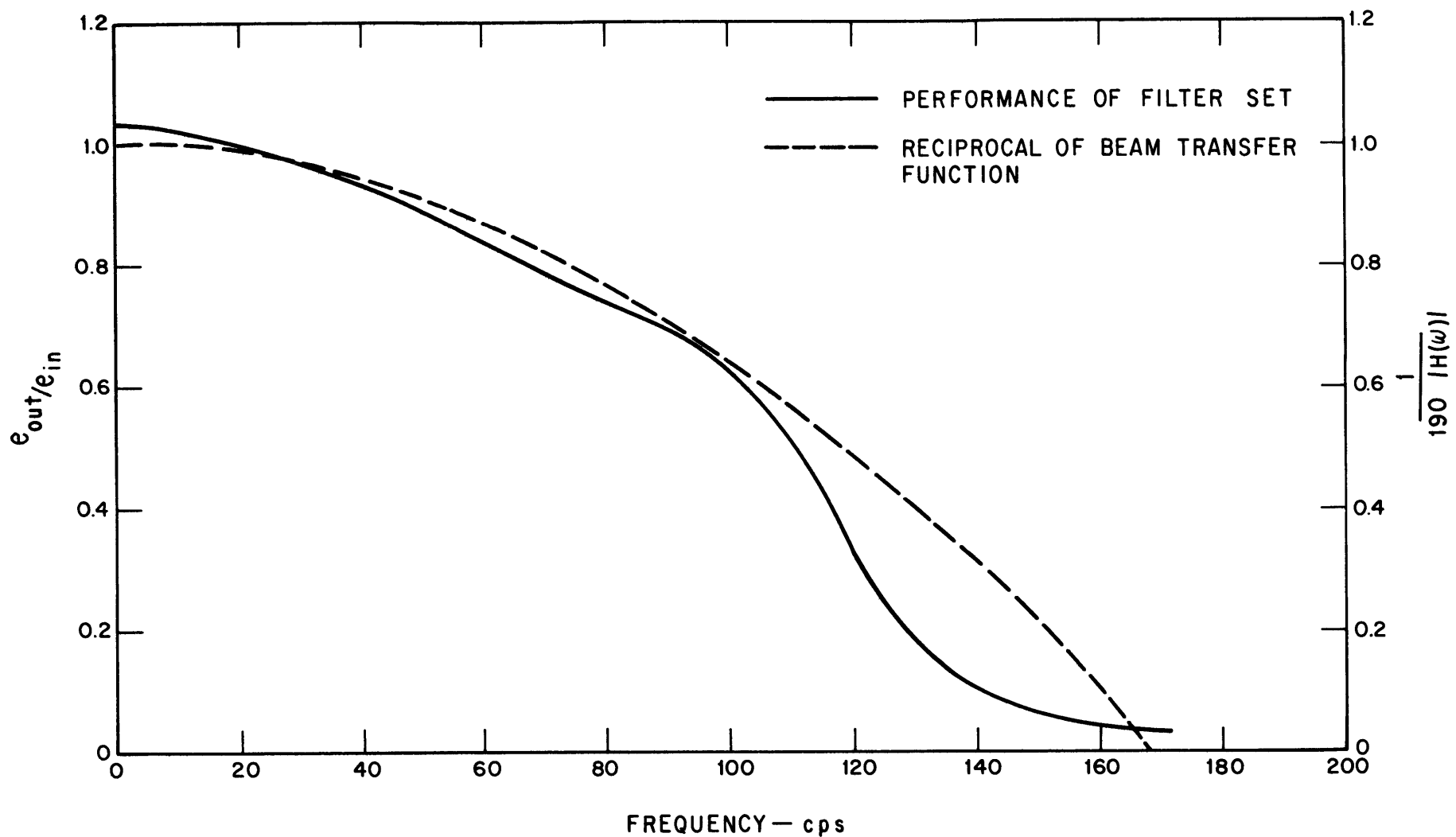


FIGURE 3.9 PERFORMANCE CURVE OF FILTER SET (B) AND RECIPROCAL OF BEAM-TEE TRANSFER FUNCTION

coefficient was thus obtained with the unit of volts/lb_f.

3.4.3 Checking the Function of the Turning Tee

The inlet of the test pipe was temporarily connected to the laboratory steam supply line. A steam jet of known flow conditions impinged on the turning tee. The momentum of this single-phase steam flow was computed and compared with the value indicated by the VTVM. These two values were in good agreement. During actual two-phase flow tests, the flow conditions from the test pipe to the turning tee were frequently watched through the glass window on the tank to assure that all the fluid leaving the tee was travelling in the horizontal plane. Under these conditions the force applied on the beam is equal to the total axial momentum of the two-phase flow from the test pipe.

3.4.4 Preliminary Tests

The purpose of running preliminary tests is to provide guide lines and assure smooth operation for the formal tests from which systematic data were obtained. Limitations of the apparatus found in the preliminary tests were; the maximum water flow rate for different test pipes and the highest regulated air supply pressure that would remain stable in tests. For stable operation with the 1/4 inch diameter test pipe, the regulated air supply pressure was about 90 psig; with other pipes it was only about 65 psig. Also determined in these tests was the proper magnification factor of the amplifier through which the signals of large fluctuations would still be within the recording capacity of the magnetic tape; the signals of small fluctuations would also have to be large enough for data processing.

3.4.5 Systematic Tests

Each set of the formal tests having the same average flow velocity V consists of 5 to 8 runs with different values of volumetric quality β . To investigate the effect of velocity on the unsteady momentum fluxes, 5 sets of experiments using the 5/8 inch diameter test pipe were conducted with values of V ranging from 70 ft/sec to 250 ft/sec. Two sets of experiments with V equal to 100 ft/sec and 150 ft/sec were planned for the rectangular, triangular and annular pipes to observe the effect of channel geometry. For investigating the effect of pipe size, experiments at average velocities of 70 ft/sec and 100 ft/sec were planned for three round test pipes. Due to the high flow resistance in the 1/4 inch diameter test pipe, two sets of experiments were conducted at average velocities of 70 ft/sec and 55 ft/sec.

All the experiments mentioned above were carried out at atmospheric pressure inside the tank. There were two sets of experiments with V equal to 70 ft/sec and 100 ft/sec, using 5/8 inch diameter test pipe conducted at 2 atmospheric pressure. For running these tests the valve before the water outlet of the tank was closed and the water coming out from the turning tee was circulated in the system. The pressure inside the tank was controlled by the valve before the air outlet.

The air flow rate Q_g and the water flow rate Q_f of each run were computed from the predetermined values of V and β . After the orifice manometer and the Flowrator Meter gave stable readings corresponding to the computed values of Q_g and Q_f , the tape recorder began to record signals. The recording period of each run was about 11 minutes which was equal to the necessary data processing time plus some overhead time.

Between the consecutive runs, signals from the sine wave generator were fed into the amplifier and were recorded on the tape for a period of about 30 seconds. These sine wave signals served to distinguish the signals recorded during the consecutive runs and to check any irregularities in the recording circuit. Signals from the playback of the tape recorder were monitored on the Brush recording chart with a duration of about 1 minute for each test. The magnitude of the steady momentum fluxes was obtained from the VTVM readings.

4. DATA PROCESSING

4.1 Random Vibration Techniques

The random nature of the two-phase flow fluctuations suggests the application of statistical analysis to the recorded signals of unsteady momentum fluxes in two-phase flow. Some basic definitions and equations in the theory of random vibration are re-stated below because they are essential to an understanding of this method of data processing.

If $x(t)$ is the value of a random process at any time t and $x(t + \tau)$ is its value at time $(t + \tau)$ its auto-correlation function is $E[x(t) x(t + \tau)]$, where τ is a time lag. If this random process is stationary, then the auto-correlation function is a function only of τ ,

$$E[x(t) x(t + \tau)] = R(\tau) \quad (4.1)$$

A random process is defined as being stationary if any translation in time leaves its probability distributions unaffected. This appears to be the case with the fluctuations of momentum fluxes in two-phase flow.

In the frequency domain the auto-correlation function $R(\tau)$ and the power density spectrum $S(\omega)$ are related to each other by the Fourier transform given as

$$R(\tau) = \int_{-\infty}^{\infty} S(\omega) e^{i\omega\tau} d\omega \quad (4.2)$$

where ω is the angular frequency in radians per second. Consider the limiting case of equation (4.1) in which $\tau = 0$.

$$R(0) = E[x^2] = \int_{-\infty}^{\infty} S_x(\omega) d\omega \quad (4.3)$$

The mean square of the process equals the sum over all frequencies of

$S(\omega) d\omega$ so that $S(\omega)$ can be interpreted as a mean square spectral density. In experimental work the spectral density is denoted by $W(f)$ where f is frequency in cycles per second. The relation between $S(\omega)$ and $W(f)$ is

$$W(f) = 4\pi S(\omega) \quad (4.4)$$

Equation (4.3) then takes the form

$$E[x^2] = \int_0^{\infty} W_x(f) df \quad (4.5)$$

This is the basic equation being used in the data processing.

4.2 Measurement of Spectral Density

The block diagram in Fig. 4.1 is the procedure commonly used in experimental measurement of spectral density (Ref. 17, p. 30). In this procedure a sample function $f(t)$ is filtered, squared, and averaged over an interval T . The measured quantity $Z(t)$ is an approximation to $\Delta\omega G(\omega_0)$ where $G(\omega)$ is the individual spectral density of $f(t)$.

A stationary random process is said to be ergodic if its ensemble averages are equal to the corresponding temporal averages taken along any representative sample function (Ref. 17, p. 21). For an ergodic process, the process spectral density $S(\omega_0)$ is identical to the individual densities $G(\omega_0)$ of representative samples. The recorded signals of unsteady momentum fluxes may be assumed to be ergodic because in the experimental work the same apparatus has been used for tests of particular flow conditions. Therefore, to estimate the process spectral density $S(\omega)$ of the unsteady momentum fluxes, it is only necessary to perform the measurement of a single sample function.

The block diagram in Fig. 4.2 shows the actual arrangement of

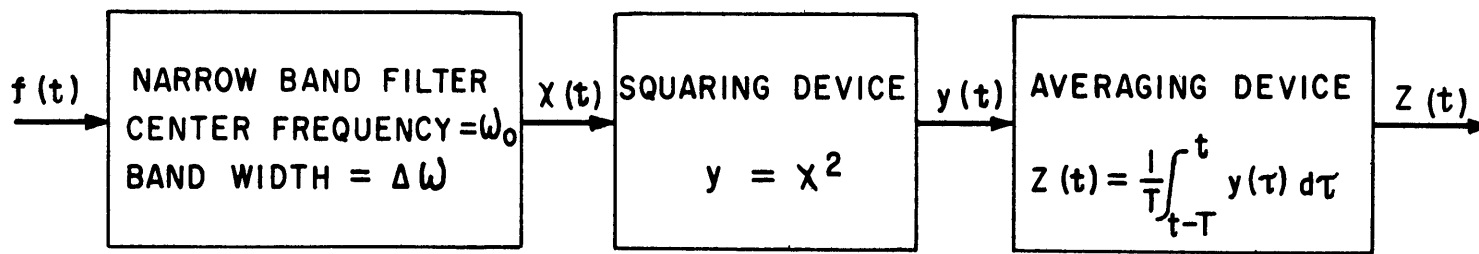


FIGURE 4.1 SCHEMATIC DIAGRAM OF MEASUREMENT OF SPECTRAL DENSITY $G(\omega_0)$ OF SAMPLE FUNCTION $f(t)$

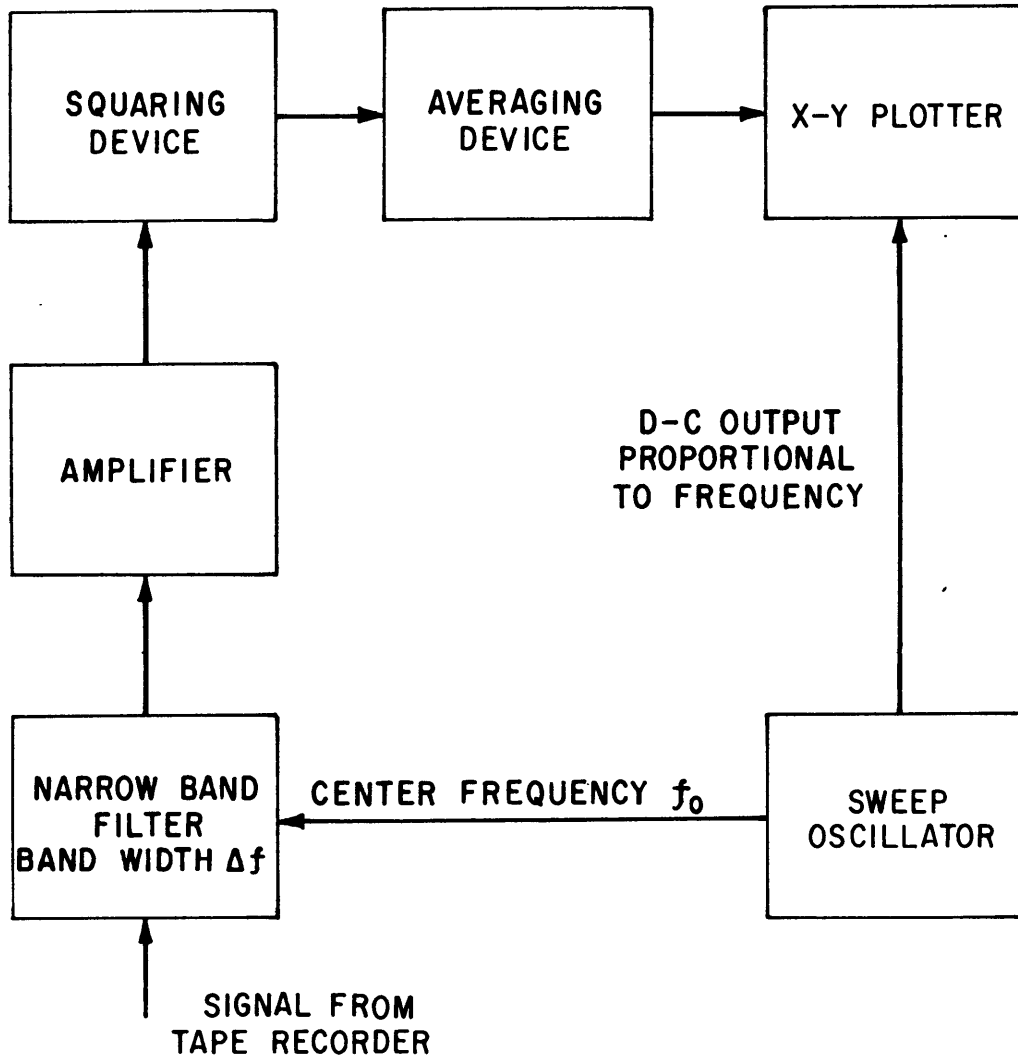


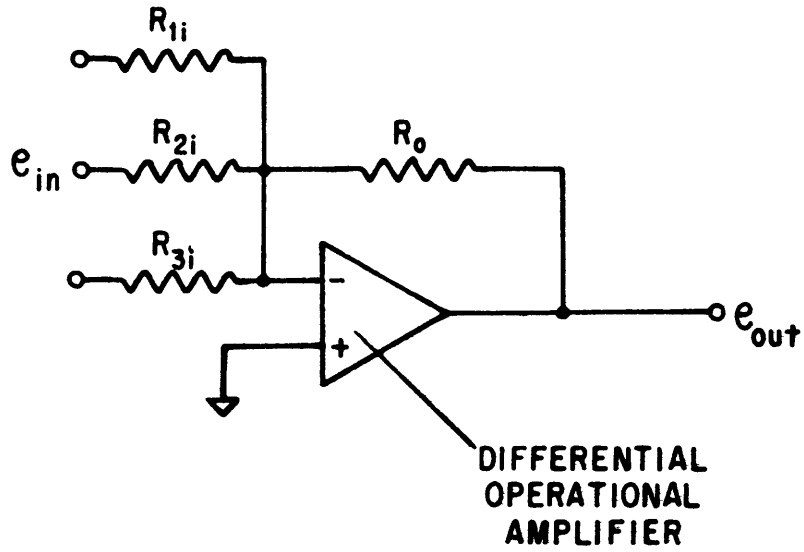
FIGURE 4.2 SPECTRAL ANALYSIS SYSTEM

instruments for obtaining the spectral density as a function of frequency. The signal played back from the tape recorder is fed into the SD 101 A Dynamic Analyzer in which there is a narrow band filter with a fixed band width $\Delta f = 5$ cps. The SD 104-5 Sweep Oscillator is used to perform an automatic sweep of the filter center frequency f_0 . It also drives the pen of the X-Y Plotter to move in the X direction in accordance with the sweeping center frequency. The filtered signal is amplified and goes through the squaring device and the averaging device. The measured quantity $Z(t)$ is then plotted versus the filter center frequency. This $Z(t) \sim f_0$ plot is the spectral density curve of the unsteady momentum fluxes if the Y axis is properly scaled.

Both the Dynamic Analyzer and the Sweep Oscillator are made by the Spectral Dynamics Corporation and the squaring device is the GPS MU401 Multiplier. Depending upon the intensity of the momentum flux fluctuations, three different magnification factors can be selected from the amplifier whose circuit diagram is shown in Fig. 4.3. The circuit diagram of the averaging device with 10 seconds time constant is shown in Fig. 4.4.

4.3 Root Mean Square Value

There are commercial instruments which can measure the rms value directly from random signals. Due to the presence of the beam-tee system in the momentum flux measuring process a considerable portion of the energy in the recorded signals is at the natural frequency of the beam system, even after severe attenuation. Thus by direct measurement one would expect to get an rms value of momentum flux much higher than its true value. Under these circumstances, the indirect measurement



$$e_{out} = \frac{R_o}{R_i} e_{in}$$

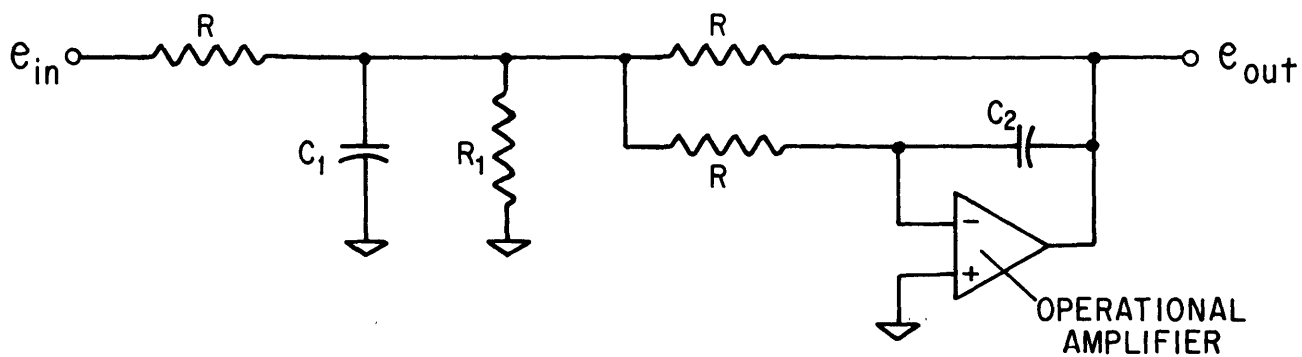
$$R_{1i} = 66 \text{ K } \Omega$$

$$R_{2i} = 50 \text{ K } \Omega$$

$$R_{3i} = 33 \text{ K } \Omega$$

$$R_o = 100 \text{ K } \Omega$$

FIGURE 4.3 AMPLIFIER IN SPECTRAL ANALYSIS SYSTEM



$$R = 1 \text{ Meg } \Omega$$

$$R_1 = 1.68 \text{ Meg } \Omega$$

$$C_1 = 6 \mu\text{f}$$

$$C_2 = 1.4 \mu\text{f}$$

FIGURE 4.4 AVERAGING DEVICE IN SPECTRAL ANALYSIS SYSTEM

of rms value must be adopted. In this method, the rms value is obtained by measuring the area under the power spectral density curve $W_p(f)$. From equation (4.5) the mean square of the unsteady momentum fluxes is

$$E [P^2] = \int_0^{\infty} W_p(f) df \quad (4.6)$$

and the rms value is the square root of equation (4.6). From the spectral density curves obtained in the preliminary tests it has been seen that beyond 50 cps the magnitude of unsteady momentum flux in two-phase flow is very small. As an approximation, the upper integration limit in equation (4.6) can be replaced by 50. In other words, to calculate the rms value one need only measure the area under the curve up to 50 cps. Thus, the trouble due to the beam natural frequency can be avoided.

4.4 Calibration of Power Spectral Density Curve

Similar to the calibration procedure described in Section 3.4.2, a calibration coefficient in terms of volts reading on the oscilloscope per pound force applied upon the beam was determined. Then from the sine wave generator a sine wave of 20 cps was fed into the recording system and recorded on the magnetic tape for a few minutes. In the meantime, the amplitude of this sine wave appeared on the oscilloscope was noted, and was converted into units of pound force by the calibration coefficient. The rms value of this sinusoidal "force" was also determined and denoted by F_s . The power spectral density measurement was carried out for the recorded sine wave and the area under this spectral density curve was measured as $A_r \text{ in}^2$. If the scale on the X axis of the graph paper used

on the X-Y Plotter is n cps per inch, then the scale on the Y axis is

$C_Y = \frac{F_s^2}{A_r \cdot n}$ with the unit of $\text{lb}_f^2/\text{cps per inch}$. After the scale of the spectral density curve was fixed, the mean square as well as the rms value of the unsteady momentum flux can be computed by measuring the area under its own power spectral density curve.

5. PRESENTATION AND DISCUSSION OF EXPERIMENTAL RESULTS

The experimental data, both raw and reduced, are tabulated in Appendix A. The steady component of momentum fluxes P_{st} was measured directly in the experiments; the root mean square value of the unsteady momentum fluxes P_{rms} was obtained from the power spectral density curve. The energy in the spectral density curves was distributed in a very broad frequency band. However, in most of the curves there was a region which contained more energy than the rest. The central location of this region is termed as the predominant frequency f_c . This is another quantitative description of the unsteady momentum fluxes. As a measure of the relative magnitude of the fluctuation, the ratio P_{rms}/P_{st} is defined to be the unsteadiness of the momentum fluxes. The primary experimental results are given in curves showing the effect of flow velocity, system pressure, channel size and geometry upon the variations of the four quantities, i.e., P_{st} , P_{rms} , P_{rms}/P_{st} and f_c , along with the volumetric quality β .

5.1 Some Particular Phenomena

In the experiments using rectangular pipe, appreciable transverse vibrations of the test pipe occurred. No such structural vibrations were observed in the tests using other pipes. This is probably due to the fact that the rectangular pipe has a low natural frequency of vibration in the direction of its small dimensions. This natural frequency falls in the range which contains the major part of the fluctuation energy of momentum fluxes.

When experiments were run with the annular test pipe, the flow resistance to the two-phase mixture was much higher than in other test

pipes. Consequently, the average flow velocity in the annulus was not able to reach 150 ft/sec for β less than 98%. The power spectral density curves of these runs are quite different from those using test pipes of other geometries. Shown in Fig. 5.1 is a typical set of spectral density curves of the unsteady momentum flux under the same flow conditions but with different channel geometries. For the annular test pipe, the energy in the spectral density curve is so evenly distributed that no specific location along the frequency axis can be assigned as the predominant frequency f_c . The spacers between the inner and outer tubes and the relatively small hydraulic diameter were both suspected of being responsible for the high flow resistance. Regarding the even distribution of the energy in the spectral density curve, the spacers were thought to have broken some of the large disturbances in the two-phase flow and increased the number of small disturbances. It resulted in a reduction of the total fluctuation energy.

When the volumetric quality β was less than 70%, another pattern of spectral density curves appeared. A sample curve of this pattern is shown in Fig. 5.2(a). In contrast to the curve pattern shown in Fig. 5.2(b), it seems impossible to assign a single value of f_c to curve (a). Since at high volumetric quality, the waves or the slugs of the liquid phase are the disturbances in the two-phase flow, whereas in the relatively low β region, presumably the slug flow regime, the lengths of liquid slugs and gas bubbles are comparable and both may be viewed as the disturbances. Therefore, there is no single value of frequency that can be assigned as f_c .

5.2 General Trends

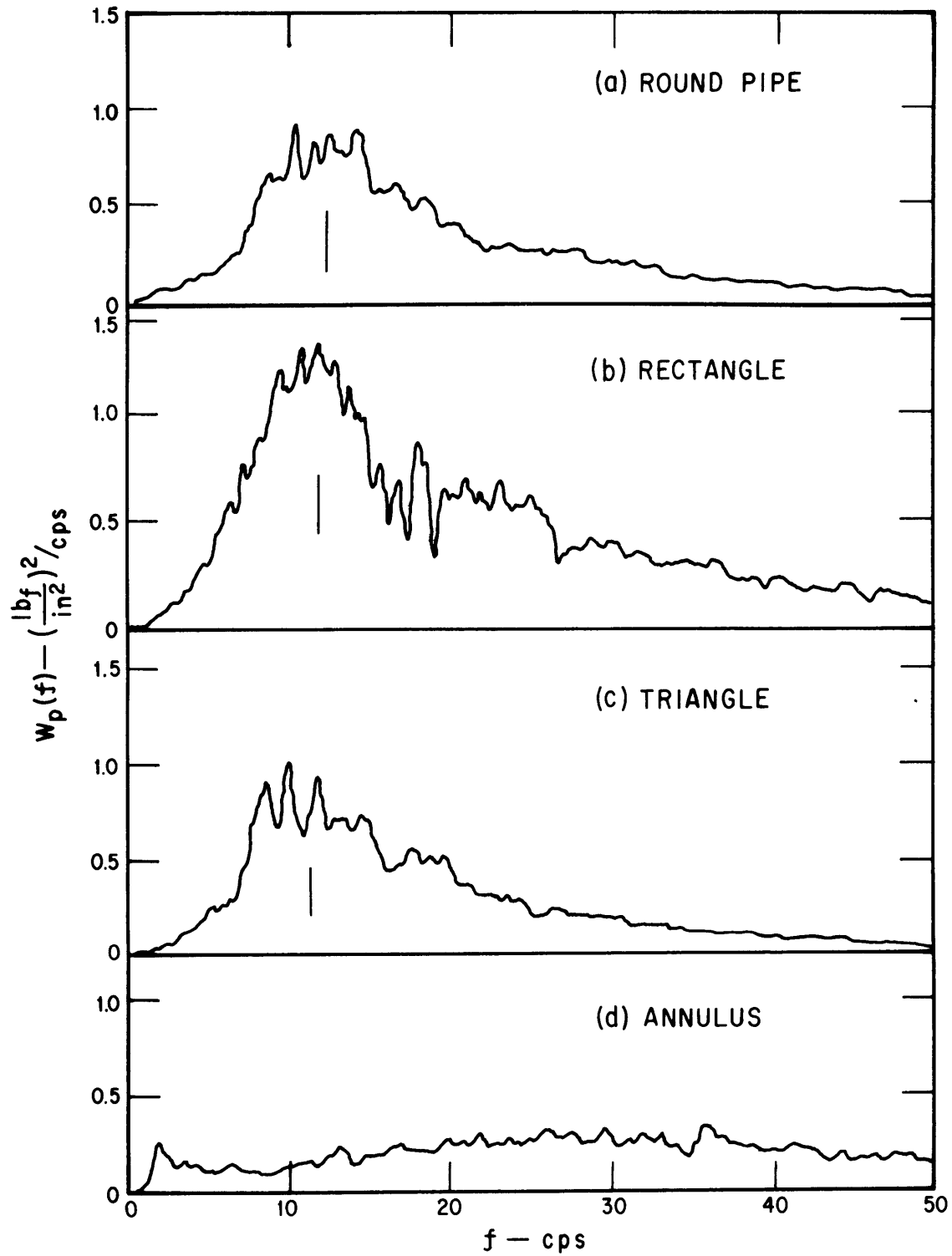


FIGURE 5.1 POWER SPECTRAL DENSITY CURVES OF UNSTEADY MOMENTUM FLUXES. $V = 100 \text{ ft}^t/\text{sec}$. $\beta = 95.5 \%$

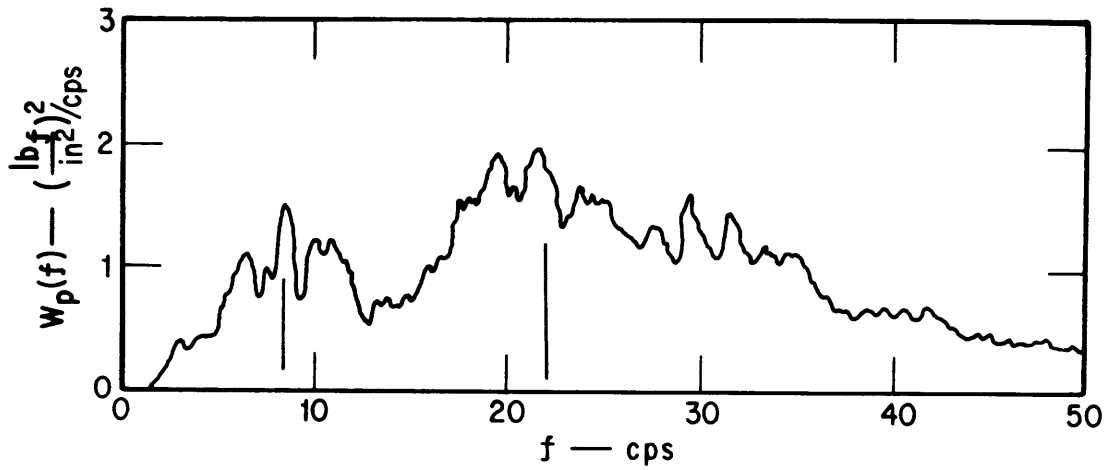
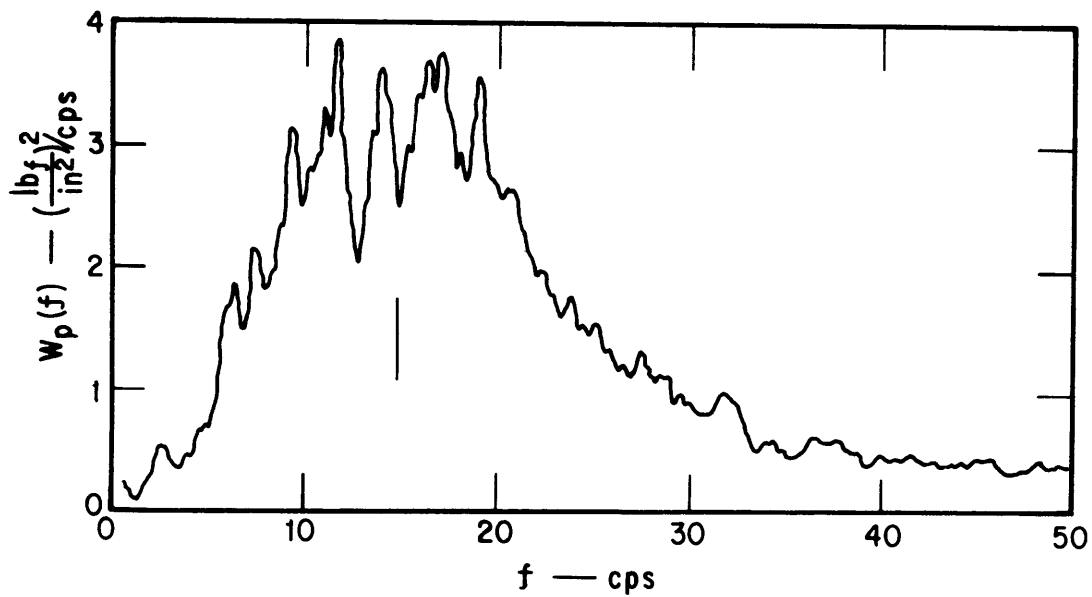
(a) $\beta = 60\%$ (b) $\beta = 70\%$

FIGURE 5.2 POWER SPECTRAL DENSITY CURVES OF UNSTEADY MOMENTUM FLUXES. $\frac{1}{4}$ " DIA. ROUND PIPE, $V = 55 \text{ ft}/\text{sec}$.

5.2.1 Effect of Average Flow Velocity

It can be seen in Figs. 5.3 and 5.4 that, for the same volumetric quality β , the rms value of the unsteady momentum fluxes P_{rms} increases with increasing average flow velocity V as one would expect. For a given value of V there appears a maximum value of P_{rms} . Although this maximum value was attained only for V equal to 55 and 70 ft/sec there is the tendency that the curves of higher velocities will reach their maximum values of P_{rms} . If the values of β and V , at which the maximum values of P_{rms} occur, are referred to the flow regime map in reference (14) it is seen that they all fall in the annular flow regime. If these values of β are first converted into α using the void fraction and volumetric flow concentration correlation in reference (20) then the values of α and V are referred to the annular-slug transition diagram in reference (21), the maximum values of P_{rms} would appear in the flow regime around the annular-slug transition line but somewhat closer to the side of the slug flow regime. Thus one can expect the maximum value of P_{rms} of a given V to appear in either low void annular or high void slug (semiannular) flow regime.

Figures 5.5 and 5.6 show that the unsteadiness of momentum fluxes P_{rms}/P_{st} increases with decreasing V . This implies that when V increases the unsteady component of momentum fluxes increases at a slower pace than the steady component. The value of β , at which the maximum value of P_{rms}/P_{st} appears, also increases with V . For the same value of V , the maximum of P_{rms}/P_{st} occurs at higher β than the maximum of P_{rms} does, since P_{st} always goes up with decreasing β . The greatest unsteadiness of momentum fluxes appear in the high β range above 90%, as shown in

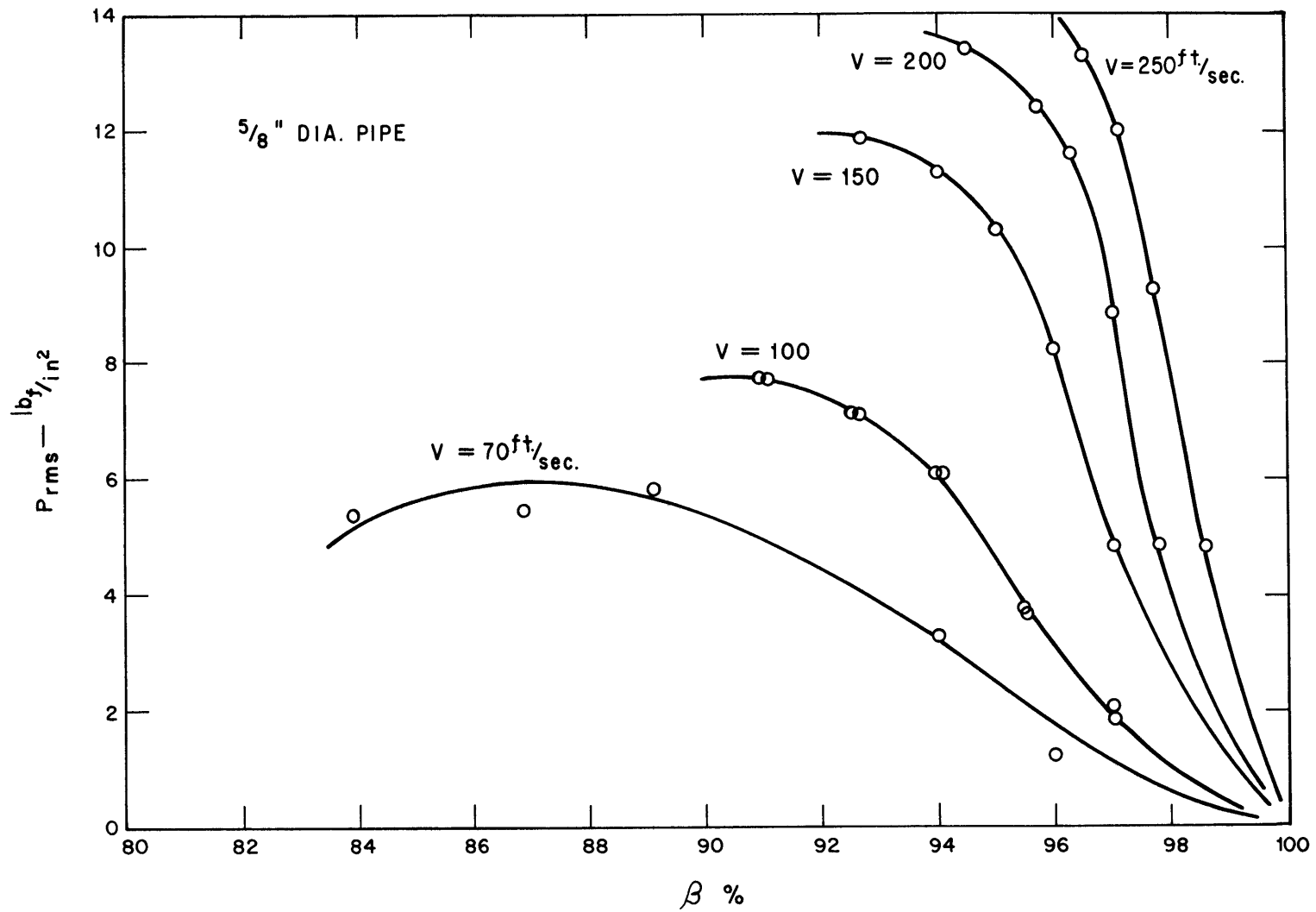


FIGURE 5.3 EFFECT OF AVERAGE FLOW VELOCITY ON RMS VALUE OF UNSTEADY MOMENTUM FLUXES

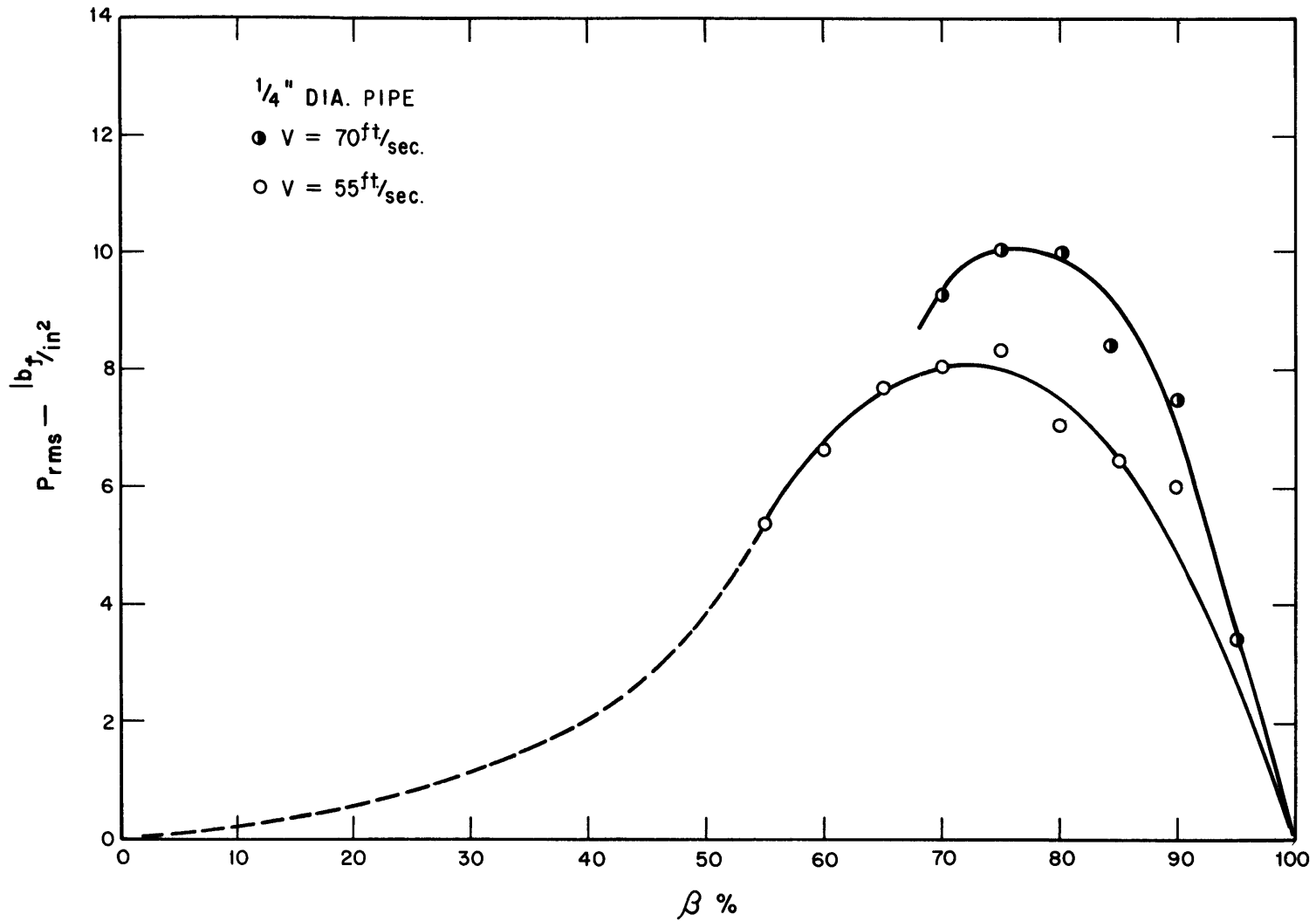


FIGURE 5.4 EFFECT OF AVERAGE FLOW VELOCITY ON RMS VALUE OF UNSTEADY MOMENTUM FLUXES

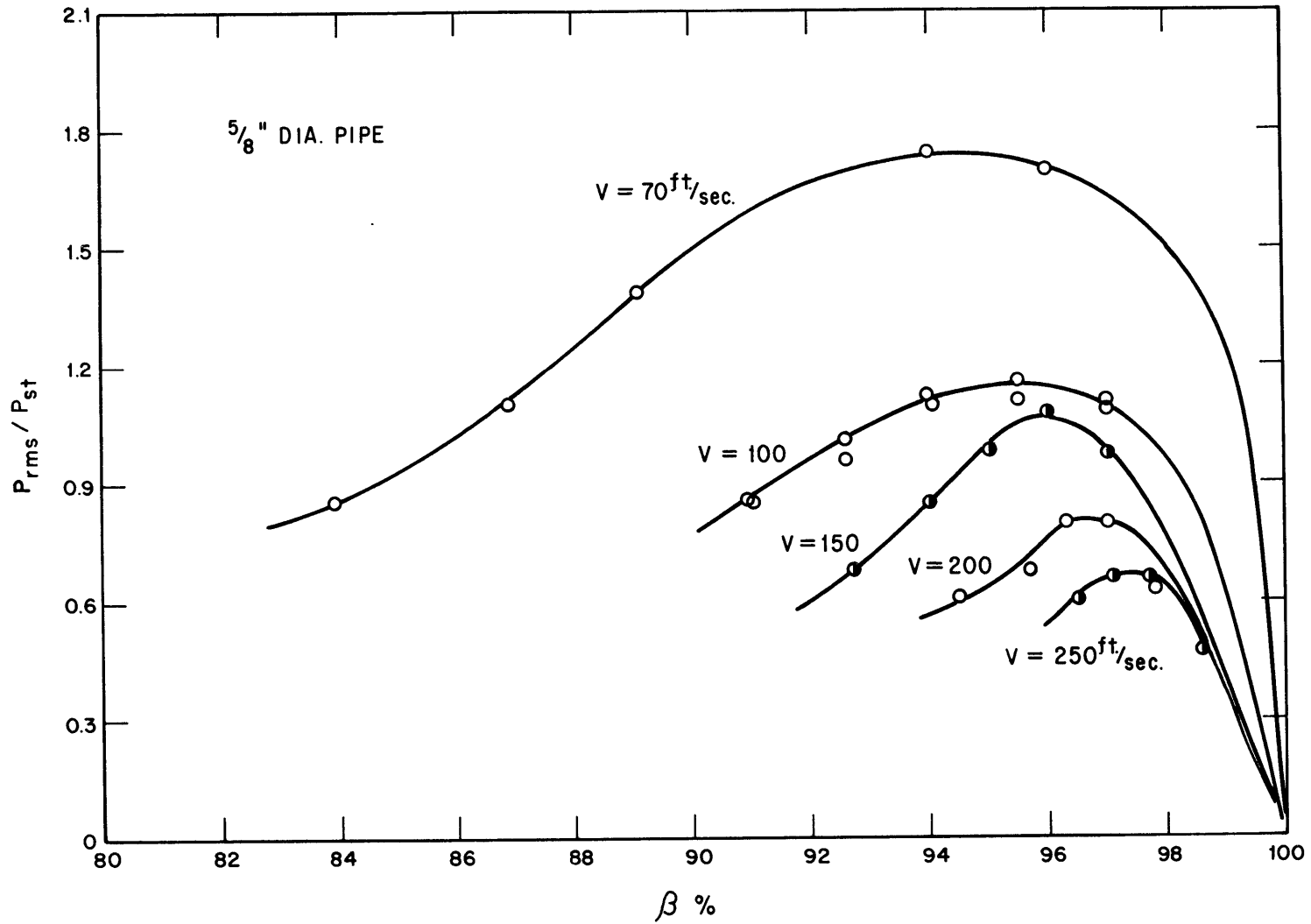


FIGURE 5.5 EFFECT OF AVERAGE FLOW VELOCITY ON THE UNSTEADINESS OF MOMENTUM FLUXES

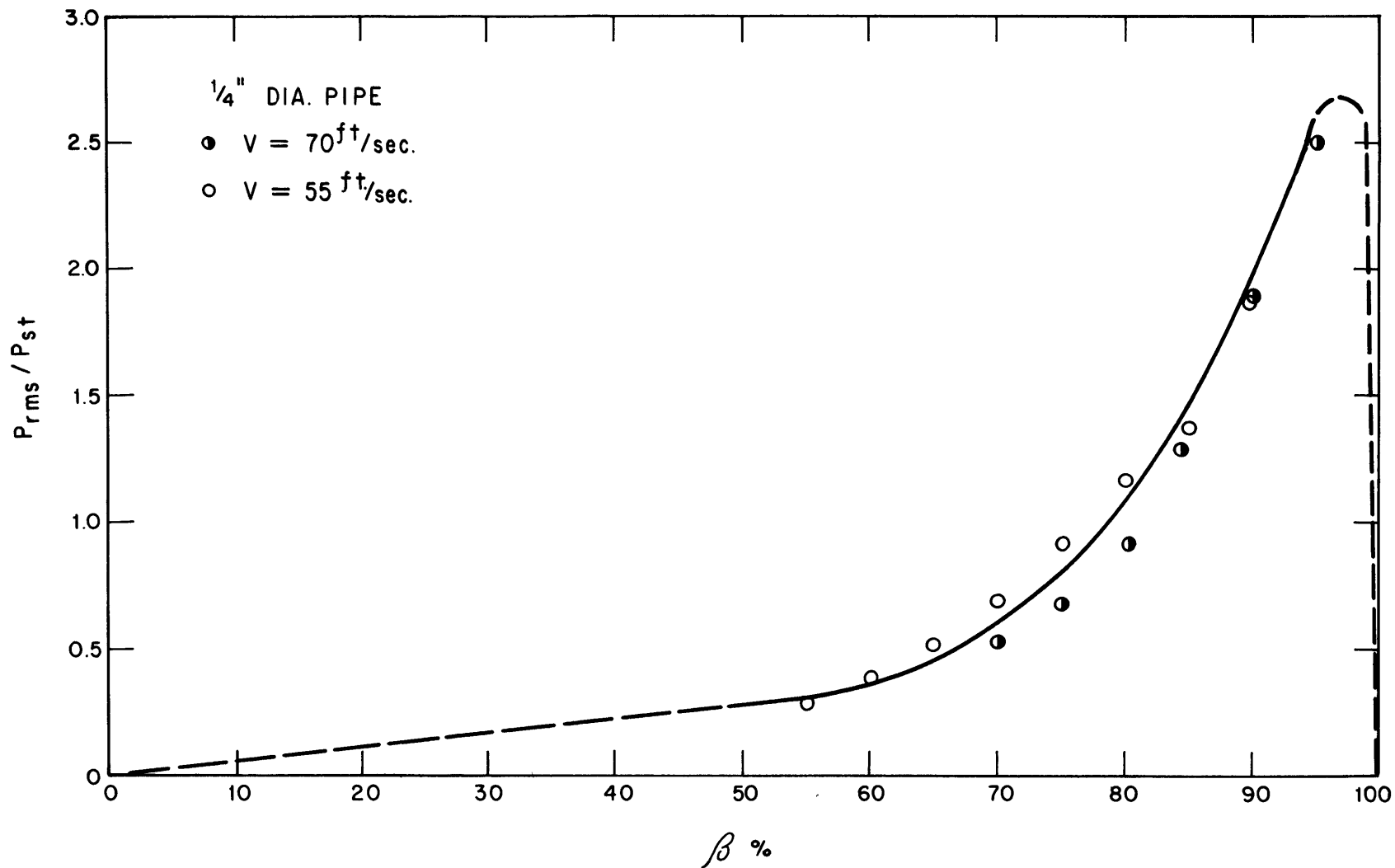


FIGURE 5.6 EFFECT OF AVERAGE FLOW VELOCITY ON THE UNSTEADINESS OF MOMENTUM FLUXES

Figs. 5.5 and 5.6. The greatest wall pressure fluctuation in the two-phase flow was reported to occur at about 90% $\beta(1)$. Although the data of these two kinds of fluctuation were obtained and expressed in different ways, one may expect that the most severe fluctuation of a two-phase flow will occur in the high β range around or above 90%.

As shown by the graphs in Figs. 5.7 and 5.8, the predominant frequency f_c increases with velocity. Within the tested range of β , f_c increases almost linearly as β goes down and the rate of increase of f_c is higher for larger values of V . In the relatively high β range, the increase of V is equivalent to the increase of gas flow rate; the decrease of β is equivalent to the increase of liquid flow rate. Both of them will increase the number of liquid slugs or waves in a two-phase flow which is the frequency of disturbance in the flow. It has been reported in references (12) and (22) that the disturbance wave frequency in a two-phase flow does increase with liquid or gas flow rate.

5.2.2 Effect of Pressure

Figures 5.9 and 5.10 show that both the steady and the unsteady components of the momentum flux increases as the system pressure increases. The ratio P_{rms}/P_{st} decreases with increasing pressure as shown in Fig. 5.11. This means that a higher system pressure tends to depress the unsteadiness of momentum fluxes. Since in a low or moderate pressure system the density of the gas phase is increased almost in proportion with pressure, the difference between the densities of the liquid and the gas phase is reduced. As a result, the density fluctuation as well as the momentum fluctuation is reduced too. This concept may be expanded to take care of the temperature effect. However, the validity of this concept needs

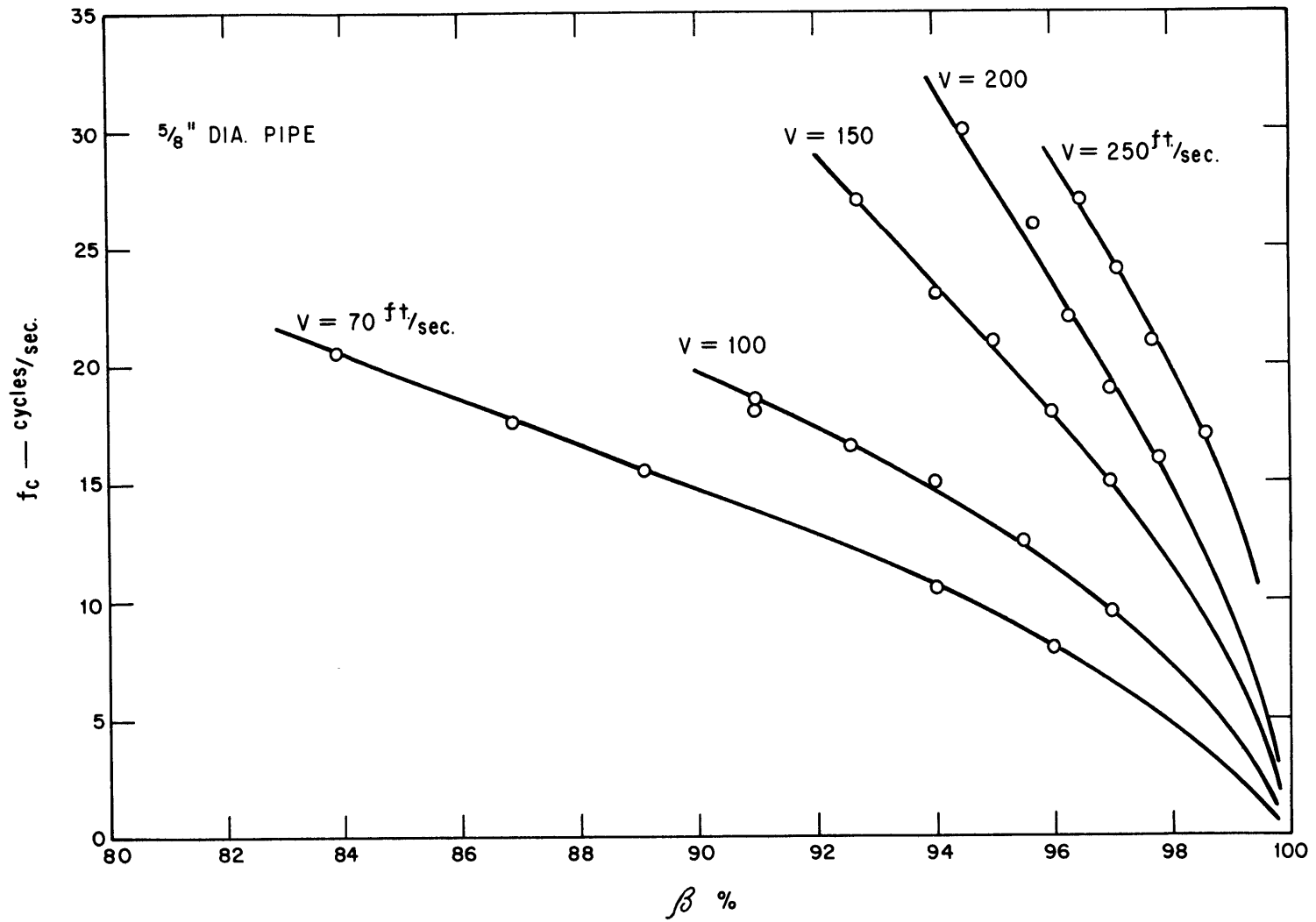


FIGURE 5.7 EFFECT OF AVERAGE FLOW VELOCITY ON PREDOMINANT FREQUENCY OF UNSTEADY MOMENTUM FLUXES

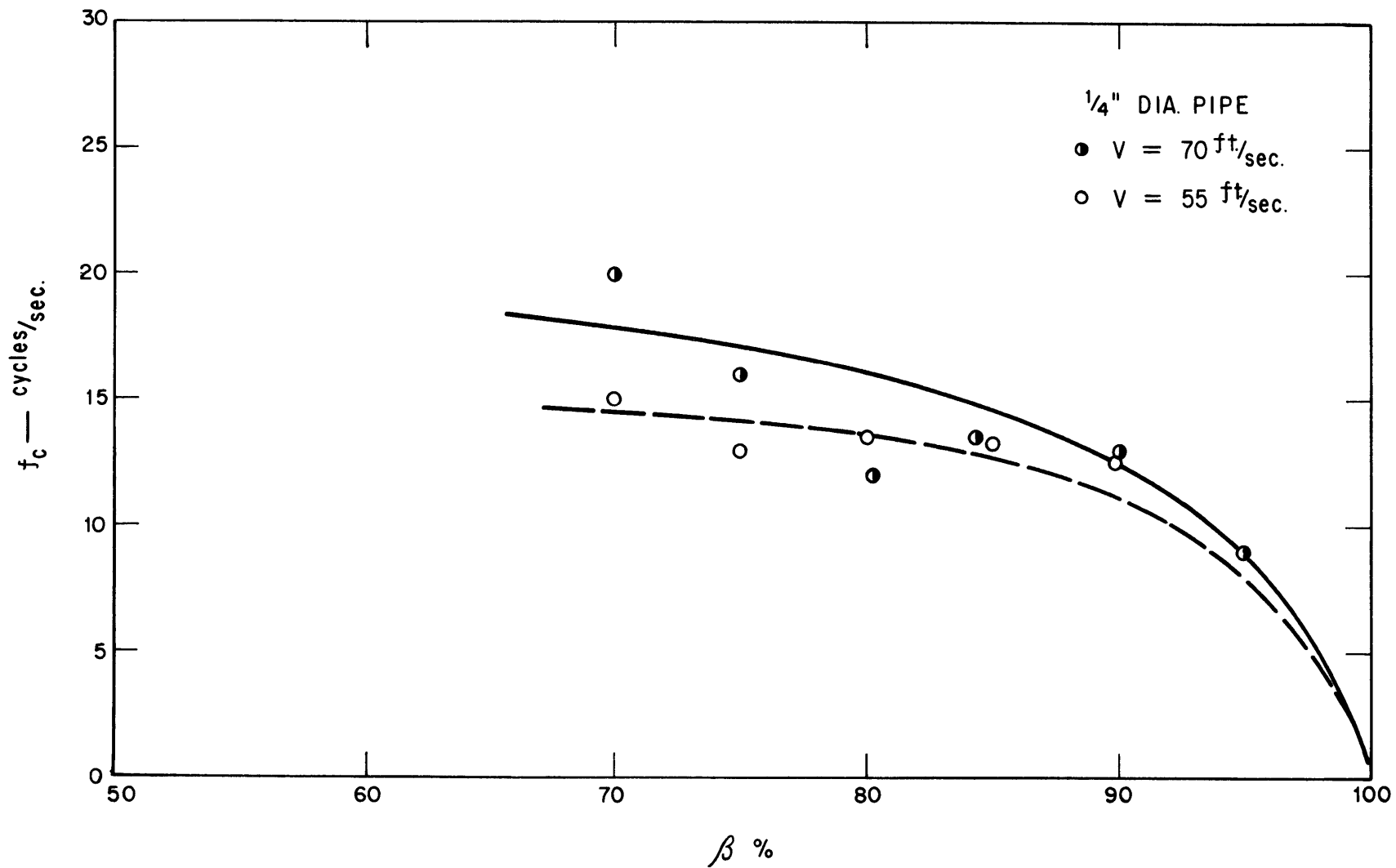


FIGURE 5.8 EFFECT OF AVERAGE FLOW VELOCITY ON PREDOMINANT FREQUENCY OF UNSTEADY MOMENTUM FLUXES

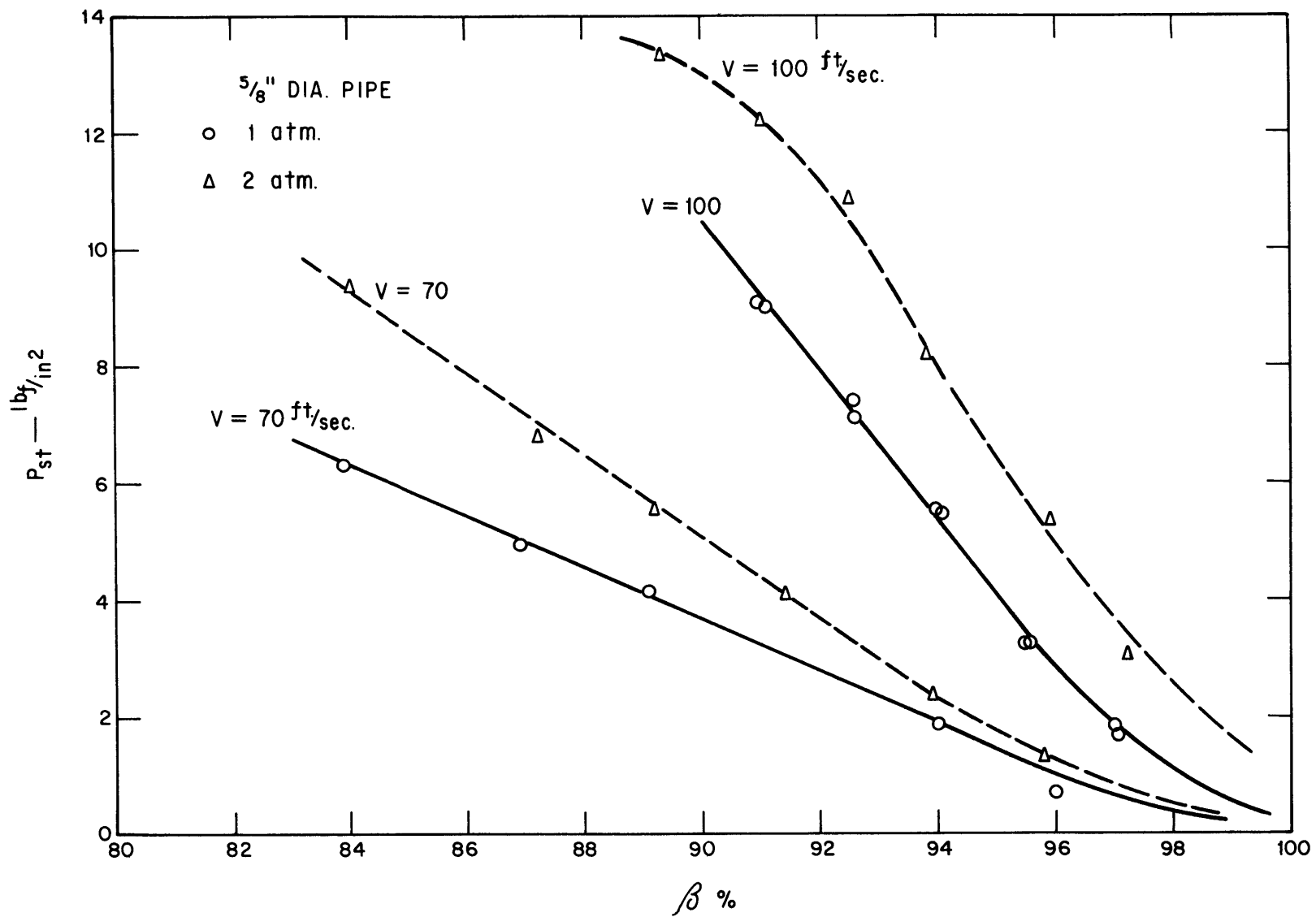


FIGURE 5.9 EFFECT OF PRESSURE ON STEADY MOMENTUM FLUXES

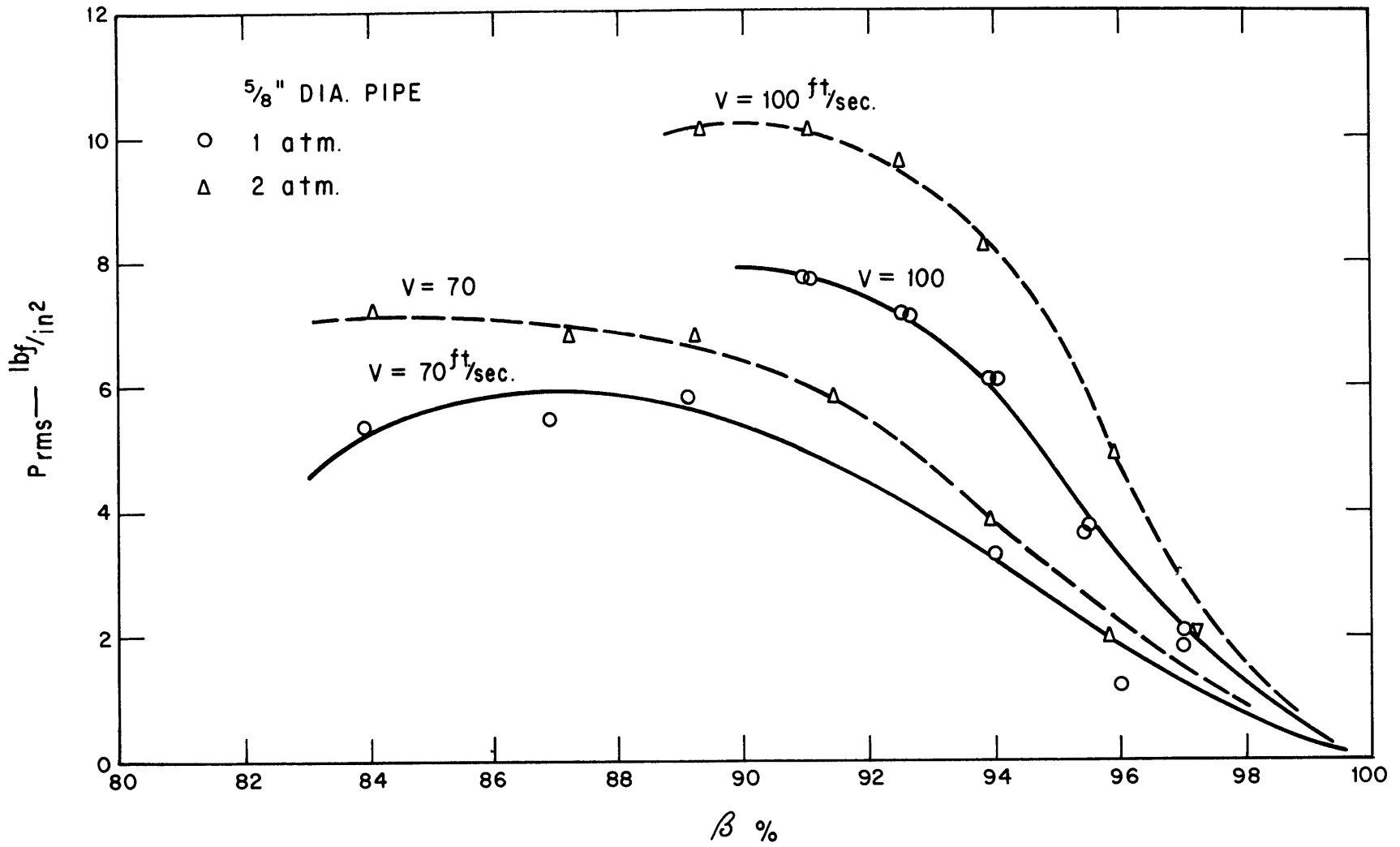


FIGURE 5.10 EFFECT OF PRESSURE ON RMS VALUE OF UNSTEADY MOMENTUM FLUXES

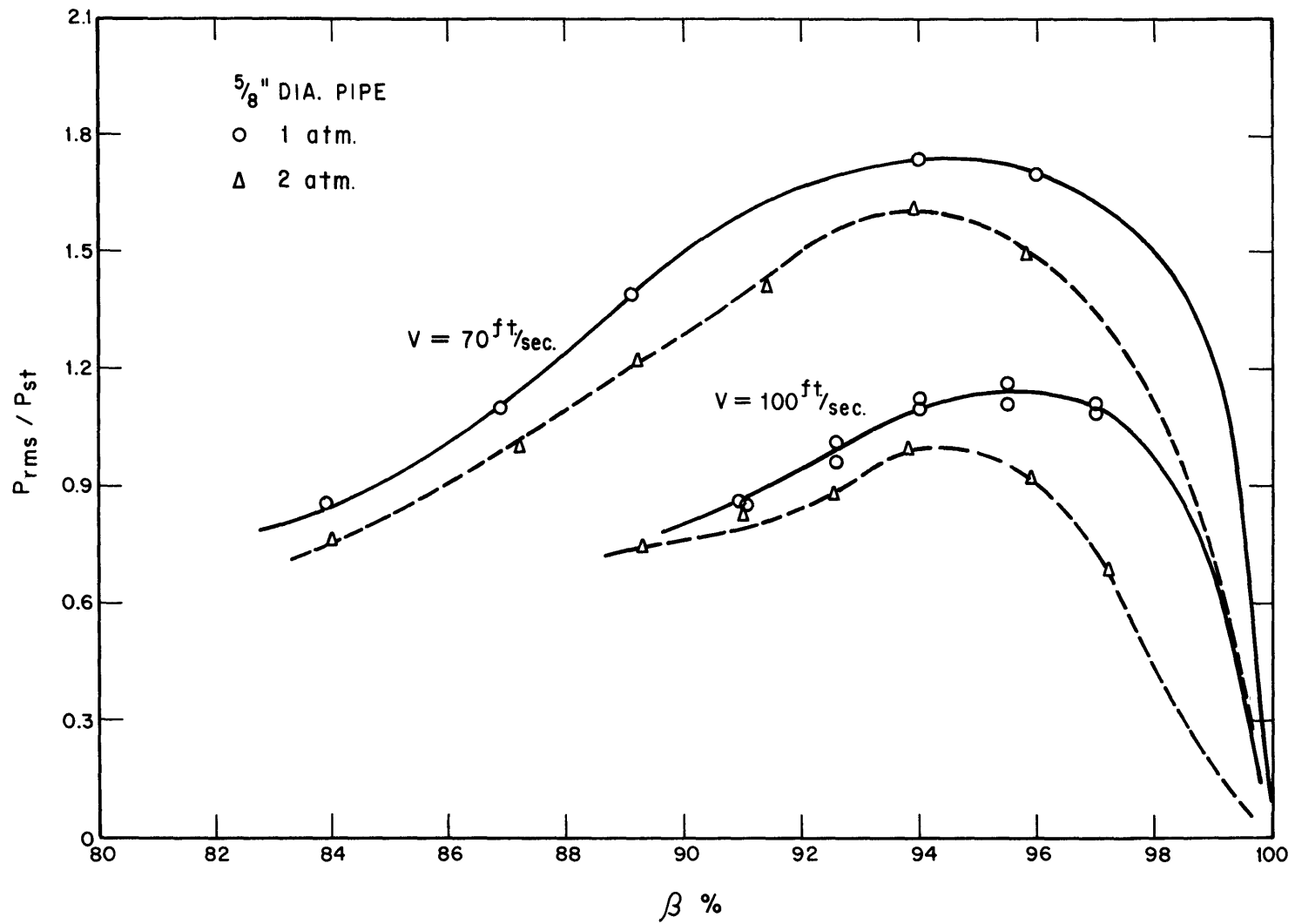


FIGURE 5.11 EFFECT OF PRESSURE ON THE UNSTEADINESS OF MOMENTUM FLUXES

to be checked.

It can be seen from Fig. 5.12 that the predominant frequency is slightly increased under higher system pressure.

5.2.3 Effect of Pipe Size

It is shown in Fig. 5.13 that the size of pipes has no effect on the steady momentum fluxes. Figure 5.14 shows that the unsteady component of momentum fluxes is larger in small pipes. Therefore, the unsteadiness of momentum fluxes in small pipes is greater than that in larger pipes as indicated in Fig. 5.15. This indicates that the gas and liquid phases are better mixed in a large pipe than in a small pipe. Probably surface tension (through the Weber number) determines the size of the dispersion.

By comparing the data obtained from tests using 5/8 inch and 1 inch diameter pipes, the values of f_c decrease slightly with increasing pipe diameter as shown in Fig. 5.16. However, for very small pipes such as 1/4 inch diameter pipe, values of f_c seem to decrease with decreasing pipe size. In either case, the size of pipes has only little effect on the predominant frequency of momentum fluxes.

5.2.4 Effect of Pipe Geometry

The steady component of momentum fluxes P_{st} is slightly affected by the pipe geometry. It can be seen from Fig. 5.17 that, for the same flow conditions, the value of P_{st} in the rectangular pipe is higher than that in the triangle pipe but lower than that in the round pipe. The value of P_{st} is the highest for flow in the annular pipe. It is likely that, for the same flow area, the value of P_{st} of a two-phase flow in the pipe of smaller hydraulic diameter is lower. The high value of P_{st} of the

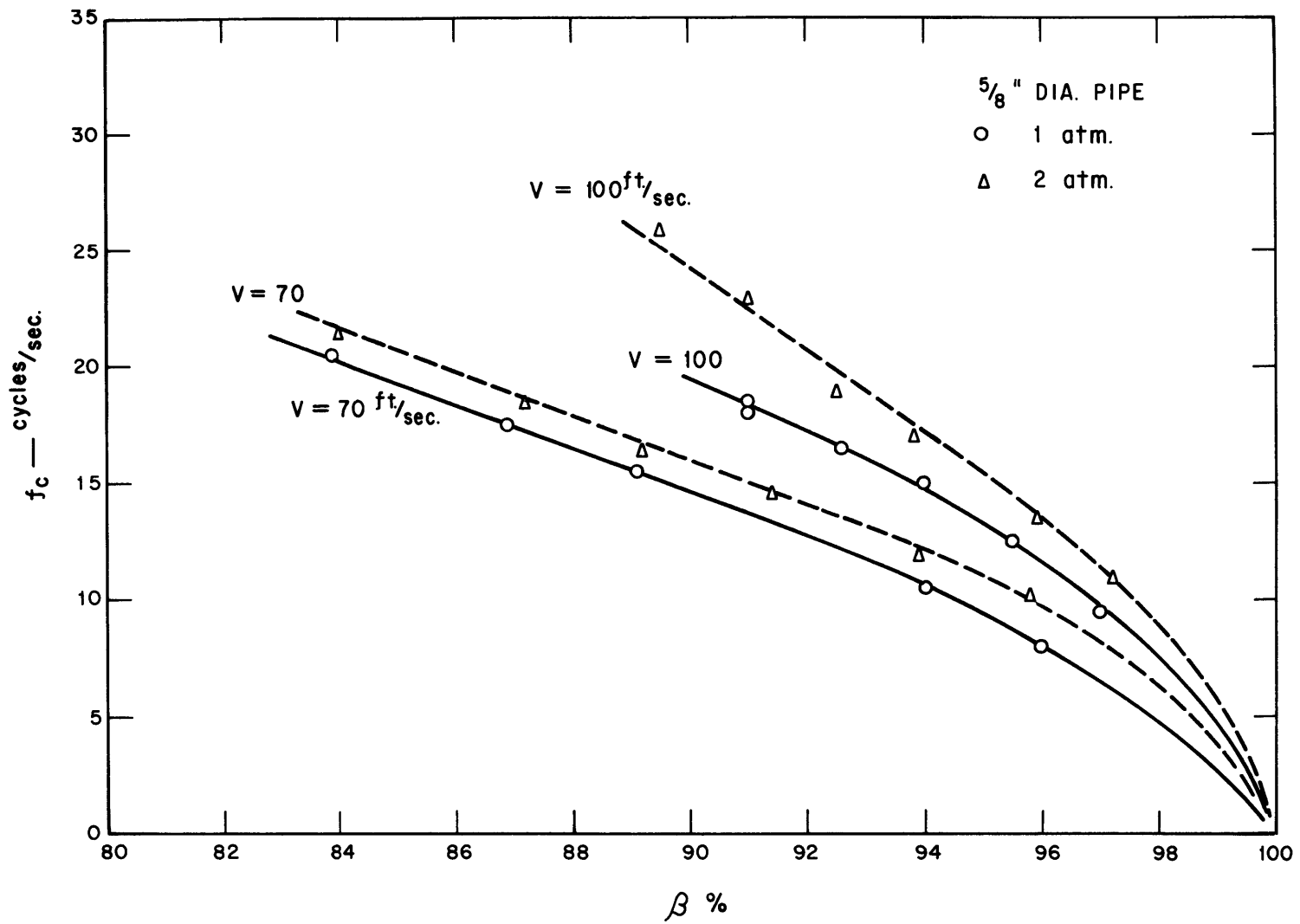


FIGURE 5.12 EFFECT OF PRESSURE ON PREDOMINANT FREQUENCY OF UNSTEADY MOMENTUM FLUXES

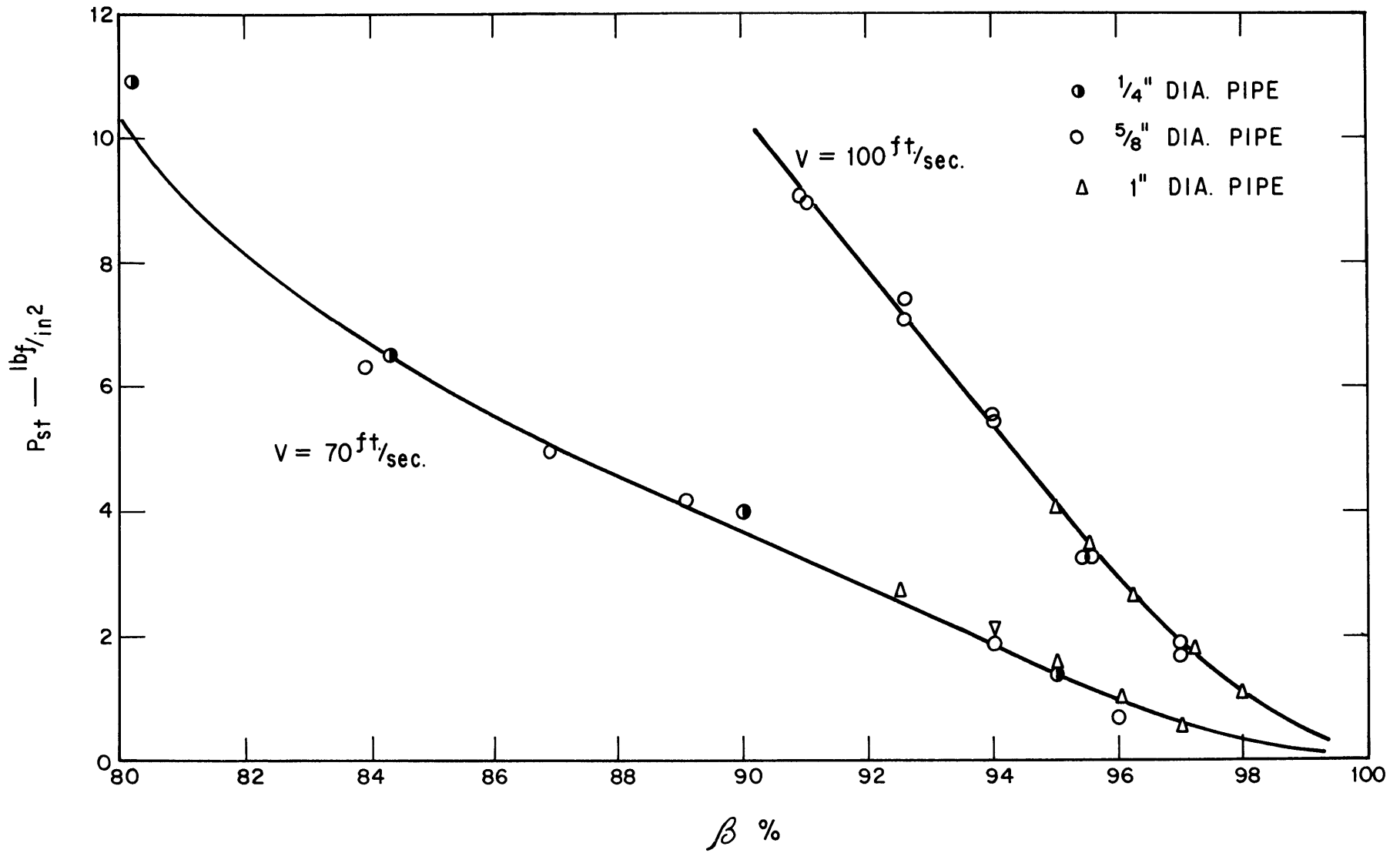


FIGURE 5.13 EFFECT OF PIPE SIZE ON STEADY MOMENTUM FLUXES

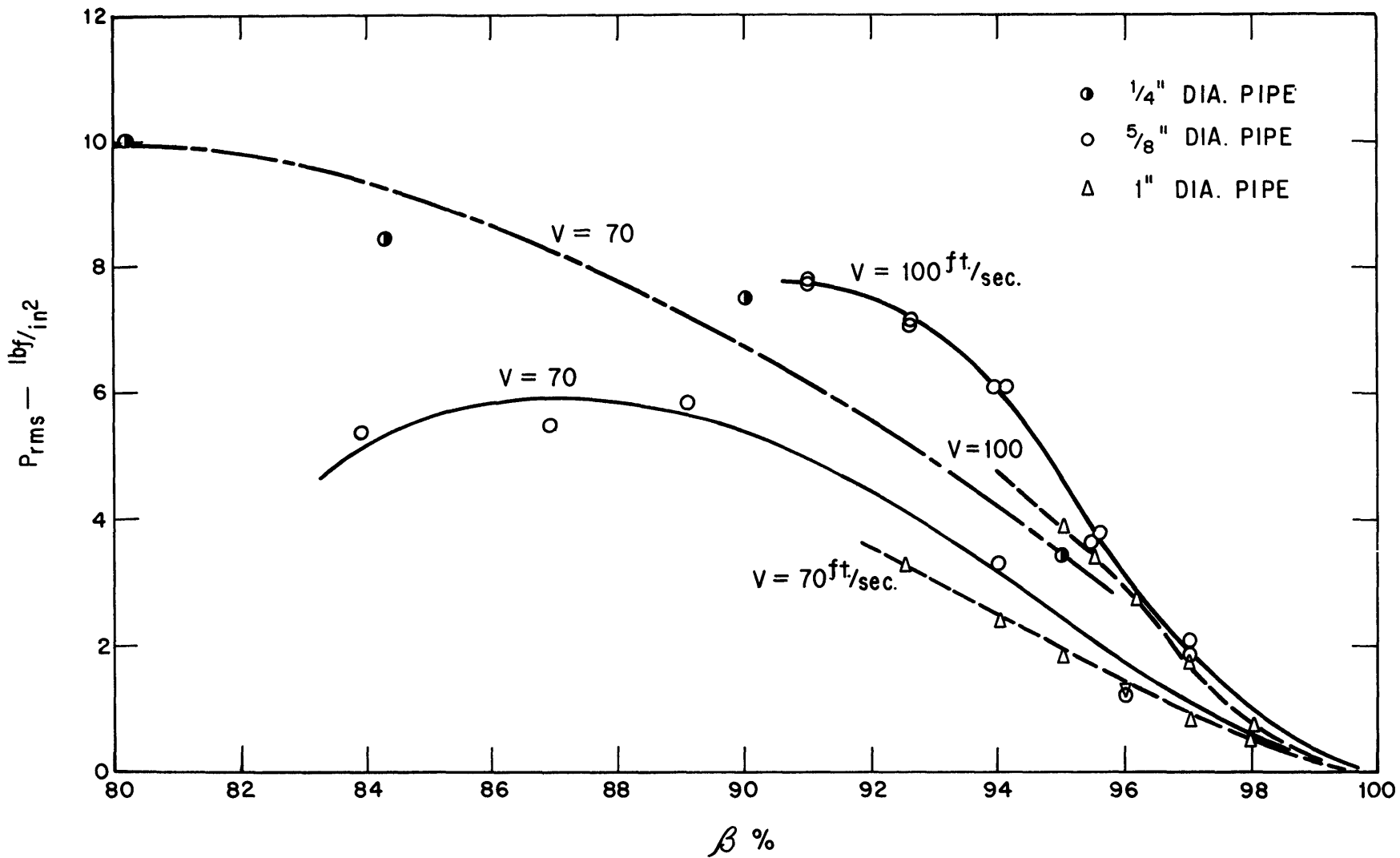


FIGURE 5.14 EFFECT OF PIPE SIZE ON RMS VALUE OF UNSTEADY MOMENTUM FLUXES

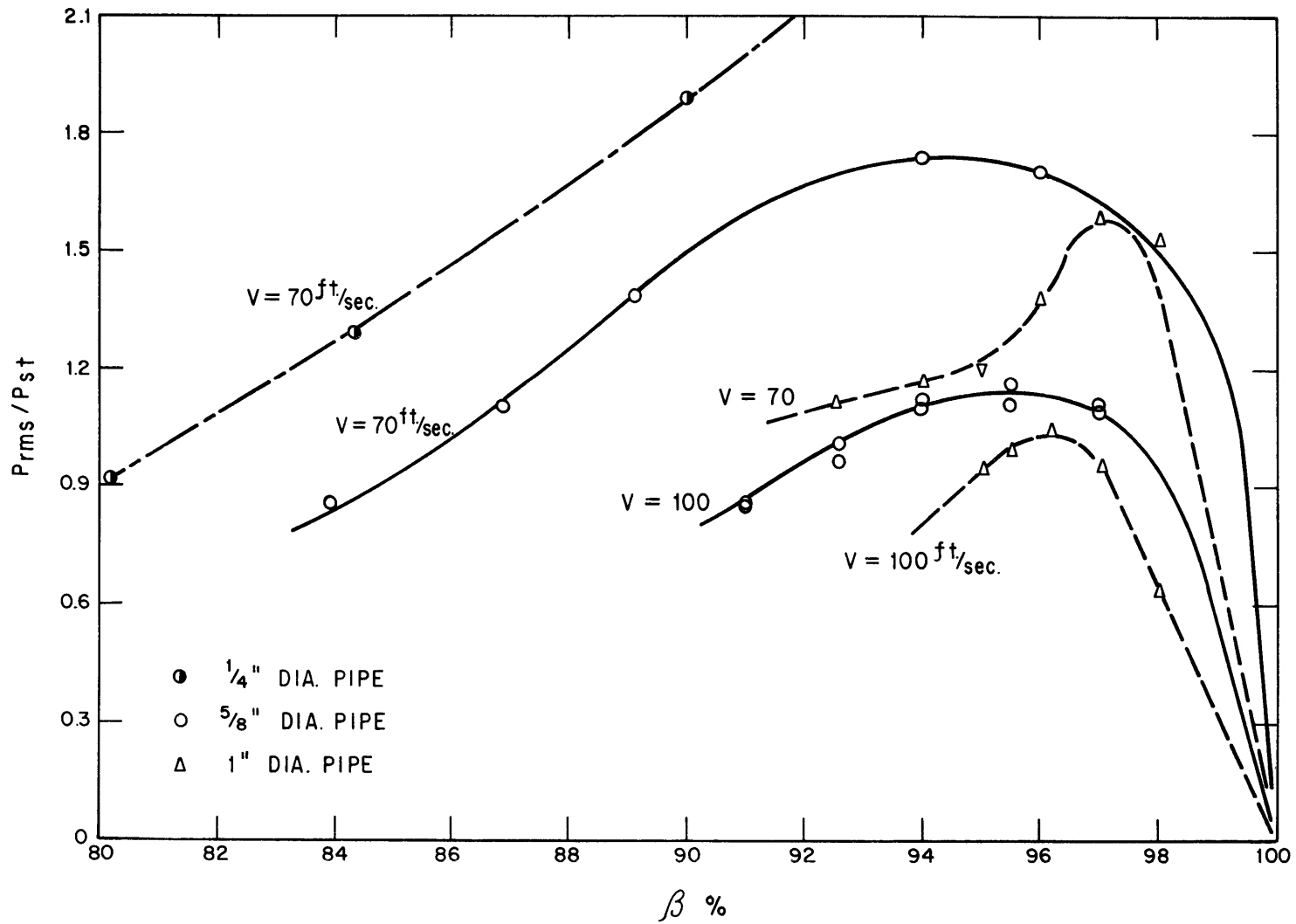


FIGURE 5.15 EFFECT OF PIPE SIZE ON THE UNSTEADINESS OF MOMENTUM FLUXES

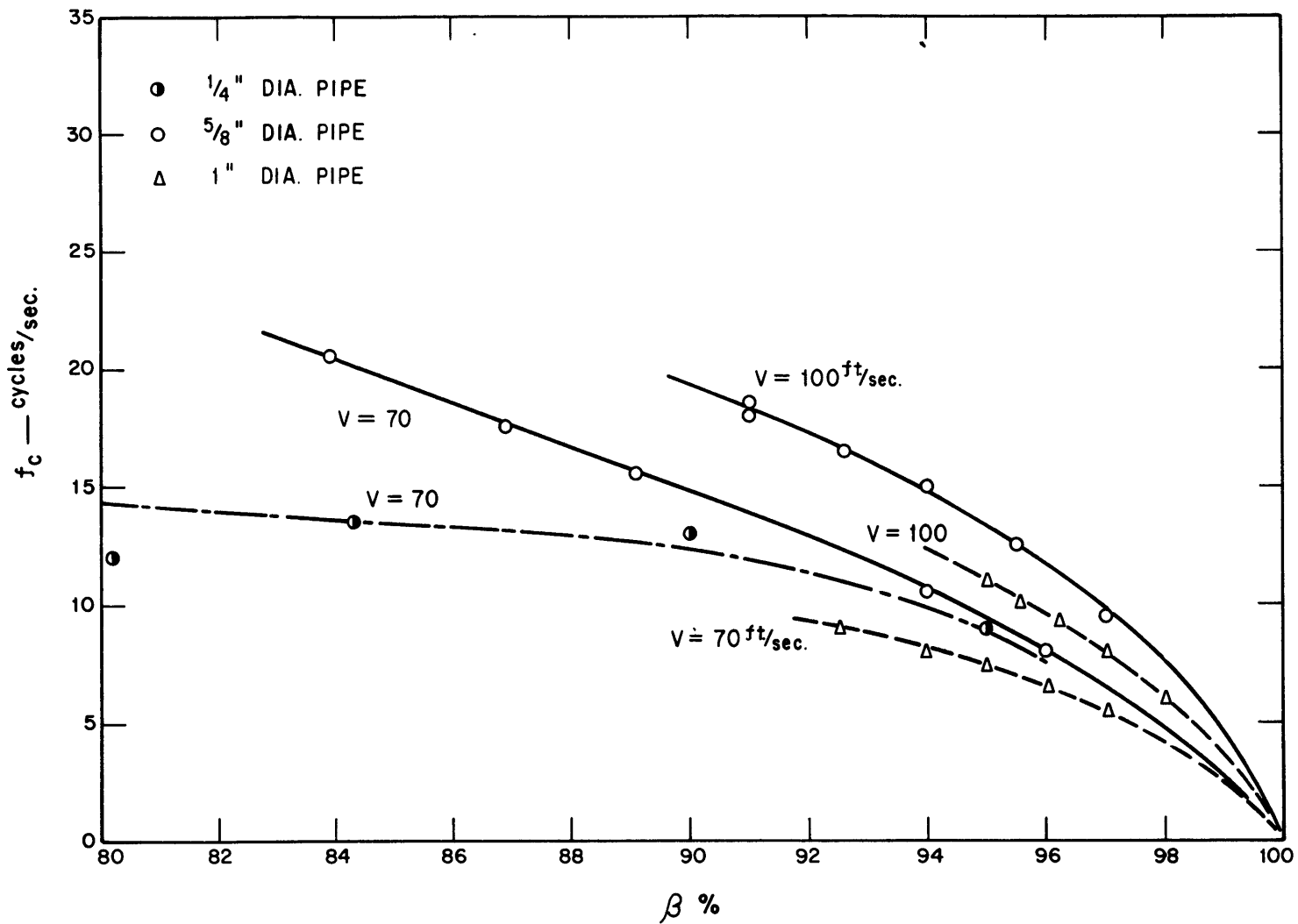


FIGURE 5.16 EFFECT OF PIPE SIZE ON PREDOMINANT FREQUENCY OF UNSTEADY MOMENTUM FLUXES

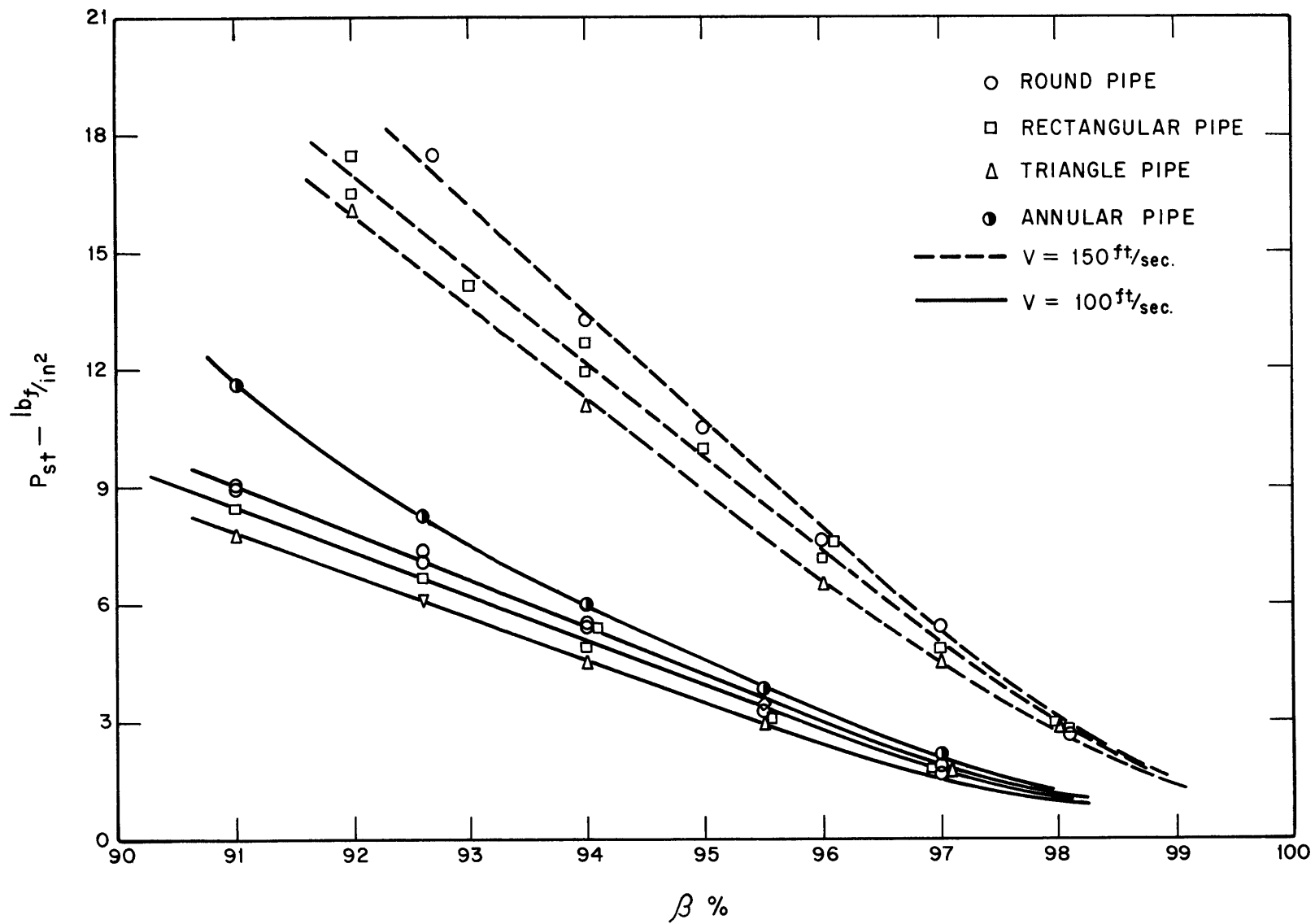


FIGURE 5.17 EFFECT OF PIPE GEOMETRY ON STEADY MOMENTUM FLUXES

flow inside the annulus may be owing to the presence of the spacers which have reduced the actual flow area in the annulus. Hence, for the same flow rate, the true velocity is higher than the computed value of V .

It can be observed from Fig. 5.18 that, for the same flow conditions; the unsteady component of momentum fluxes in a triangular pipe is smaller than that in a round or rectangular pipe but larger than that in an annular pipe. The unsteadiness P_{rms}/P_{st} is the greatest for the flow in the rectangular pipe and is the smallest in the annular pipe as shown in Fig. 5.19. Spacers for the annulus perhaps tend to break up the flow.

Figure 5.20 shows that the pipe geometry has no significant effect on the predominant frequency of the unsteady momentum fluxes.

5.3 Correlations

Efforts have been made to correlate the unsteady momentum flux data with flow parameters being used as experimental variables in all tests. For the unsteadiness of momentum fluxes, the experimental results presented in Figs. 5.5, 5.6 and 5.15 were correlated together in the form of $V^{0.8} D^{0.4} P_{rms}/P_{st}$ versus β as shown in Fig. 5.21 where V is the average flow velocity in ft/sec and D is the pipe diameter in inches. For the predominant frequency of unsteady momentum fluxes, all the experimental results were correlated together in the form of f_c/V versus β and presented in Fig. 5.22 where F_c has the unit of cycles/sec and V has the unit of ft/sec. In the range of β above 70%, f_c is proportional to V and increases with decreasing β . The frequency of pressure fluctuation in the two-phase flow has a similar trend except it has been reported to be inversely proportional to the pipe diameter (1),

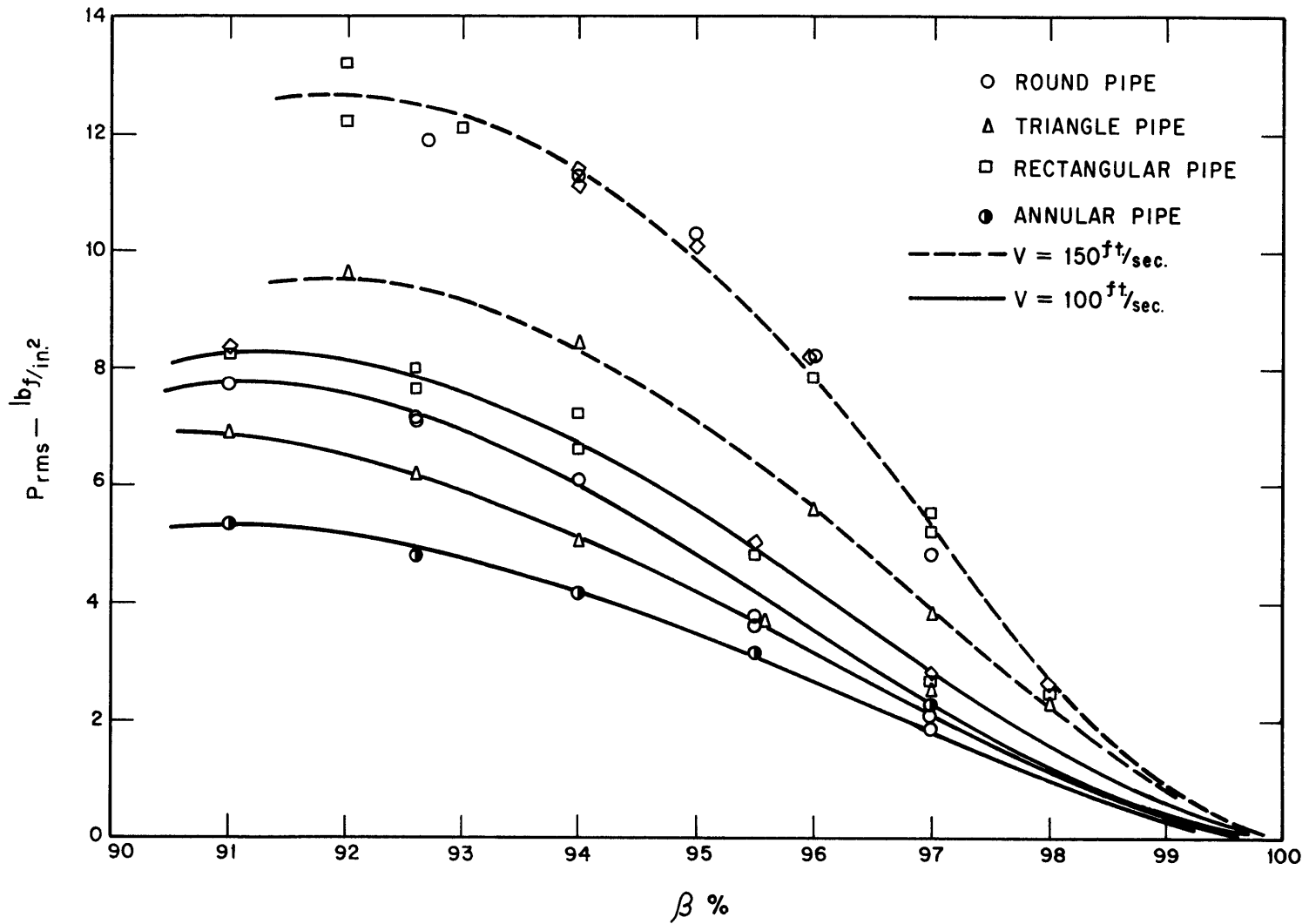


FIGURE 5.18 EFFECT OF PIPE GEOMETRY ON RMS VALUE OF UNSTEADY MOMENTUM FLUXES

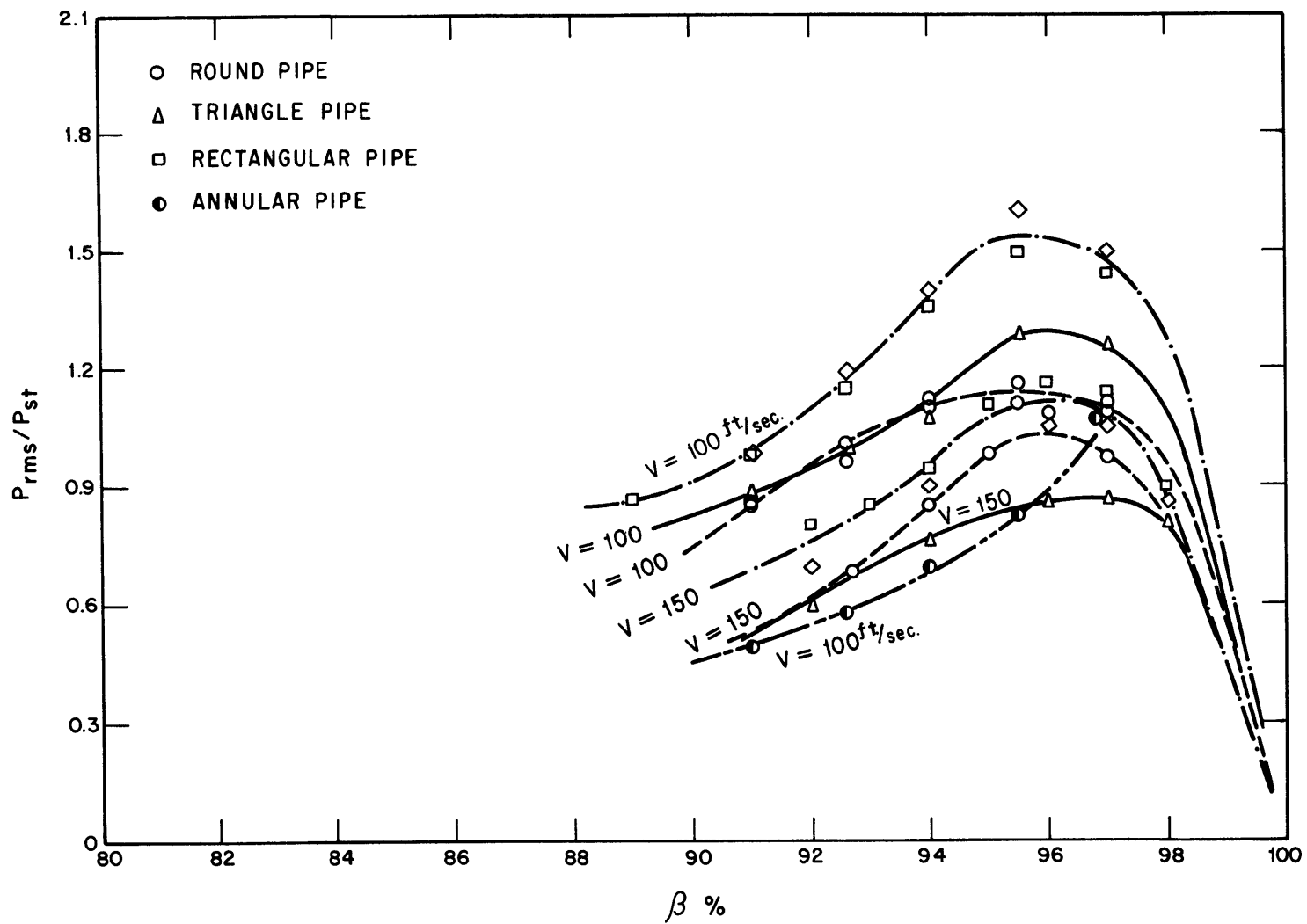


FIGURE 5.19 EFFECT OF PIPE GEOMETRY ON THE UNSTEADINESS OF MOMENTUM FLUXES

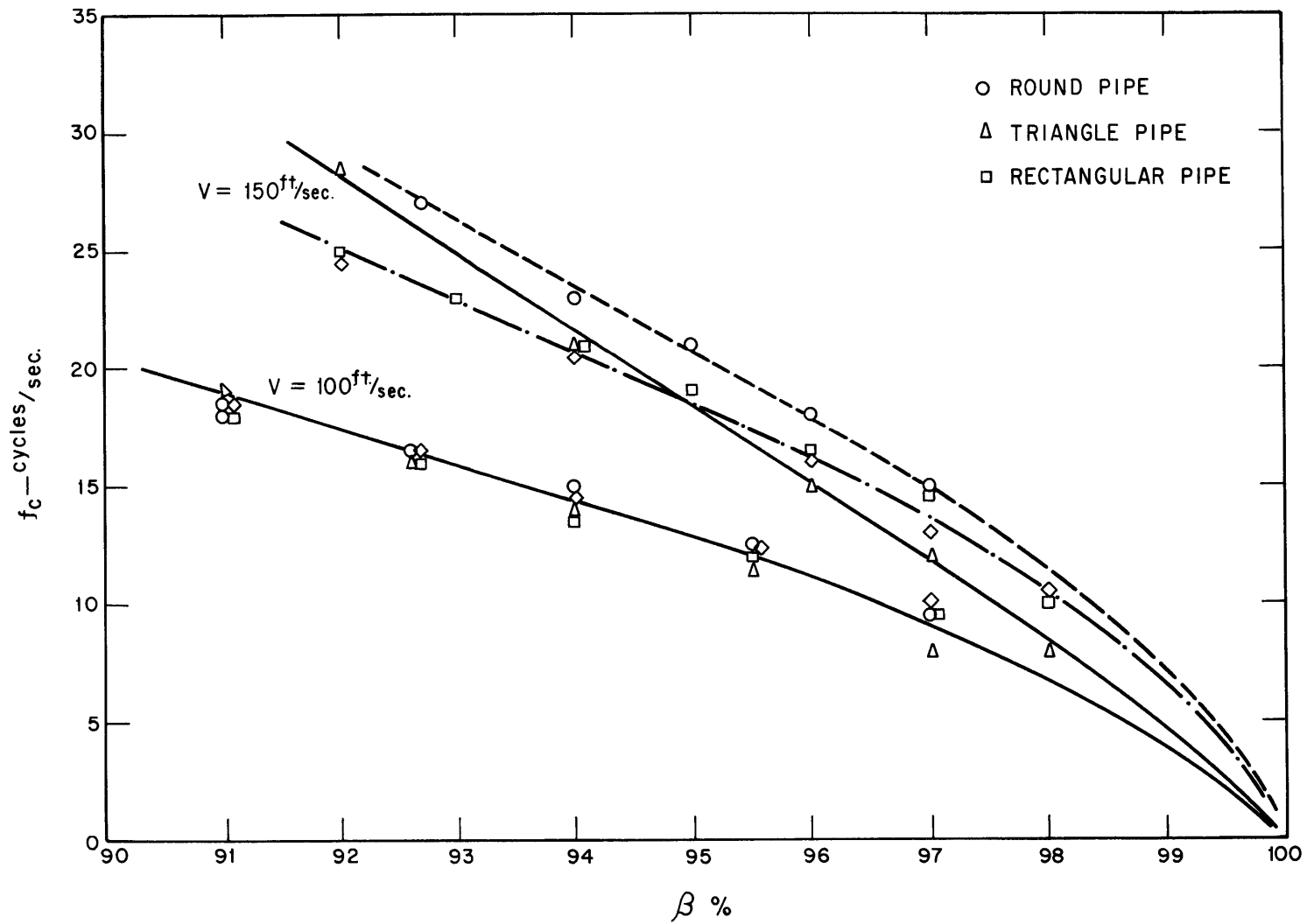


FIGURE 5.20 EFFECT OF PIPE GEOMETRY ON PREDOMINANT FREQUENCY OF UNSTEADY MOMENTUM FLUXES

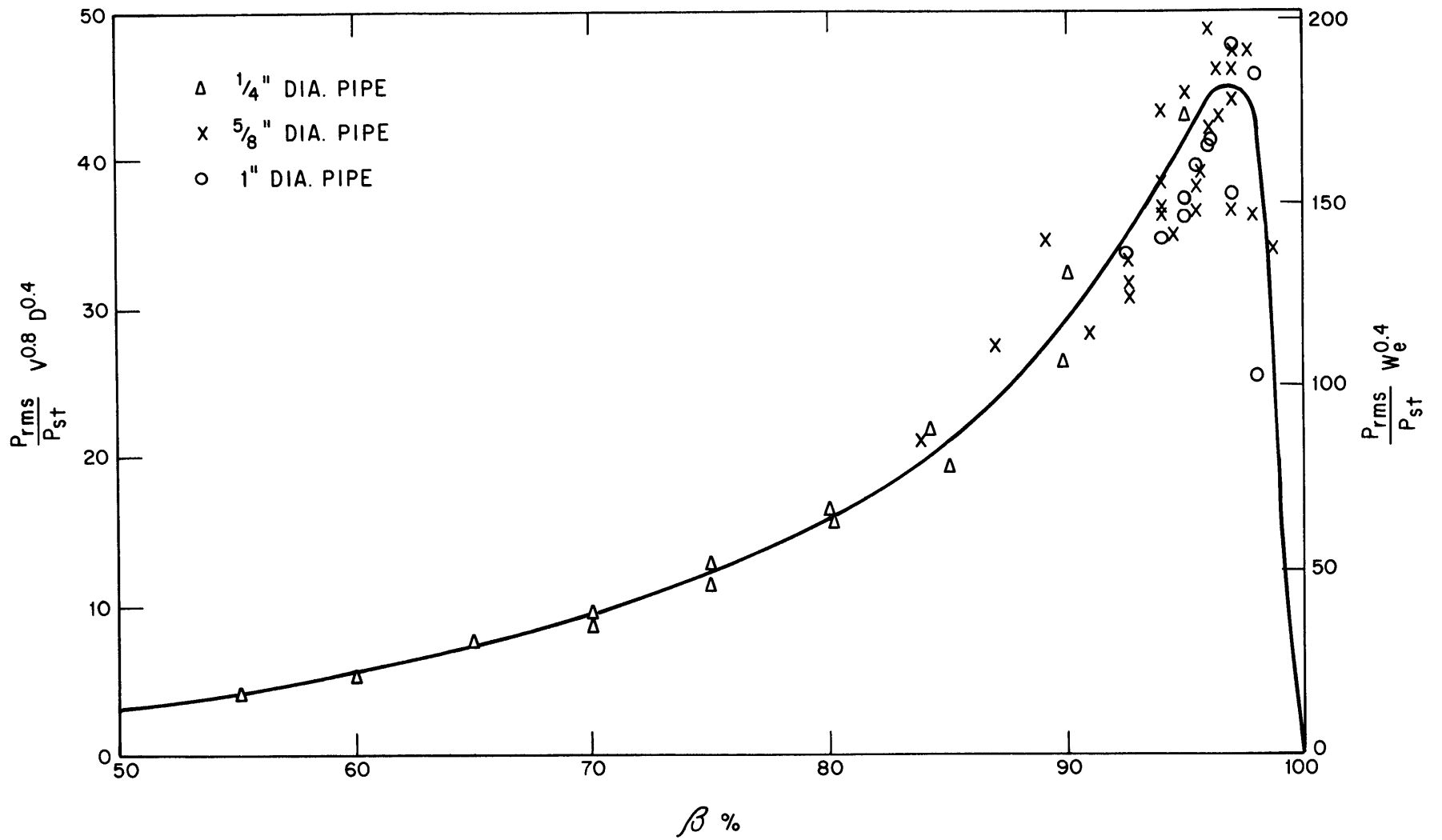


FIGURE 5.21 CORRELATION OF THE UNSTEADINESS OF MOMENTUM FLUXES

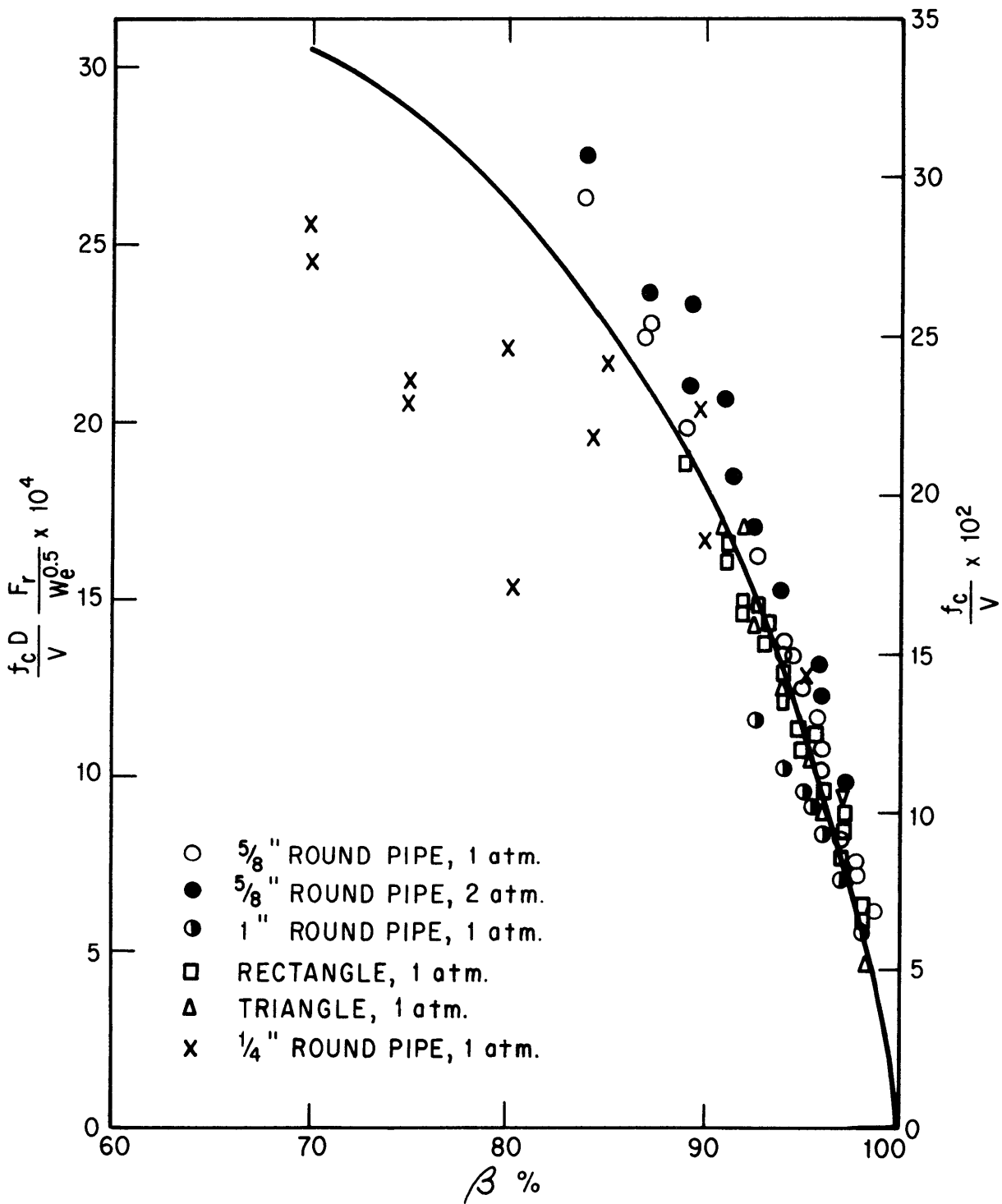


FIGURE 5.22 CORRELATION OF PREDOMINANT FREQUENCY OF UNSTEADY MOMENTUM FLUXES.

whereas f_c has been found almost independent of pipe diameter.

Since the unsteady momentum fluxes of a two-phase flow may be affected by surface tension and gravity force, it is suggested to correlate the P_{rms}/P_{st} data and the f_c data by the dimensionless groups, $W_e^{0.4} P_{rms}/P_{st}$ and $(f_c D/V) (F_r/W_e^{0.5})$ respectively. Scales in terms of these dimensionless groups are also shown in Figs. 5.21 and 5.22.

5.4 Reliability and Reproducibility

When an ergodic random process is being measured, it can be shown that the uncertainty or the percentage deviation of the measurement described in Section 4.2 is

$$\frac{\sigma_z}{E[Z]} = \frac{1}{\sqrt{\Delta f T}} \quad (5.1)$$

where $E[Z]$ is the mean value of the reading and σ_z is the standard deviation of the reading (Ref. 18, p. 58). The equivalent number of statistical degrees of freedom has the form

$$K_{eq} = 2 \Delta f T \quad (5.2)$$

With the filter band width $\Delta f = 5$ cycles/sec and the averaging time $T = 10$ sec, the percentage deviation of the measurement is 14.2% and K_{eq} is 100. Reproduced in Fig. 5.23 is a plot of statistical reliability for 80% confidence limits (Ref. 18, p. 40). For $K_{eq} = 100$, Fig. 5.23 yields the 80% confidence limits for true $E[Z]$ as

$$0.8 Z < E[Z] < 1.2 Z \quad (5.3)$$

On different days, the same measurements of the momentum fluxes in a two-phase flow were made for the 5/8 inch round pipe with $V = 100$ ft/sec, and for the rectangular pipe with $V = 100$ ft/sec and 150 ft/sec.

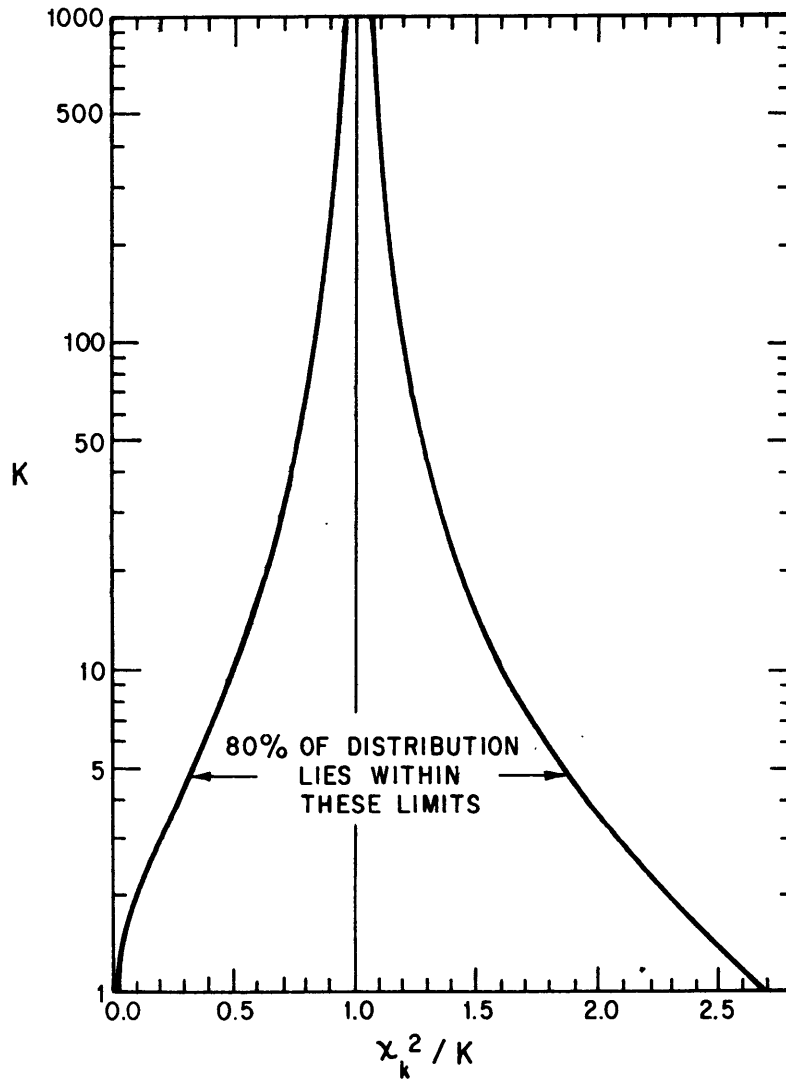


FIGURE 5.23 NUMBER OF DEGREES-OF-FREEDOM K REQUIRED TO HAVE THE CENTRAL 80% OF THE DISTRIBUTION OF χ_k^2 / K WITHIN THE INDICATED LIMITS

As shown in Figs. 5.18 and 5.19, the greatest deviation of P_{rms} and P_{rms}/P_{st} were found to be less than 10% for the rectangular pipe. Two sets of samples showing the reproducibility of spectral density curve are presented in Fig. 5.24. The pair of curves in Fig. 5.24(a) is an example of bad reproducibility while that in (b) is an example of good reproducibility.

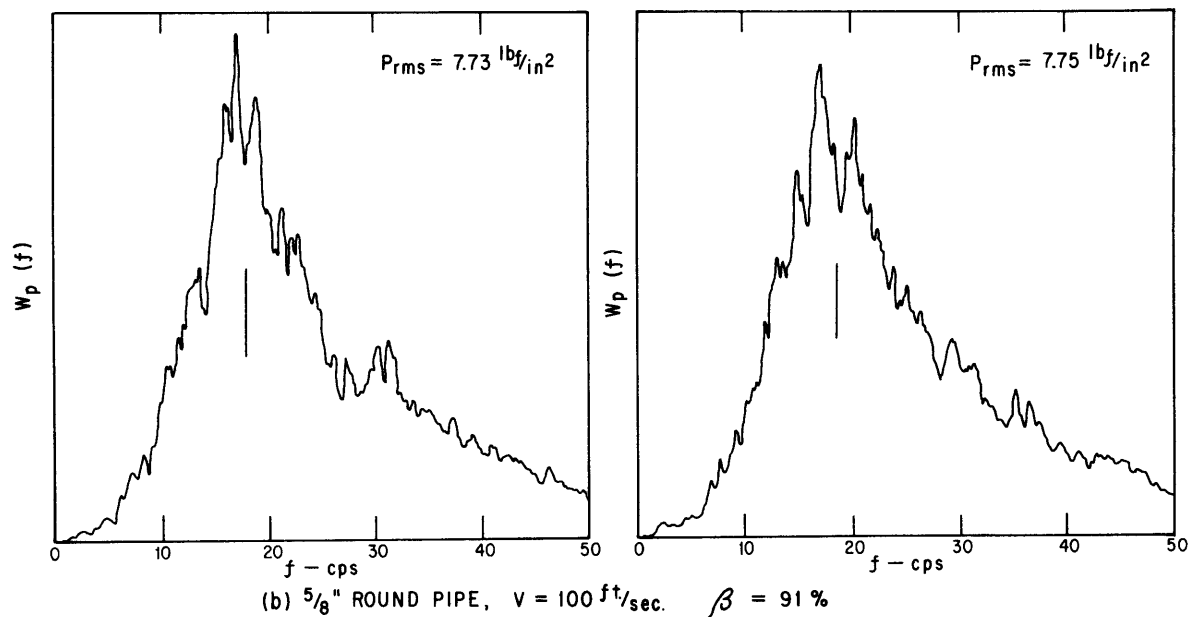
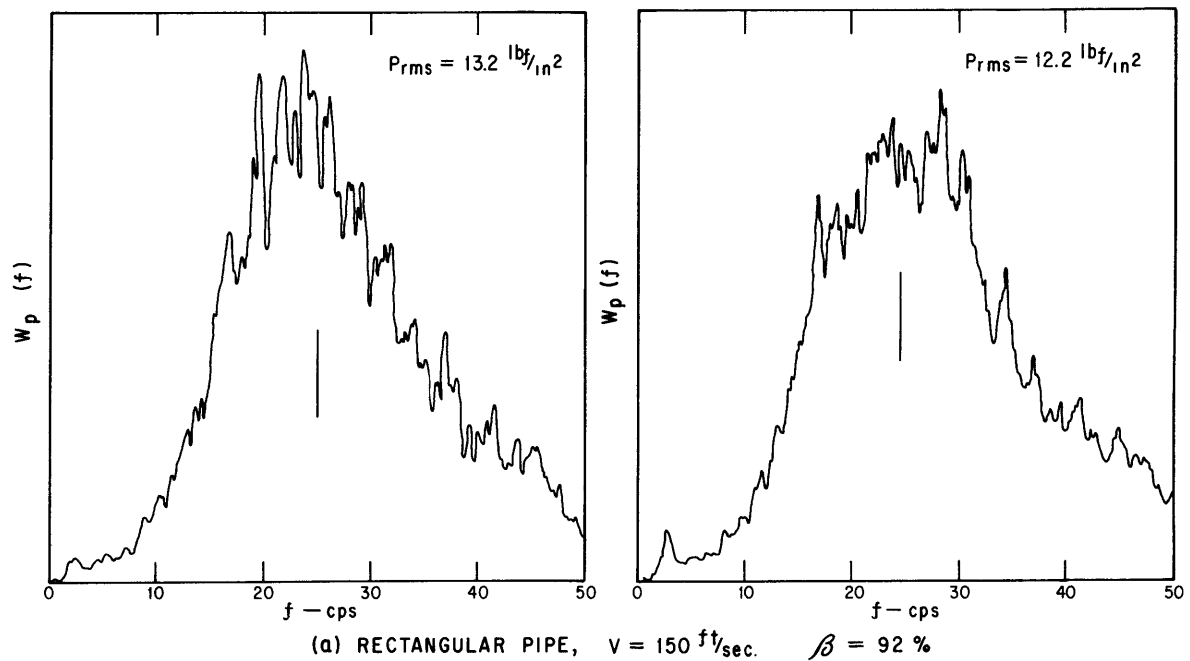


FIGURE 5.24 SAMPLES SHOWING REPRODUCIBILITY OF SPECTRAL DENSITY CURVE

6. CONSTRUCTING A SPECTRAL DENSITY CURVE FOR UNTESTED CONDITIONS

For a two-phase mixture with flow parameters close to the ranges being tested in this investigation, the rms value and the predominant frequency of the unsteady momentum fluxes in this two-phase flow can be obtained from the results presented graphically in Chapter 5. However, the power spectral density curve, which contains more information than the values of P_{rms} and f_c , are available only for the two-phase flows with exactly the same conditions as those which have been tested. The method to be presented below will permit one to construct the spectral density curve for untested conditions.

From the observation made on the spectral density curves plotted in the experiments, it has been found that most of the curves can be represented approximately by a triangle as shown in Fig. 6.1(a). If the area under the spectral density curve is denoted by A_{psd} then equation (4.6) can be written as

$$A_{psd} = \int_0^{\infty} W_p(f) df = (P_{rms})^2 \quad (6.1)$$

The area of the triangle is

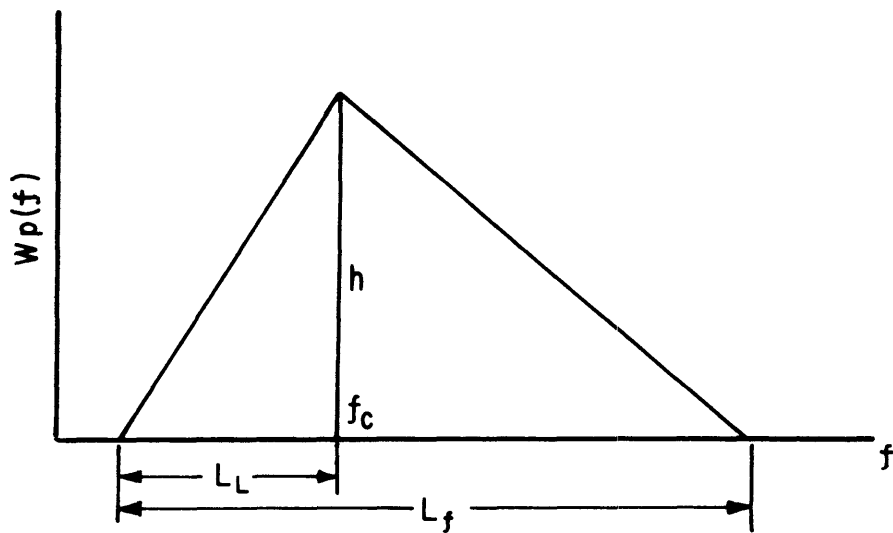
$$\frac{1}{2} h L_f = (P_{rms})^2 \quad (6.2)$$

Two empirical equations relating the value of f_c to the length and position of the triangle base line were obtained statistically from available spectral density curves. The two equations have the form

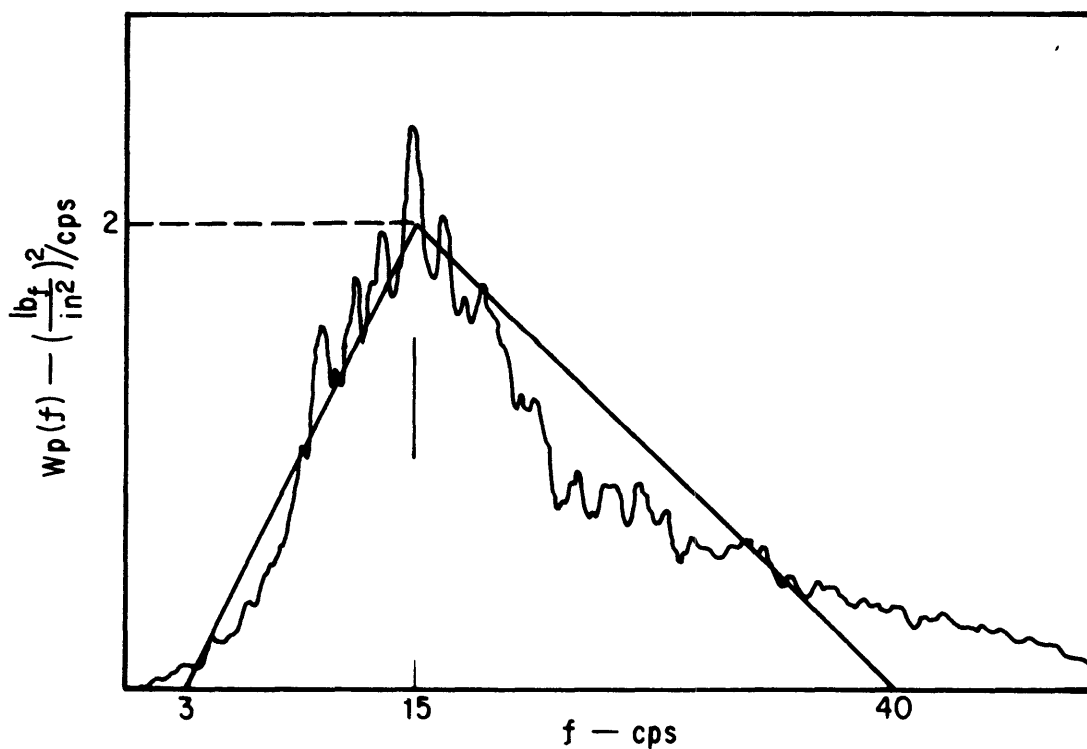
$$L_f = f_c + 22 \quad (6.3)$$

$$L_L = 0.6 f_c + 3 \quad (6.4)$$

where L_f and L_L are all in unit of cycles per second. With the aid of equations (6.2), (6.3) and (6.4) one can construct an approximate



(a) TRIANGLE SIMULATING POWER SPECTRAL DENSITY CURVE



(b) TRUE AND APPROXIMATE SPECTRAL DENSITY CURVES OF TEST NO. 74

FIGURE 6.1 CONSTRUCTION OF POWER SPECTRAL DENSITY CURVE

spectral density curve from given values of P_{rms} and f_c . For the purposes of comparison, the true and the approximate spectral density curves of Test No. 74 are shown in Fig. 6.1(b).

For a two-phase flow with $\beta < 70\%$ or a two-phase mixture passing through an annular pipe with spacers inside, the spectral density curves are close to the band-limited white noise spectrum. In these cases a rectangle can be used to simulate the spectral density curves for untested conditions.

In general it is possible to estimate the values of P_{rms} and f_c of the unsteady momentum fluxes in any two-phase flow from the limited results of this investigation then to construct the spectral density curve except in the case of relatively low volumetric quality or extremely high system pressure. For a two-phase flow with low values of β , the unsteady component of momentum fluxes is not important as shown in Fig. 5.21. For a two-phase flow under very high pressure, the density difference between the liquid and the gas phases is small and the unsteady momentum fluxes are also unimportant as explained in Chapter 2. The general procedure of constructing a power spectral density curve for untested conditions is suggested as the following:

(1) To estimate the steady component of momentum fluxes either from reference (13) or by the simplified relation

$$P_{st} = \rho_f (1 - \beta) V^2 \quad (6.5)$$

for low system pressure and by

$$P_{st} = [\rho_f (1 - \beta) + \rho_g \beta] V^2 \quad (6.6)$$

for high system pressure. In the case of low system pressure the steady momentum flux estimated by the homogeneous model is often higher than

its true value because most contributions of the momentum flux come from the liquid phase whose velocity is, in general, lower than the average velocity V of the two-phase flow. In equation (6.5) although the term $\rho_f(1 - \beta)$ is somewhat smaller than the homogeneous density, the value of P_{st} will not be underestimated in most cases.

(2) For given values of V , D and β , pick P_{rms}/P_{st} from Fig. 5.21 and designate this value as $(P_{rms}/P_{st})_0$.

(3) The unsteadiness of the momentum flux being concerned is

$$\frac{P_{rms}}{P_{st}} = \left(\frac{P_{rms}}{P_{st}} \right)_0 (0.85)^{\log_2 \left(\frac{\rho_g}{\rho_a} \right)} \quad (6.7)$$

where ρ_g is the density of the gas phase in the two-phase flow to be studied and ρ_a is the density of air under standard conditions. This adjustment of the value of unsteadiness is made on the grounds that the increase of gas density will reduce the difference between the densities of liquid and the gas phases and depress the fluctuations of momentum fluxes as discussed in Chapter 2. In Fig. 5.11 the average reduction rate of P_{rms}/P_{st} by doubling the system pressure is about 15%. Since no other information is available, it is suggested to use the result in Fig. 5.11 as a rule of thumb, i.e., when the density of the gas phase is doubled the unsteadiness is reduced by 15%. This rule can take care of the pressure change as well as the temperature change of the two-phase flow system.

(4) Combining equation (6.5) or (6.6) with equation (6.7), the value of P_{rms} can be determined.

(5) For given values of V and β obtain f_c from Fig. 5.22.

(6) Construct the desired power spectral density curve by applying equations (6.2), (6.3) and (6.4).

7. APPLICATION SAMPLES

Two sample problems to be presented are the two-phase flow induced vibrations of a U-tube in a steam generator and a pipe simply supported at both ends with two phases flowing within. Aimed at demonstrating the usefulness of the unsteady momentum flux information, both the models and the treatment of these two problems are much simplified. Nevertheless, these examples will provide insight into the effect of unsteady momentum fluxes on two-phase flow systems and give engineering estimations of the effect.

In the analysis of these problems the major assumption is that both the U-tube and the simply supported pipe are treated as equivalent mass spring systems of single degree of freedom, since an excessive amount of energy is required to cause a mechanical system to vibrate with significant amplitude at a mode higher than the fundamental one. It has been found in the experiment of flow induced vibration of cylinders in parallel flow that the first mode is dominant (5,6).

Numerical examples of these two problems are given in Appendix D.

7.1 U-Tube Example

The U-tube model is shown in Fig. 7.1. Being treated as a vibrating system of single degree of freedom, its equation of motion is

$$M_e \ddot{x} + C \dot{x} + kx = F \quad (7.1)$$

where k is the stiffness of a cantilever beam

$$k = \frac{3EI_Y}{L^3} \quad (7.2)$$

and M_e is the equivalent mass of the U-tube and equal to 24% of the mass of the two long pipes (see Appendix E) plus the mass of the short pipe.

The transfer function of this system takes the form

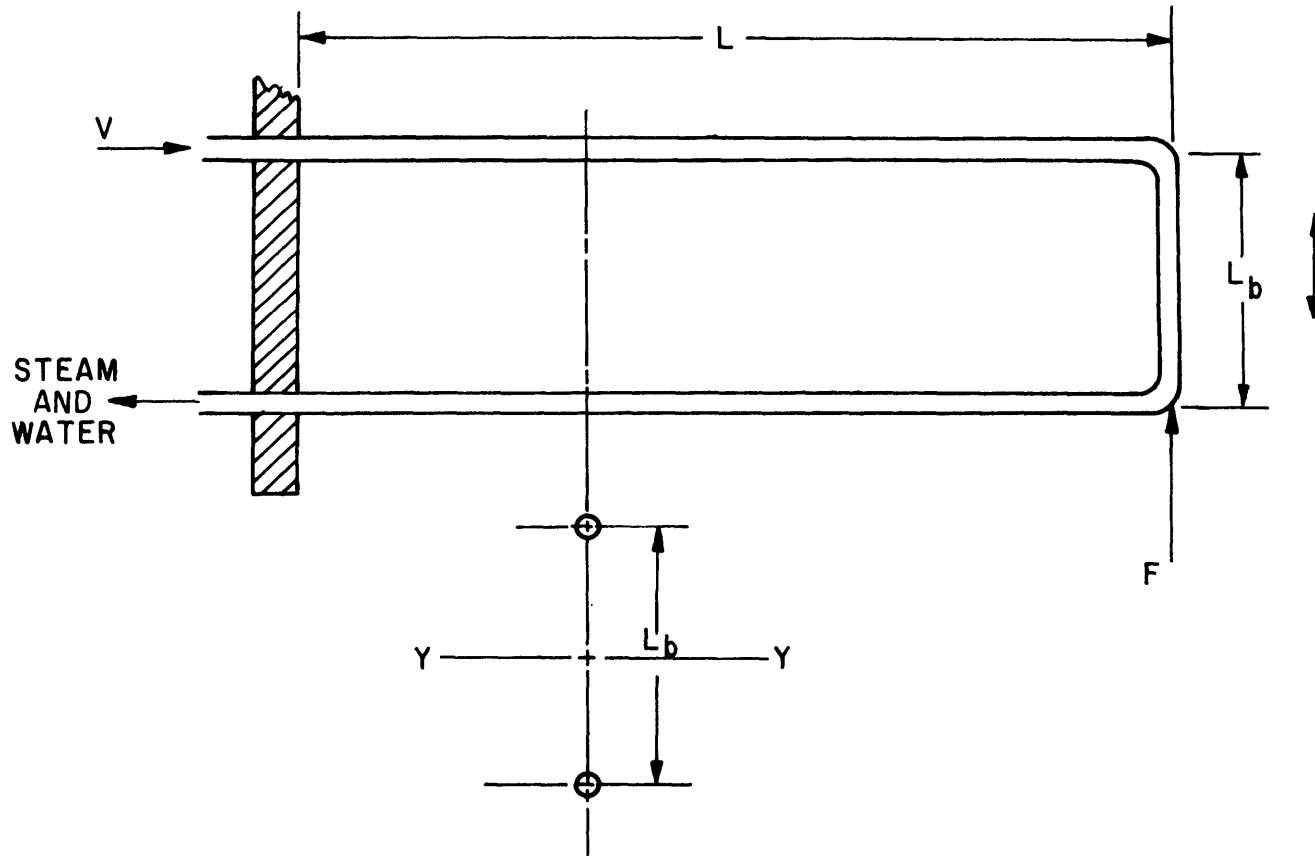


FIGURE 7.1 U-TUBE MODEL

$$H(\omega) = \frac{1}{k - M_e \omega^2 + i C \omega} \quad (7.3)$$

It can be shown that the relations between the spectral density of the excitation $F(t)$ and the spectral density of the response $x(t)$ has the following form (reference 17, p. 69-71)

$$S_x(\omega) = |H(\omega)|^2 S_F(\omega) \quad (7.4)$$

Consequently, the power density spectrum of the response is

$$S_x(\omega) = \frac{S_F(\omega)}{(k - M_e \omega^2)^2 + C^2 \omega^2} \quad (7.5)$$

In terms of experimental spectral density,

$$W_x(f) = \frac{W_F(f)}{[k - M_e (2\pi f)^2]^2 + C^2 (2\pi f)^2} \quad (7.6)$$

Now, the remaining problem is to find the spectral density of the transverse force F . Referring to the model in Fig. 7.1, at time t , if the momentum flux in the two-phase flow at the upper bend is $P(t)$ then that at the lower bend is $P(t + \tau_o)$, where τ_o is the time interval for the flow to travel through the distance L_b and can be expressed as

$$\tau_o = \frac{L_b}{V} \quad (7.7)$$

Therefore, the total vertical force acting on the U-tube is

$$F(t) = A_t [P(t) - P(t + \tau_o)] \quad (7.8)$$

where A_t is the flow area inside the U-tube. The auto-correlation function of F is

$$R_F(\tau) = E[F(t) F(t + \tau)] \quad (7.9)$$

Substitute equation (7.8) into (7.9) and consider the limiting case of $\tau = 0$.

$$R_F(0) = A_t^2 [2R_p(0) - 2R_p(\tau_0)] \quad (7.10)$$

where

$$R_p(0) = \int_{-\infty}^{\infty} S_p(\omega) d\omega \quad (7.11)$$

$$R_p(\tau_0) = \int_{-\infty}^{\infty} S_p(\omega) e^{i\omega\tau_0} d\omega \quad (7.12)$$

as defined in Chapter 4. Therefore, equation (7.10) becomes

$$\int_{-\infty}^{\infty} S_F(\omega) d\omega = 2A_t^2 \int_{-\infty}^{\infty} (1 - e^{i\omega\tau_0}) S_p(\omega) d\omega \quad (7.13)$$

Since

$$|1 - e^{i\omega\tau_0}| = \sqrt{2} (1 - \cos \omega\tau_0)^{1/2} \quad (7.14)$$

equation (7.13) can be expressed in the form

$$\int_{-\infty}^{\infty} S_F(\omega) d\omega = 2\sqrt{2} A_t^2 \int_{-\infty}^{\infty} (1 - \cos \omega\tau_0)^{1/2} S_p(\omega) d\omega \quad (7.15)$$

The relation between the power spectral density curves of F(t) and P(t) is thus found to be

$$S_F(\omega) = 2\sqrt{2} A_t^2 (1 - \cos \omega\tau_0)^{1/2} S_p(\omega) \quad (7.16)$$

or

$$W_F(f) = 2\sqrt{2} A_t^2 (1 - \cos 2\pi f\tau_0)^{1/2} W_p(f) \quad (7.17)$$

The term $(1 - \cos 2\pi f\tau_0)^{1/2}$ is a periodic function. It is sketched in Fig. 7.2.

From the spectral density curve of the momentum flux in the two-phase mixture flowing within a U-tube, one can construct the spectral density curve of the vibration amplitude by using the relation

$$W_x(f) = \frac{2\sqrt{2} A_t^2 (1 - \cos 2\pi f\tau_0)^{1/2}}{[k - M_e(2\pi f)^2]^2 + C^2(2\pi f)^2} W_p(f) \quad (7.18)$$

The mean square of the vibration amplitude of the U-tube is

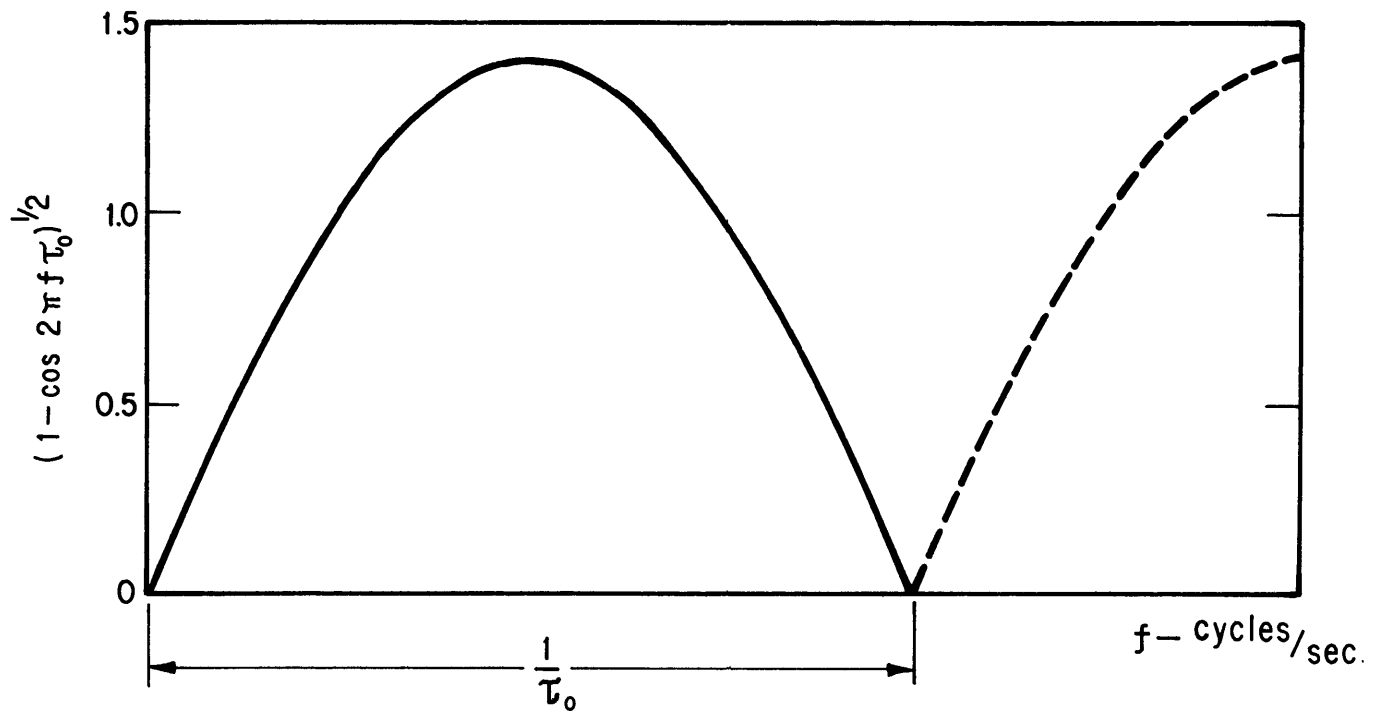


FIGURE 7.2 PERIODIC FUNCTION IN EQUATION (7.17)

$$E[\chi^2] = \int_0^{\infty} W_x(f) df \quad (7.19)$$

7.2 Fuel Rod Example

In this example, the vibration of fuel rod is supposed to be excited only by the unsteady momentum fluxes while the effects of cross flow, viscosity, etc. are neglected.

7.2.1 The Model

As shown in Fig. 7.3, this model is a rod simply supported at both ends immersed in a much simplified two-phase flow which is flowing in the longitudinal direction of the rod. It is assumed that the velocities of the liquid and gas phases are the same and equal to V , a constant.

By defining the void fraction of the two-phase mixture

$$\alpha = \frac{l_g}{l_f + l_g} = \beta \quad (7.20)$$

and the period of the liquid slug

$$T_s = \frac{l_f + l_g}{V} \quad (7.21)$$

then we have its frequency

$$\omega_k = \frac{2\pi\alpha V}{l_g} \quad (7.22)$$

Suppose the density of the flow at a section varies sinusoidally.

It can be expressed as

$$\rho = \rho_m [1 + \sin \omega_k (t - \tau)] \quad (7.23)$$

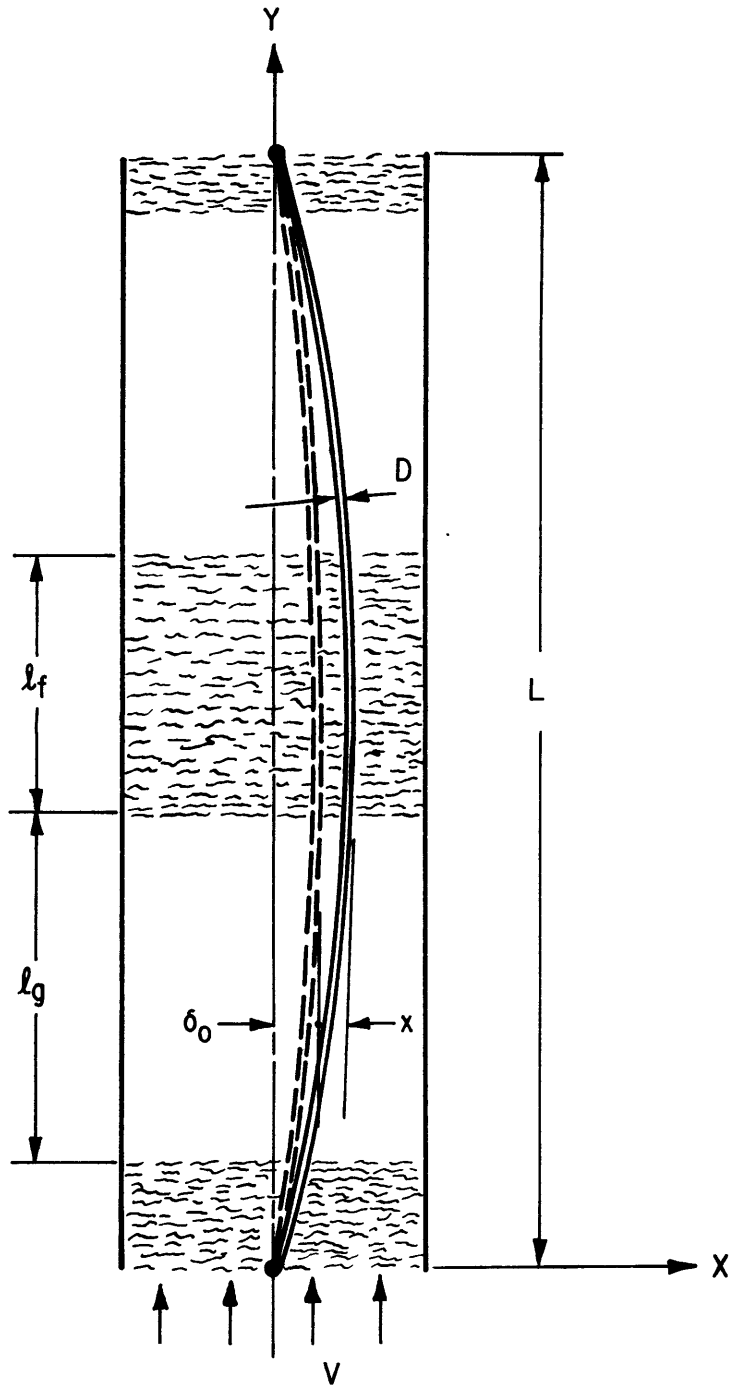


FIGURE 7.3 FUEL ROD MODEL

where

$$\tau = \int_{L-y}^L \frac{d\eta}{V} = \frac{y}{V} \quad (7.24)$$

As an approximation, the relative velocity component perpendicular to the rod is $\frac{2\delta}{L} V$. The normal force acting on an element length dy of the rod is

$$dF = \rho \left(\frac{2\delta}{L} V \right)^2 D dy \quad (7.25)$$

The total transverse force acting on the rod is

$$F = \int_{L/2}^L \rho \left(\frac{2\delta}{L} V \right)^2 D dy - \int_0^{L/2} \rho \left(\frac{2\delta}{L} V \right)^2 D dy \quad (7.26)$$

where $\delta = \delta_0 + \chi$ and δ_0 is the initial deflection of the rod. Having combined with equations (7.23) and (7.24) equation (7.26) becomes

$$F = \frac{4DV}{\omega_k L^2} \rho_m V^2 \delta^2 \left(6 - 8 \cos \frac{\omega_k L}{2V} + 2 \cos \frac{\omega_k L}{V} \right)^{1/2} \sin(\omega_k t + \phi) \quad (7.27)$$

Since in the present analysis the phase angle ϕ is of no interest, it can be discarded. Then Equation (7.27) can be written in the form

$$F = \frac{4DV}{\omega_k L^2} B^{1/2} \delta^2 P \sin \omega_k t \quad (7.28)$$

where P is the mean momentum flux and is

$$P = \rho_m V^2 \quad (7.29)$$

The system geometric variables are in the term "B" which is defined as

$$B = 6 - 8 \cos \frac{\omega_k L}{2V} + 2 \cos \frac{\omega_k L}{V} \quad (7.30)$$

The substitution of equation (7.22) into (7.30) yields

$$B = 6 - 8 \cos \frac{\alpha L \pi}{l_g} + 2 \cos \frac{2\alpha L \pi}{l_g} \quad (7.31)$$

It can be seen from Equations (7.30) and (7.31) that B has a minimum value equal to zero when $\omega_k = 0$, i.e., in the bubbly flow or mist flow regime; it has a maximum value equal to 16 when $\alpha L/l_g = 1$, i.e., along the whole length of the rod there is only one bubble and one slug.

If we treat the fuel rod model as a simple spring-mass system without considering the effect of damping then the equation of motion of the rod is

$$M_e \ddot{x} + kx = F \quad (7.32)$$

where M_e is the equivalent mass of the rod (see Appendix E) and k is the spring constant of a uniformly loaded beam with freely supported ends, namely

$$k = \frac{384EI}{5L^3} \quad (7.33)$$

The natural frequency of the system is

$$\omega_n = \sqrt{\frac{k}{M_e}} \quad (7.34)$$

Based on the assumption that $\delta_o > x$, one can have the relation

$$\delta^2 \cong \delta_o^2 + 2\delta_o x \quad (7.35)$$

The combination of equations (7.28), (7.32) and (7.35) gives the following differential equation

$$M_e \ddot{x} + (k - 2\delta_o NP \sin \omega_k t) x = N\delta_o^2 P \sin \omega_k t \quad (7.36)$$

where

$$N = \frac{4DVB^{\frac{1}{2}}}{\omega_k L^2} \quad (7.37)$$

Equation (7.36) describes the motion of a system having variable elasticity. This implies that owing to the fluctuation of momentum flux in two-phase flow, there is a nonlinear restoring force acting upon the rod. Thus, a time varying stiffness is added to the original constant stiffness of the rod. This time varying terms has the same frequency of the pulsating momentum flux.

7.2.2 Stability

The stability of the system with variable elasticity will depend on the relative magnitudes of ω_n and ω_k as well as those of the original stiffness k of the rod and the amplitude of the time dependent stiffness $2\delta_o NP$.

Figure 7.4 is the diagram showing the stability of a system with variable elasticity (Ref. 19, p. 346). The periodic variation of stiffness in this system is not sinusoidal but rectangular. Nevertheless, the general behavior of both systems will be much the same. Referring to Fig. 7.4, the product $2\delta_o NP$ in equation (7.36) is the term corresponding to Δk in Fig. 7.4. In Fig. 7.4, the shaded regions are stable and the blank regions are unstable. From the diagram it is obvious that, for stable operation of the system, one would like to have conditions such that $\omega_n > \omega_k$ and $k > 2\delta_o NP$. In other words, a stiff rod and a low flow velocity are to be preferred. If the re-

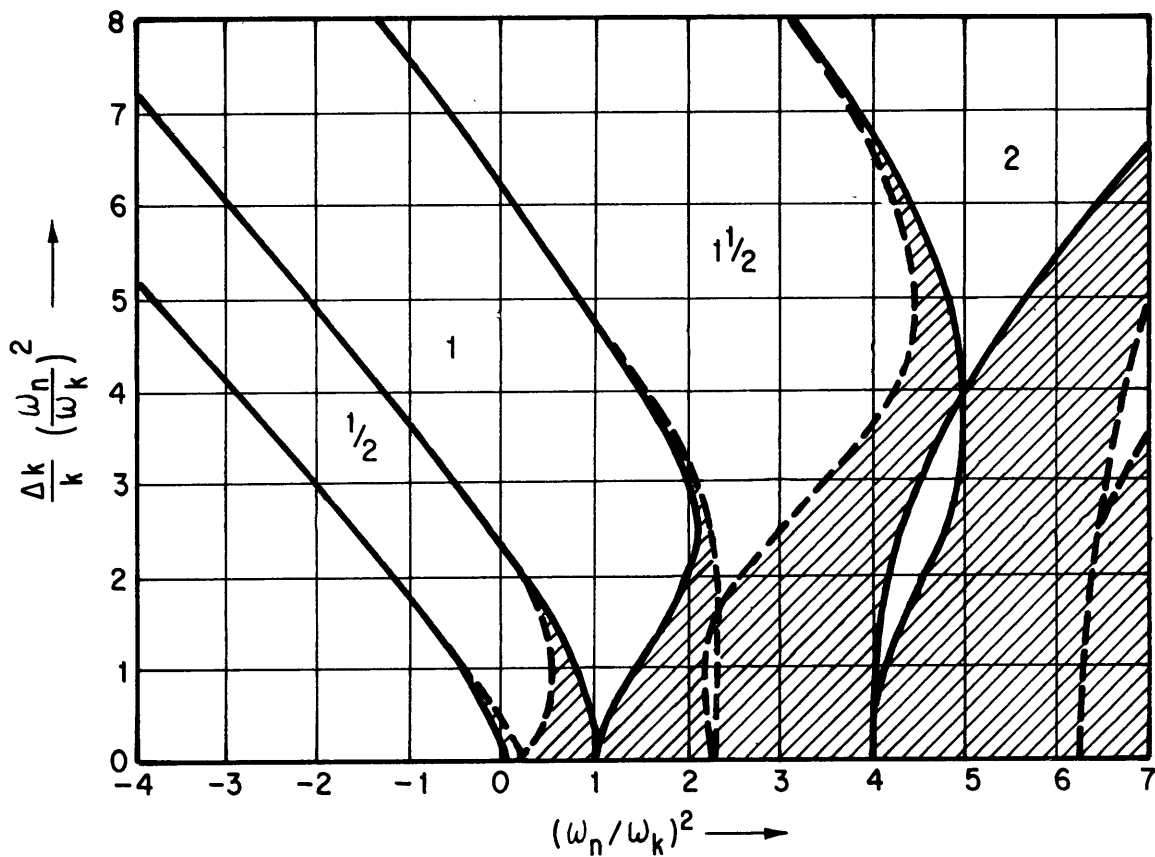


FIGURE 7.4 FUNDAMENTAL DIAGRAM DETERMINING THE STABILITY OF A SYSTEM WITH VARIABLE ELASTICITY. THE SHADED REGIONS ARE STABLE AND THE BLANK REGIONS ARE UNSTABLE.

quirements of stable operation were based entirely on this diagram, one would probably get an extremely low flow velocity and very high stiffness of rod. This may not be a practical fuel rod design. Thus, as a stabilizing factor, the damping of such a system must be taken into consideration in any practical design. In this respect a hollow bar filled with fuel pellets may be a good fuel rod structure because this would have higher damping than a solid fuel rod. The damping properties of fuel element structure are, however, only slightly studied.

7.2.3 Prediction of the Vibration Amplitude of the Fuel Rod

It is a reasonably good approximation to use the average stiffness of the rod, i.e., the original stiffness k , in the calculation of this variable elasticity system provided that $k > 2\delta_o NP$ and the system is stable. The term $P \sin \omega_k t$ in the right hand side of equation (7.36) should be replaced by the real history of momentum flux $P(t)$ and a damping term must be added to the equation of motion. Thus equation (7.36) becomes

$$\ddot{x} + \frac{C}{M_e} \dot{x} + \omega_n^2 x = \frac{\delta_o^2 N}{M_e} P(t) \quad (7.38)$$

The transfer function of the system is

$$H(\omega) = \frac{\frac{N}{M_e} \delta_o^2}{\omega_n^2 - \omega^2 + i \frac{C}{M_e} \omega} \quad (7.39)$$

Similar to equation (7.6) the spectral density of the vibration amplitude of the rod is

$$W_x(f) = \frac{\frac{4}{\pi^2} \left(\frac{DV\delta_o^2}{L^2} \right)^2 \frac{6 - 8 \cos \frac{\pi L}{V} f + 2 \cos \frac{2\pi L}{V} f}{f^2}}{\left[k - M_e (2\pi f)^2 \right]^2 + C^2 (2\pi f)^2} W_p(f) \quad (7.40)$$

Hence the mean square as well as the rms value of the vibration amplitude of the rod can be obtained.

7.3 Discussion

In the foregoing examples, the average flow velocity V of the two-phase flow was used in computing the time lag of the momentum fluctuations. In reality, one should use the actual disturbance velocity, such as the liquid slug velocity in a slug flow or the wave velocity in an annular flow, instead of the average velocity of the mixture.

The damping coefficient of a vibration system is important in predicting the amplitude and in determining the stability of the system. In a two-phase flow system both the mechanical structure and the two-phase flow may affect the damping term in the equation of motion. Therefore, reliable information about the damping coefficients of typical two-phase flow systems is very desirable.

From the analysis of fuel rod model, it can be seen that, without the initial deflection of the rod, there will be no exciting force for the vibration if the momentum fluctuation is the only cause. Applying the same analysis to a pipe, which is freely supported at both ends with two-phase flowing within, one would obtain a similar result. In these two cases, the mechanism is the self-excited vibration. The U-tube problem is essentially a forced vibration case because the tube bend will still receive the impulses of the two-phase flow even if it is rigidly fixed by some means.

On the subject of flow induced vibration, many investigations have proceeded from the flow conditions directly to the vibration

solutions without studying the interactions between the flow and the mechanical structure. Obviously, the results of these investigations can be applied only to systems similar to those which have been investigated. Furthermore, following this approach, it is difficult to understand the actual mechanism of the flow induced vibration. For instance, the vibration frequencies of rods subjected to parallel flow are found close to the natural frequencies of rods in many experimental studies. Based on this fact, Burgreen (3), Quinn (4) and some other investigators believe the mechanism of parallel flow induced vibration to be a self-excited vibration. It has been shown in the U-tube vibration problems that the frequencies of forced vibrations may also be close to the natural frequencies of the mechanical systems in case the excitation is random. In the present study, the flow induced vibration problems were solved by applying the exciting forces of known magnitude and frequency to models appropriate to the systems being studied. This is a more fundamental way of approaching such problems although the models and the analysis in this study are by no means perfect.

8. CONCLUSIONS

The conclusions of this investigation may be summarized as follows:

1. The fluctuation of momentum fluxes is important only in a relatively low frequency range. Under all the tested flow conditions, the major part of the fluctuation energy is contained in the frequency range below 50 cycles/sec.

2. The unsteady component of the momentum fluxes in a two-phase flow increases with increasing average flow velocity at a smaller rate than the steady component does. At a given velocity, the steady momentum fluxes increase with decreasing volumetric quality through the entire quality range, while the unsteady momentum fluxes reach the maximum at certain value of volumetric quality. The maximum values of unsteady momentum fluxes appear in either the high void slug flow or the low void annular flow regime.

3. The unsteadiness of momentum fluxes, the ratio of the rms value of the unsteady momentum flux to the steady momentum flux is inversely proportional to the average flow velocity to the 0.8 power and pipe diameter to the 0.4 power. Among the tested pipe geometries the unsteadiness is the greatest in the rectangular pipe. High system pressures repress the unsteadiness of momentum fluxes.

4. Above 70% volumetric quality, the predominant frequency of unsteady momentum fluxes increases in proportion with the average flow velocity and increases almost linearly with decreasing volumetric quality. At higher flow velocity, the increasing rates of the predominant frequency are higher. The system pressure, the size and

geometry of flow channel do not have significant effect on the predominant frequency. Below 70% volumetric quality, the fluctuation energy of unsteady momentum fluxes is distributed rather evenly in the low frequency region.

5. Based on the experimental results, a method of constructing the power spectral density curves for untested conditions has been suggested.

6. The presence of obstacles in the flow channel, such as the spacers between the reactor fuel elements, depresses the pulsation of momentum fluxes and results in an even distribution of the fluctuation energy in the low frequency range.

7. In two-phase flow systems, appreciable structural vibrations can be excited by the unsteady momentum fluxes. With the experimental results in the present investigation, the rms value of the vibration amplitude can be predicted by applying random vibration techniques. In either self-excited or forced vibrations, the vibration energy of the mechanical system is concentrated around its natural frequency. Under some conditions, the vibration may be unstable.

9. SUGGESTIONS FOR FUTURE WORK

The results of this study should be regarded as preliminary and subject to refinement when more work on this problem has been done.

Suggestions about the unsteady momentum flux data are:

1. The effect of the gas phase density on the unsteadiness of momentum fluxes needs to be studied in wide pressure and temperature ranges because the suggestion of equation (6.7) is based on very limited experimental data.

2. It is necessary to verify or modify the proposed correlations of the unsteadiness and predominant frequency of momentum fluxes with Weber number and Froude number by studying the effects of surface tension and gravity.

Suggestions concerning the application of unsteady momentum flux data in solving problems of two-phase flow induced vibrations are:

1. The measurements of disturbance velocities in a two-phase flow as a function of flow regime are necessary because the true velocities of the two-phase momentum fluctuations are important in some applications such as the two-phase flow induced vibration of U-tubes in a steam generator.

2. The measurements of damping coefficients for typical two-phase flow systems are required in the determination of vibration amplitudes and the stability of the vibrations.

3. The predicted rms amplitudes of the two-phase flow induced vibrations should be checked experimentally.

APPENDIX A

Experimental Data

TABLE 1.

(1)	(2)	(3)	(4)	(5)	(6)	(7)	(8)
Test No.	Roto-meter Reading %	Supply Air Pressure psig	Mano-meter Reading in. oil (in.Hg)	VTVM Reading volt	Q_f ft ³ /sec x10 ²	Q_g ft ³ /sec	$(A/A_R)^{\frac{1}{2}}$
1	76.0 *	56.0	18.7	.029	0.960	0.305	0.851
2	51.0 *	56.0	18.7	.014	0.640	0.305	
3	25.0 *	56.0	18.7	.007	0.320	0.305	
4	30.0	56.0	18.7	.040	1.28	0.305	1.45
5	37.0	56.0	18.7	.055	1.59	0.305	1.81
6	45.0	56.0	18.7	.070	1.92	0.305	1.99
7	56.0	56.0	18.7	.092	2.40	0.305	2.10
8	30.0	55.0	34.6	.058	1.28	0.413	1.56
9	25.0 *	55.0	34.6	.017	0.320	0.413	
10	51.0 *	55.0	34.6	.025	0.640	0.413	
11	76.0 *	55.0	34.6	.040	0.960	0.413	0.856
12	37.0	55.0	34.6	.075	1.59	0.413	2.04
13	45.0	55.0	34.6	.095	1.92	0.413	2.18
14	56.0	55.0	34.6	0.115	2.40	0.413	2.36
15	37.0	54.0	(3.40)	.095	1.59	0.518	2.12
16	25.0 *	54.0	(3.40)	.025	0.320	0.518	
17	51.0*	54.0	(3.40)	.035	0.640	0.518	
18	76.0 *	54.0	(3.40)	.053	0.960	0.518	0.851
19	30.0	54.0	(3.40)	.073	1.28	0.518	1.63
20	45.0	54.0	(3.40)	0,115	1,92	0.518	2.34
21	54.0	59.5	28.0	.070	2.32	0.191	1.77
22	45.0	59.5	28.3	.064	1.92	0.192	1.77
23	37.0	59.5	29.6	.057	1.59	0.196	1.68
24	30.0	59.5	30.5	.043	1.28	0.200	1.56
25	76.0 *	59.5	32.1	.028	0.960	0.206	0.865
26	51.0 *	59.3	32.5	.016	0.640	0.205	0.370
27	25.0 *	59.3	33,1	.004	0.320	0.208	

TABLE 1.

(1)	(2)	(3)	(4)	(5)	(6)	(7)	(8)
28	56.0	60.2	12.0	.049	2.40	0.216	1.26
29	45.0	60.0	12.8	.036	1.92	0.130	1.21
30	37.0	60.0	13.0	.029	1.59	0.131	1.20
31	30.0	60.0	13.4	.022	1.28	0.133	1.02
32	76.0 *	60.0	14.7	.012	0.960	0.140	0.678
33	51.0 *	60.0	15.1	.007	0.640	0.141	0.351
34	25.0 *	60.0	15.8	.001	0.320	0.145	
35	24.3 *	61.3	(4.00)	.001	0.304	0.146	
36	48.5 *	61.3	(3.80)	.004	0.609	0.143	0.214
37	72.7 *	61.5	(3.70)	.010	0.913	0.141	0.580
38	38.2	61.5	(3.30)	.022	1.63	0.133	1.02
39	45.0	61.5	(3.10)	.026	1.92	0.129	0.961
40	56.0	61.5	(2.90)	.033	2.40	0.125	0.946
41	60.4 *	60.0	25.8	.045	0.759	0.370	0.288
42	90.8 *	60.0	25.3	.067	1.15	0.366	0.446
43	35.6	60.0	24.8	0.130	1.52	0.362	0.748
44	44.0	60.0	24.1	0.200	1.89	0.357	1.01
45	54.0	60.0	23.5	0.270	2.32	0.352	1.30
46	65.0	60.0	22.8	0.355	2.79	0.347	1.66
47	65.0	58.5	(3.12)	0.530	2.79	0.517	2.08
48	57.1	58.5	(3.17)	0.450	2.45	0.521	1.87
49	48.0	58.0	(3.21)	0.345	2.06	0.525	1.50
50	38.2	58.5	(3.25)	0.235	1.63	0.527	0.930
51	86.1 *	58.5	(3.33)	0.140	1.09	0.534	0.377
52	45.0 *	58.5	(3.37)	.060	0.576	0.537	
53	45.0	61.0	7.0	0.460	1.92	0.193	1.63
54	37.3	61.0	7.3	0.375	1.60	0.199	1.50
55	30.0	61.0	7.5	0.275	1.28	0.201	1.29
56	76.0 *	61.0	7.7	0.165	0.960	0.205	0.766
57	51.0 *	60.5	8.1	.085	0.640	0.208	0.395

TABLE 1.

(1)	(2)	(3)	(4)	(5)	(6)	(7)	(8)
58	55.0	61.5	6.7	0.560	2.36	0.190	2.03
59	45.0	61.0	7.0	0.450	1.92	0.193	1.85
60	37.3	61.0	7.3	0.360	1.60	0.199	1.78
61	30.0	60.5	7.7	0.275	1.28	0.201	1.62
62	76.0 *	60.5	7.9	0.180	0.960	0.205	1.12
63	51.0 *	60.5	8.1	.095	0.640	0.208	0.637
64	59.6	60.0	16.1	0.880	2.56	0.295	2.94
65	45.0	60.0	17.1	0.630	1.92	0.302	2.48
66	30.0	60.0	17.8	0.380	1.28	0.308	1.84
67	51.0	60.0	18.5	0.155	0.640	0.313	0.583
68	52.0	60.0	16.7	0.755	2.24	0.297	2.69
69	37.3	60.0	17.5	0.530	1.60	0.304	2.23
70	76.0 *	60.0	18.2	0.260	0.960	0.310	1.24
71	25.0 *	60.0	18.9	.080	0.320	0.317	
72	45.0	61.0	7.0	0.455	1.92	0.193	1.64
73	37.3	61.0	7.3	0.360	1.60	0.199	1.52
74	30.0	61.0	7.5	0.280	1.28	0.201	1.29
75	76.0 *	61.0	7.7	0.615	0.960	0.205	0.800
76	51.0 *	60.5	8.1	.095	0.640	0.208	0.435
77	59.6	60.0	16.1	0.910	2.56	0.295	2.71
78	45.0	60.0	17.1	0.675	1.92	0.302	2.52
79	30.0	60.0	17.8	0.405	1.28	0.308	1.76
80	76.0 *	60.0	18.2	0.260	0.960	0.310	1.16
81	51.0 *	60.0	18.5	0.150	0.640	0.313	0.536
82	45.0	61.0	7.0	0.450	1.92	0.193	1.83
83	37.3	61.0	7.3	0.400	1.60	0.199	1.70
84	30.0	61.0	7.5	0.260	1.28	0.201	1.47
85	76.0 *	61.0	7.7	0.165	0.960	0.205	1.07
86	51.0 *	60.5	8.1	.095	0.640	0.208	0.602

TABLE 1.

(1)	(2)	(3)	(4)	(5)	(6)	(7)	(8)
87	45.0	61.0	7.0	0.395	1.92	0.193	1.46
88	37.3	61.0	7.3	0.310	1.60	0.199	1.30
89	30.0	61.0	7.5	0.230	1.28	0.201	1.07
90	76.0 *	61.0	7.7	0.145	0.960	0.205	0.790
91	51.0 *	60.5	8.1	0.100	0.640	0.208	0.530
92	59.6	60.0	16.1	0.815	2.56	0.295	2.03
93	45.0	60.0	17.1	0.555	1.92	0.302	1.79
94	30.0	60.0	17.8	0.330	1.28	0.308	1.18
95	76.0 *	60.0	18.2	0.230	0.960	0.310	0.820
96	51.0 *	60.5	18.5	0.145	0.640	0.313	0.490
97	45.0	61.0	7.0	0.550	1.92	0.193	1.13
98	37.3	61.0	7.3	0.425	1.60	0.199	1.02
99	30.0	61.0	7.5	0.305	1.28	0.201	0.887
100	76.0 *	61.0	7.7	0.195	0.960	0.205	0.670
101	51.0 *	60.5	8.1	0.115	0.640	0.208	0.490
102	75.0 *	89.0	0.5	0.570	0.946	.0037	
103	74.0 *	89.0	1.2	0.575	0.930	.0057	
104	69.0 *	88.5	2.6	0.605	0.870	.0084	
105	66.0 *	88.5	3.5	0.585	0.831	.0098	
106	60.5 *	88.5	4.2	0.530	0.764	.0108	
107	60.6 *	88.5	5.1	0.500	0.765	.0118	
108	54.7 *	88.5	5.7	0.490	0.690	.0125	
109	54.3 *	88.5	7.1	0.465	0.687	.0139	
110	42.3 *	88.5	4.8	0.305	0.535	.0144	
111	51.0 *	88.5	7.0	0.335	0.638	.0138	
112	9.5 *	88.0	18.9	.045	0.119	.0227	0.525
113	18.9 *	88.0	17.0	0.130	0.239	.0215	1.15
114	29.7 *	88.0	14.8	0.215	0.375	.0201	1.29
115	37.4 *	88.0	13.4	0.360	0.472	.0191	1.53

TABLE 1.

(1)	(2)	(3)	(4)	(5)	(6)	(7)	(8)
116	47.2 *	88.5	11.7	0.490	0.596	.0179	1.54
117	56.7 *	88.5	10.2	0.580	0.716	.0167	1.42
118	15.1 *	88.0	10.4	0.105	0.191	.0168	0.920
119	22.2 *	88.0	9.3	0.155	0.281	.0159	0.987
120	29.7 *	88.5	8.2	0.210	0.375	.0150	1.08
121	37.1 *	88.5	7.3	0.300	0.469	.0141	1.28
122	44.6 *	88.5	6.3	0.385	0.563	.0131	1.23
123	52.0 *	88.5	5.4	0.465	0.657	.0122	1.18
124	59.4 *	88.5	4.7	0.570	0.750	.0113	1.02
125	66.8 *	88.5	3.9	0.620	0.844	.0103	0.823

* Reading on the Rotometer of smaller measuring capacity.

TABLE 2.


(1)	(9)	(10)	(11)	(12)	(13)	(14)	(15)
Test No.	Pipe	V	β	P_{st}	P_{rms}	P_{rms}/P_{st}	f_c
		ft/sec	%	lb _f /in ²	lb _f /in ²		cps
1		150	97.0	5.44	4.83	0.974	15.0
2		150	98.1	2.67			
3		150	99.0	1.34			
4		150	96.0	7.63	8.23	1.08	18.0
5		150	95.0	10.5	10.3	0.985	21.0
6		150	94.0	13.3	11.3	0.850	23.0
7		150	92.7	17.5	11.9	0.680	27.0
8		200	97.0	11.1	8.87	0.802	19.0
9		200	99.3	3.26			
10		200	98.5	4.76			
11		200	97.8	7.67	4.86	0.634	16.0
12		200	96.3	14.4	11.6	0.805	22.0
13		200	95.7	18.1	12.4	0.682	26.0
14		200	94.5	21.9	13.4	0.611	30.0
15		250	97.1	18.1	12.0	0.665	24.0
16		250	99.5	4.76			
17		250	98.8	6.68			
18		250	98.6	10.1	4.83	0.477	17.0
19		250	97.7	13.9	9.27	0.665	21.0
20		250	96.5	21.9	13.3	0.605	27.0
21 *		100	89.3	13.4	10.1	0.750	26.0
22 *		100	91.0	12.2	10.0	0.823	23.0
23 *		100	92.5	10.9	9.60	0.882	19.0
24 *		100	93.8	8.18	8.23	1.00	17.0
25 *		100	95.5	5.34	4.93	0.921	13.7
26 *		100	97.2	3.06	2.08	0.690	11.0
27 *		100	98.7	.07			

TABLE 2.

(1)	(9)	(10)	(11)	(12)	(13)	(14)	(15)	
28 *	↑ 5" D	70	84.0	9.36	7.18	0.766	21.5	
29 *		70	87.2	6.74	6.85	1.00	18.5	
30 *		70	89.2	5.54	6.80	1.22	16.4	
31 *		70	91.4	4.10	5.81	1.41	14.5	
32 *		70	93.9	2.38	3.85	1.62	12.0	
33 *		70	95.8	1.34	1.99	1.49	10.3	
34 *		70	98.0	0.20				
35		Round	70	98.0	0.20			
36		↓	70	96.0	0.72	1.22	1.70	8.0
37			70	94.0	1.89	3.30	1.74	10.5
38	70		89.1	4.16	5.81	1.39	15.5	
39	70		86.9	4.95	5.46	1.10	17.5	
40	70		83.9	6.32	5.38	0.855	20.5	
41	70		98.0	0.35	0.53	1.53		
42	70		97.0	0.52	0.82	1.59	5.5	
43	70		96.0	1.03	1.38	1.37	6.5	
44	70		95.0	1.54	1.86	1.21	7.5	
45	70		94.0	2.08	2.41	1.16	8.0	
46	1" D	70	92.5	2.74	3.07	1.12	9.0	
47	Round	100	95.0	4.09	3.85	0.94	11.0	
48	↓	100	95.5	3.48	3.45	0.99	10.2	
49		100	96.2	2.66	2.78	1.04	9.3	
50		100	97.0	1.81	1.72	0.95	8.0	
51		100	98.0	1.08	0.69	0.640	6.2	
52		100	98.8	0.51				
53		100	91.0	9.06	7.73	0.852	18.0	
54		↑ 5" D	100	92.6	7.40	7.10	0.960	16.5
55			100	94.0	5.44	6.09	1.12	15.0
56			Round	100	95.5	3.26	3.62	1.11
57		↓	100	97.0	1.69	1.86	1.09	9.5

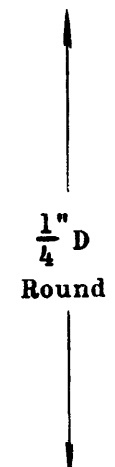
TABLE 2.

(1)	(9)	(10)	(11)	(12)	(13)	(14)	(15)
58	↑ Rec- tangle ↓	100	89.0	10.6	9.12	0.865	21.0
59		100	91.0	8.48	8.32	0.982	18.5
60		100	92.6	6.76	8.00	1.19	16.5
61		100	94.0	5.18	7.26	1.40	14.5
62		100	95.5	3.38	5.03	1.49	12.5
63		100	97.0	1.99	2.86	1.44	9.5
64		150	92.0	16.5	13.2	0.800	25.0
65		150	94.0	11.9	11.2	0.944	21.0
66		150	96.0	7.14	8.25	1.16	16.5
67		150	98.0	2.92	2.62	0.900	10.0
68		150	93.0	14.2	12.1	0.853	23.0
69		150	95.0	10.0	10.1	1.01	19.0
70		150	97.0	4.91	5.56	1.14	14.5
71	150	99.0					
72	↑ $\frac{5}{8}$ " D Round ↓	100	91.0	8.99	7.75	0.862	18.5
73		100	92.6	7.10	7.16	1.01	16.5
74		100	94.0	5.54	6.09	1.10	15.0
75		100	95.5	3.26	3.78	1.16	12.5
76		100	97.0	1.87	2.07	1.11	9.5
77		150	92.0	17.5	12.2	0.697	24.5
78		150	94.0	12.7	11.4	0.895	20.5
79		150	96.0	7.64	7.92	1.04	16.0
80		150	97.0	4.90	5.21	1.06	13.0
81		150	98.0	2.83	2.42	0.857	10.5
82		100	91.0	8.45	8.26	0.978	18.0
83		100	92.6	6.68	7.65	1.15	16.0
84		100	94.0	4.91	6.62	1.35	13.5
85	100	95.5	3.11	4.81	1.55	12.0	
86	100	97.0	1.80	2.70	1.50	10.0	

TABLE 2.

(1)	(9)	(10)	(11)	(12)	(13)	(14)	(15)
87	↑ Tri- angle ↓	100	91.0	7.76	6.91	0.890	19.0
88		100	92.6	6.13	6.14	1.00	16.0
89		100	94.0	4.53	5.05	1.08	14.0
90		100	95.5	2.87	3.75	1.31	11.5
91		100	97.0	1.99	2.53	1.26	8.0
92		150	92.0	16.1	9.59	0.600	28.5
93		150	94.0	11.1	8.45	0.760	21.0
94		150	96.0	6.52	5.58	0.860	15.0
95		150	97.0	4.53	3.88	0.860	12.0
96		150	98.0	2.87	2.32	0.810	8.0
97		↑ Annulus ↓	100	91.0	11.6	5.32	0.492
98	100		92.6	8.24	4.80	0.583	
99	100		94.0	6.00	4.18	0.697	
100	100		95.5	3.83	3.15	0.822	
101	100		97.0	2.16	2.30	1.06	
102	38		27.0				
103	44		38.0				
104	50		49.0				
105	53		54.0				
106	54		58.5				
107	57		60.6				
108	↑ $\frac{1}{4}$ " D Round ↓	57	64.5				
109		61	67.0				
110		49	68.0				
111		59	68.3				
112		70	95.0	1.37	3.42	2.50	9.0
113		70	90.0	3.97	7.50	1.89	13.0
114		70	84.3	6.54	8.41	1.29	13.5
115		70	80.2	10.9	10.0	0.915	12.0

TABLE 2.

(1)	(9)	(10)	(11)	(12)	(13)	(14)	(15)
116		70	75.0	14.9	10.1	0.674	16.0
117		70	70.0	17.6	9.27	0.526	20.0
118		55	89.8	3.20	6.00	1.87	12.5
119		55	85.0	4.71	6.44	1.37	13.3
120		55	80.0	6.00	7.05	1.17	13.5
121		55	75.0	9.11	8.35	0.916	13.0
122		55	70.0	11.7	8.03	0.686	15.0
123		55	65.0	14.1	7.70	0.546	
124		55	60.0	17.3	6.65	0.384	
125		55	55.0	18.9	5.38	0.286	

* Test run at 2 atm.

APPENDIX B

Transfer Function of Beam-Tee Systems

The beam and turning tee combination is considered to be a simple linear time-invariant vibratory system. When a force F is applied to the system its equation of motion is

$$M_e \ddot{x} + c \dot{x} + kx = F \quad (\text{B.1})$$

The beam system is excited by the momentum flux of the two-phase flow, i.e., a force F ; the quantity picked by the LVDT is the displacement of the beam x . Therefore, the excitation history to the system is $F(t)$ and the response history is $x(t)$. To find the transfer function $H(\omega)$ of the system in the frequency domain it is assumed that

$$F(t) = e^{i\omega t} \quad (\text{B.2})$$

$$x(t) = H(\omega)e^{i\omega t}$$

By substituting equation (B.2) in equation (B.1), cancelling $e^{i\omega t}$, the solution is then obtained as

$$H(\omega) = \frac{1}{k - M_e \omega^2 + i c \omega} \quad (\text{B.3})$$

For the beam-tee system with $f_n = 84$ cps, it was found that $M_e = 0.98$ lb_m, $k = 710$ lb_f/in and $c = 2.65 \times 10^{-3}$ lb_fsec/in. As a function of frequency, the reciprocal of the transfer function is

$$\frac{1}{|H(\omega)|} = (505000 - 142.8 f^2 + .0101 f^4)^{1/2} \quad (\text{B.4})$$

For the beam-tee system with $f_n = 168$ cps, the corresponding quantities are: $M_e = .0611$ lb_m, $k = 190$ lb_f/in and $c = 7.25 \times 10^{-4}$ lb_f sec/in. The reciprocal of its transfer function is

$$\frac{1}{|H(\omega)|} = (36100 - 2.57 f^2 + 4.58 \times 10^{-5} f^4)^{1/2} \quad (\text{B.5})$$

APPENDIX C

Calibration Coefficients of Steady Momentum Fluxes
and Power Spectral Density Curves

Test No.	#1 - #40	#41 - #101	#102 - #125
Calibration coefficient of Steady momentum fluxes (Section 3.4.2)	.0171 volts/lb _f	0.165 volts/lb _f	0.67 volts/lb _f
Calibration coefficient F _s of power spectral density curves (Section 4.4)	1.74 lb _f	1.45 lb _f	0.32 lb _f

Example of spectral density curve calibration:

The power spectral density curve of a sinusoidal "force" is shown in Fig. C.1. The rms value of the "force" is $F_s = 1.45 \text{ lb}_f$. The area under the spectral density curve is $A_r = 2.7 \text{ in}^2$. With the scale on X axis being $n = 10 \text{ cps per inch}$, the scale on Y axis is then determined to be $C_y = .0778 \text{ lb}_f^2/\text{cps per inch}$. This scale can be used to determine the scale of the spectral density curves of momentum fluxes which have been obtained by using the same recording and spectral analysis systems for the sinusoidal "force". One of these spectral density curves is shown in Fig. C.2. The scale on the Y axis of this graph is

$$\frac{C_y}{A_p^2} = 0.822 \left(\frac{\text{lb}_f}{\text{in}^2} \right)^2 / \text{cps per inch},$$

where A_p is the flow area of the test pipe.

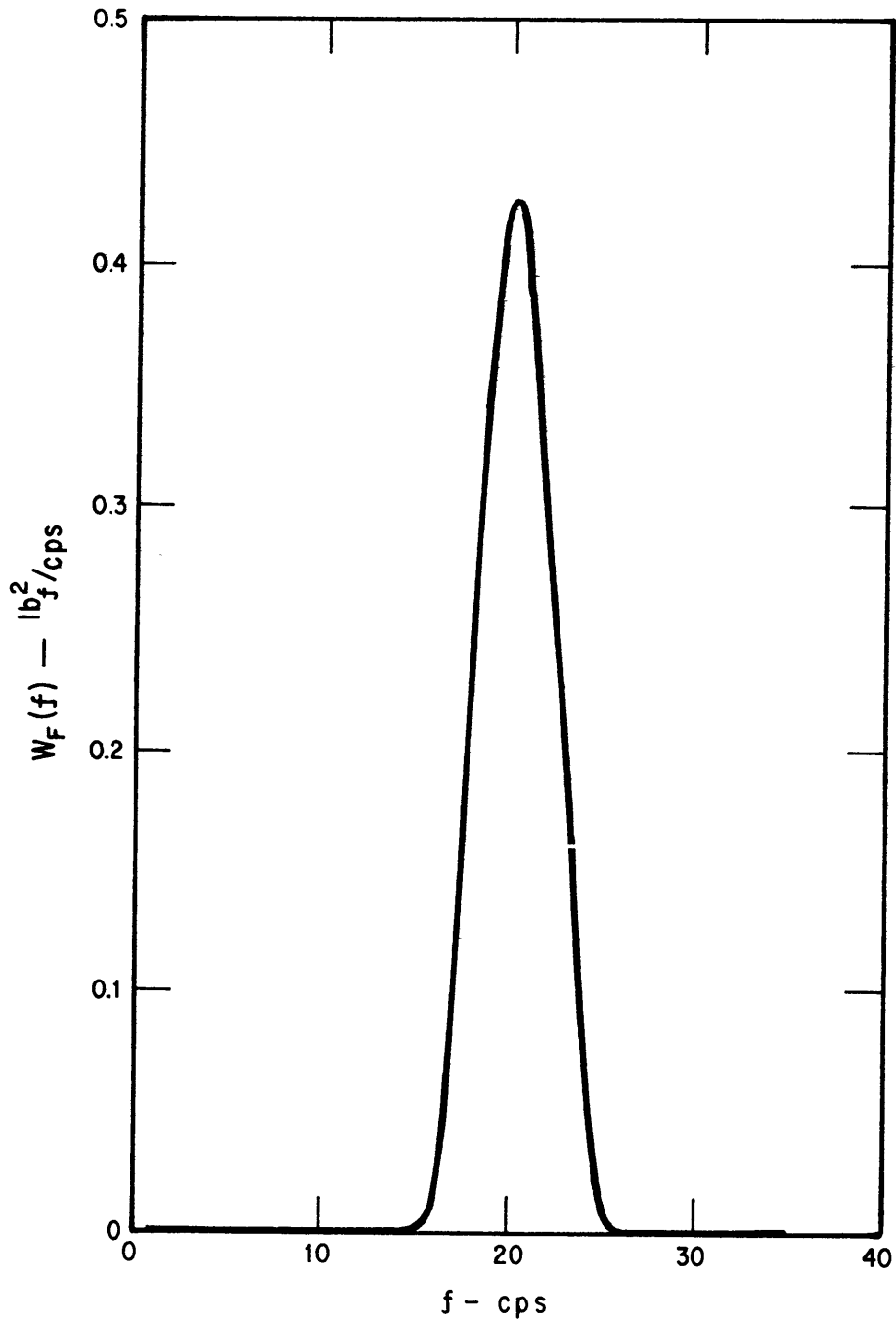


FIGURE C.1 POWER SPECTRAL DENSITY OF SINUSOIDAL FORCE

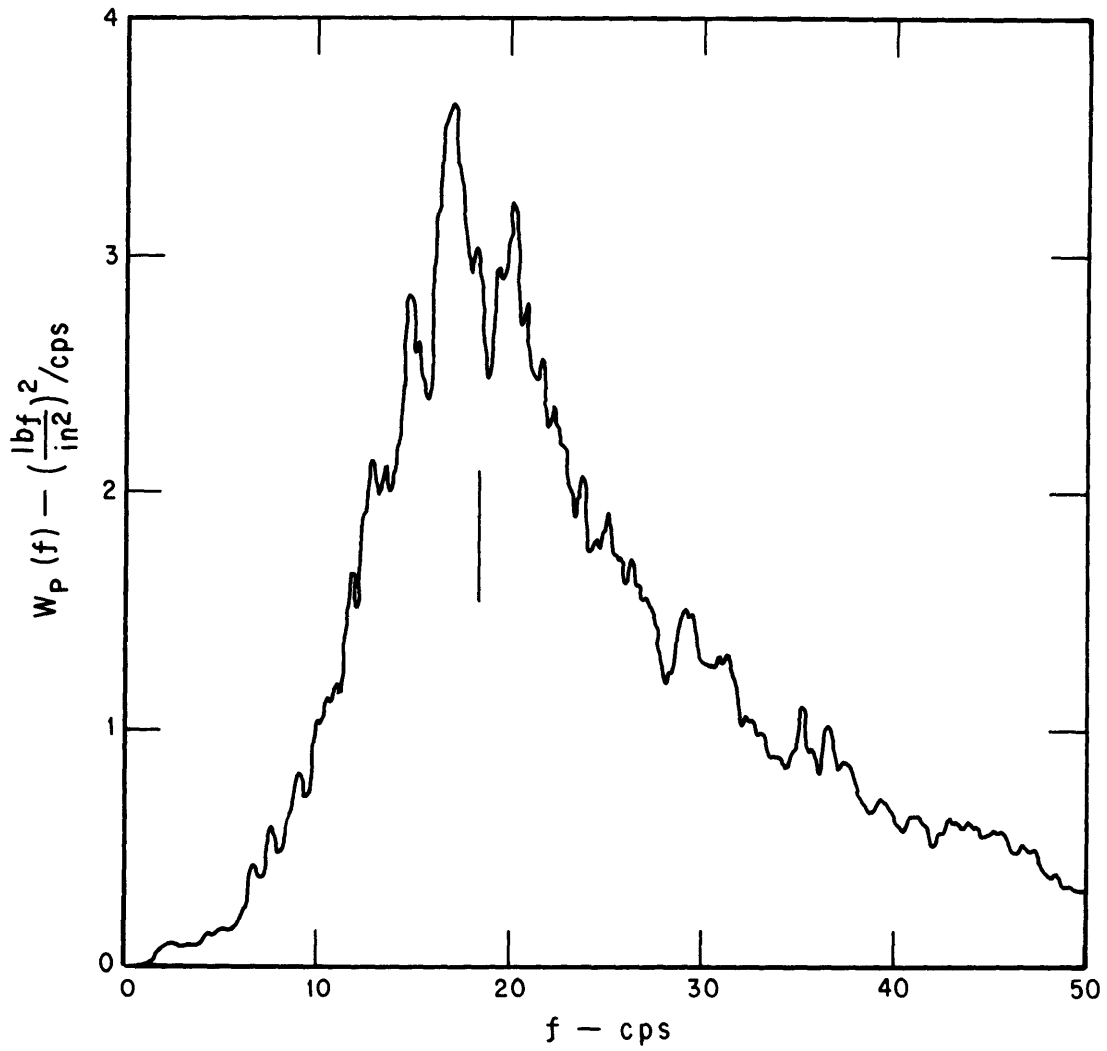


FIGURE C.2 POWER SPECTRAL DENSITY OF MOMENTUM FLUX OF TEST NO. 72

APPENDIX D

Numerical Examples for Predicting Vibration Amplitudes

Example 1. U-tube

Tube data: Stainless steel tubing

O.D. = 0.5 inches, Wall thickness = .05 inches

$$E = 30 \times 10^6 \text{ lb}_f/\text{in}^2$$

$L = 20 \text{ ft.}$, $L_b = 1 \text{ ft.}$ (see Fig. 7.1)

$C/C_c = .01$ (assumed)

Flow data: Steam and water mixture

$$p = 2400 \text{ psi} \quad T = 662 \text{ }^\circ\text{F}$$

$$V = 70 \text{ ft/sec} \quad \beta = 90\%$$

$$\rho_g = 7.1 \text{ lb}_m/\text{ft}^3 \quad \rho_f = 35.7 \text{ lb}_m/\text{ft}^3$$

$$P_{st} = 10.5 \text{ lb}_f/\text{in}^2 \quad (\text{equation(6.6)})$$

$$\left(\frac{P_{rms}}{P_{st}} \right)_o V^{0.8} D^{0.4} = 29.3 \quad (\text{Fig. 5.21})$$

$$\left(\frac{P_{rms}}{P_{st}} \right)_o = 1.41$$

$$\frac{P_{rms}}{P_{st}} = 0.487 \quad (\text{equation(6.7)})$$

$$P_{rms} = 5.11 \text{ lb}_f/\text{in}^2$$

$$\frac{f_c}{v} \times 10^2 = 20, \quad f_c = 14 \text{ cps} \quad (\text{Fig. 5.22})$$

$$L_f = 36, \quad L_L = 11 \quad (\text{equation(6.3)})$$

$$h = 1.45 \left(\frac{\text{lb}_f}{\text{in}^2} \right)^2 / \text{cps} \quad (\text{equation(6.2)})$$

With these known quantities, the power spectral density curve of the momentum flux was constructed according to Fig. 6.1(a).

$$I_Y = 5.08 \text{ in}^4 \quad (\text{see Fig. 7.1})$$

$$k = 33.1 \text{ lb}_f/\text{in} \quad (\text{equation (7.2)})$$

$$M_e = 2.53 \text{ lb}_m$$

$$\omega_n = 71 \text{ rad/sec} \quad (\text{equation (7.34)})$$

$$f_n = 11.3 \text{ cps}$$

$$C = .01 C_c = .0093 \text{ lb}_f\text{sec}/\text{in}$$

$$A_t = 0.126 \text{ in}^2$$

$$\tau_o = 1/70 \quad (\text{equation (7.7)})$$

By substituting the relevant figures into equation (7.18), it became

$$W_x(f) = \frac{5.3(1 - \cos \frac{f}{70} 2\pi)^{1/2}}{f^4 - 255f^2 + 16360} W_p(f) \quad (\text{D.1})$$

where the functions $(1 - \cos \frac{f}{70} 2\pi)^{1/2}$ and $W_p(f)$ were shown in Figs.

7.2 and 6.1(a), respectively. Equation (D.1) was plotted in Fig. D.1.

The mean square of the vibration amplitude was $E[x^2] = 0.13 \text{ in}^2$ and

$$x_{\text{rms}} = 0.36 \text{ inches.}$$

Example 2. Fuel Rod

In this example the data of the test No. 72 were used. The physical quantities regarding the fuel rod and others needed in the calculation were assumed. These data are:

$$V = 100 \text{ ft/sec}$$

$$\beta = 91\%$$

$$D = 5/8 \text{ inches}$$

$$L = 56 \text{ inches}$$

$$\delta_o = 3/8 \text{ inches}$$

$$\text{Density of rod material}$$

$$\rho_r = 0.28 \text{ lbm/in}^3$$

$$\text{Modulus of elasticity}$$

$$E = 30 \times 10^6 \text{ lb}_f/\text{in}^2$$

$$\frac{C}{C_c} = .01$$

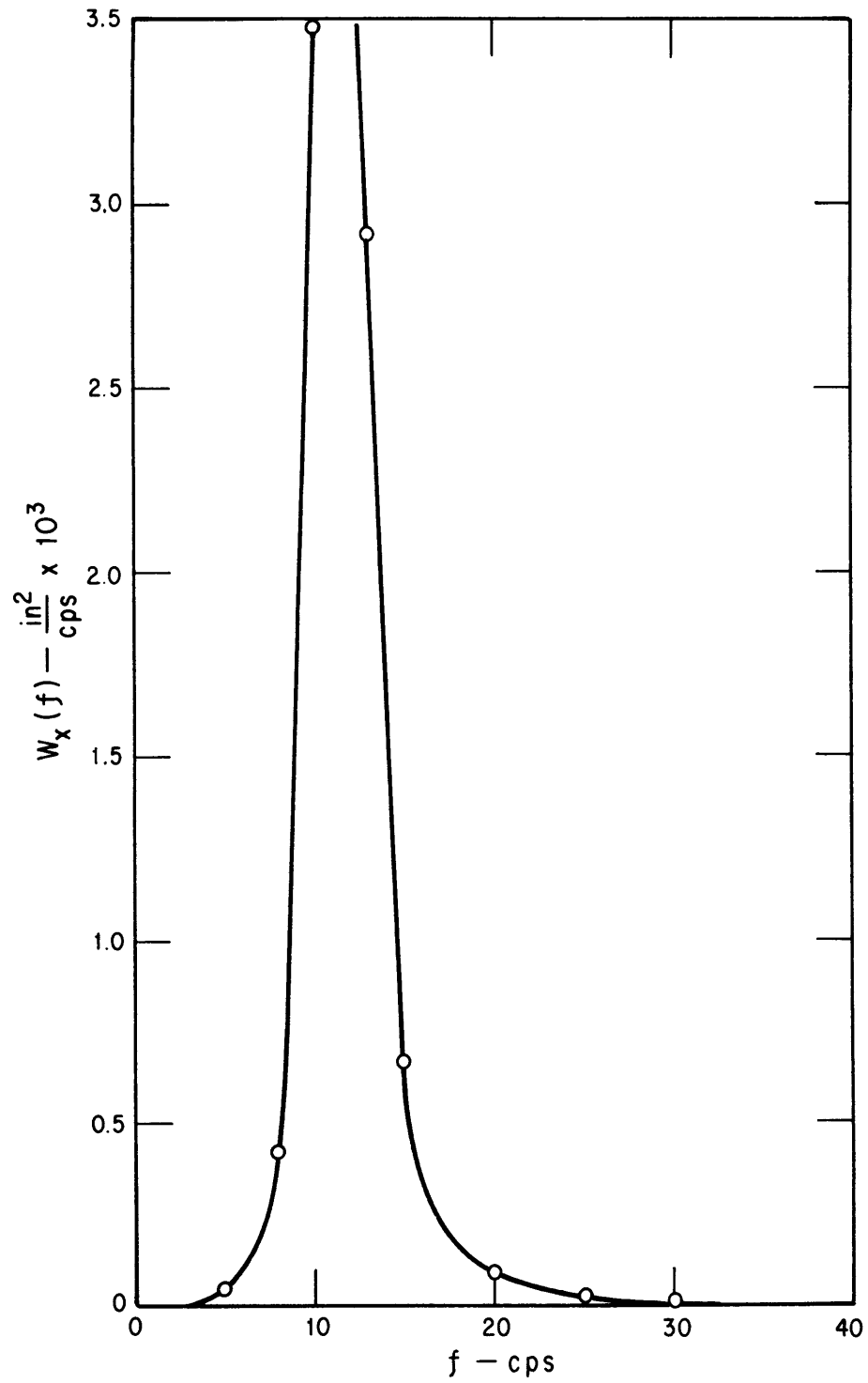


FIGURE D.1 POWER SPECTRAL DENSITY OF U-TUBE VIBRATION AMPLITUDE

$$k = 98.2 \text{ lb}_f/\text{in.} \quad (\text{equation (7.33)})$$

$$M_e = 3.82 \text{ lb}_m. \quad (\text{Appendix E})$$

$$\omega_n = 99.5 \text{ rad/sec.}, \quad f_n = 15.8 \text{ cps} \quad (\text{equation (7.34)})$$

$$C = .01 C_c = .0197 \text{ lb}_f\text{sec/in}$$

By substituting the given data into equation (7.40), it becomes

$$W_x(f) = \frac{4.57 \times 10^{-4} [6 - 8 \cos(0.1468f) + 2 \cos(0.2936f)]}{[(98.2 - 0.391f^2)^2 + .01535f^2]} W_p(f) \quad (\text{D.2})$$

With the help of the $W_p(f)$ curve in Fig. C.2, equation (D.2) was plotted in Fig. D.2. The mean square of the vibration amplitude was found to be $E[x^2] = 2.95 \times 10^{-5} \text{ in}^2$ and the rms value of the vibration amplitude $x_{\text{rms}} = .0054 \text{ inches}$.

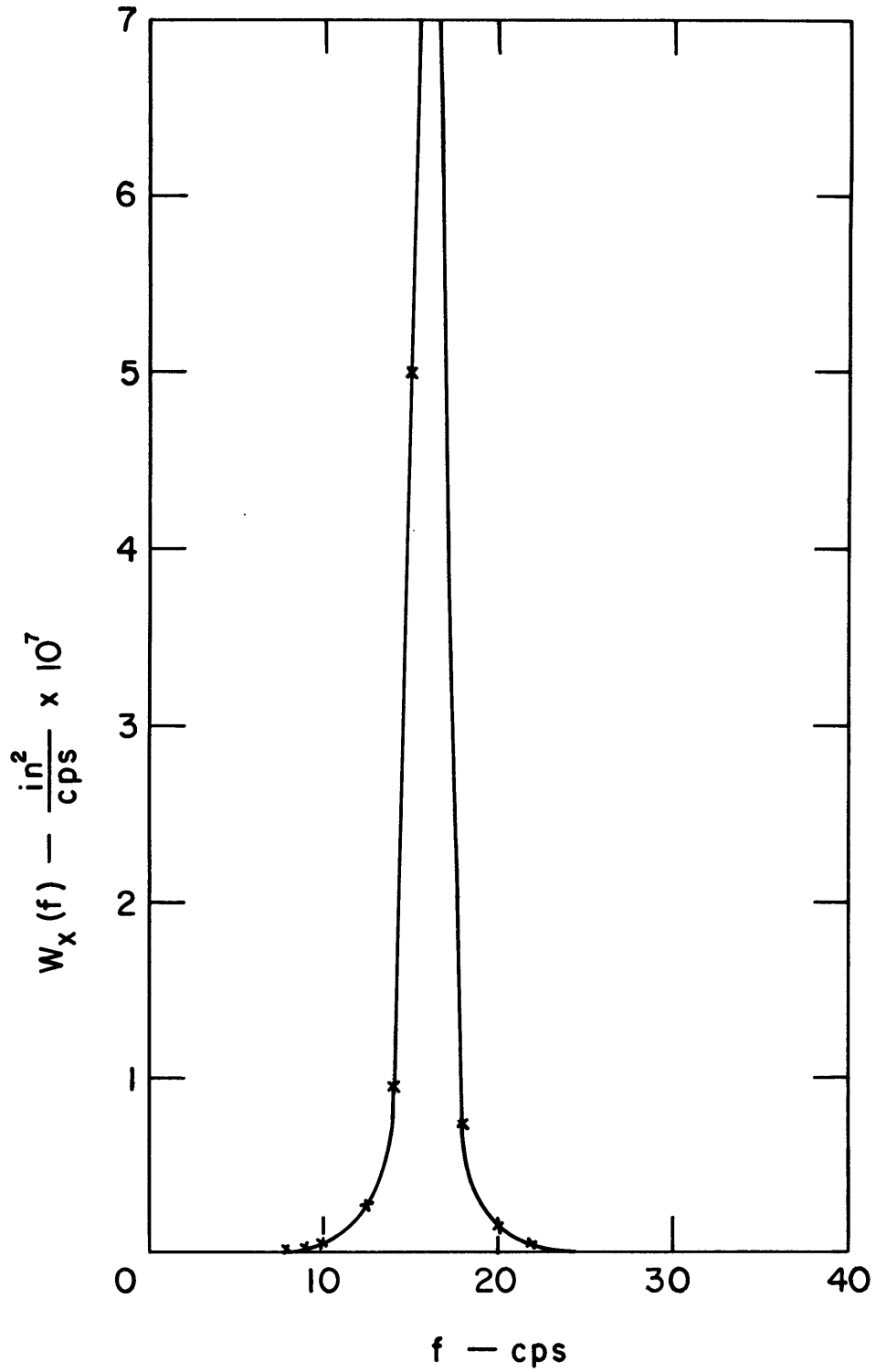


FIG. D.2 POWER SPECTRAL DENSITY OF FUEL ROD VIBRATION AMPLITUDE

APPENDIX E

Equivalent Mass of Uniform Beams in Transverse Vibrations

M_e -- Equivalent mass of the beam

M -- True mass of the beam

l -- Length of the beam

EI -- Bending stiffness

k -- Spring constant

ω_n -- Natural frequency of first mode, $\omega_n = \frac{k}{M_e}$

1. Beam-tee system

Type of beam -- Fixed at both ends, load at center.

$$\omega_n = 22 \sqrt{\frac{EI}{Ml^3}} \quad (\text{Ref. 19, p. 432})$$

$$k = 192 \frac{EI}{l^3}$$

$$M_e \cong 0.4M$$

2. U-tube

Type of beam -- Fixed at one end, load at other.

$$\omega_n = 3.52 \sqrt{\frac{EI}{Ml^3}}$$

$$k = 3 \frac{EI}{l^3}$$

$$M_e \cong 0.24M$$

3. Fuel rod

Type of beam -- Simply supported at both ends, uniform load.

$$\omega_n = \pi^2 \sqrt{\frac{EI}{Ml^3}}$$

$$k = \frac{384}{5} \frac{EI}{l^3}$$

$$M_e \cong 0.79 M$$

APPENDIX F

Accuracy of the Unsteady Momentum Flux Measurement

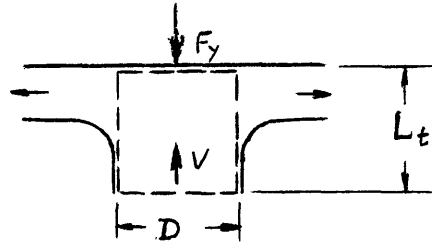
Using the Turning Tee

The vertical force acting upon the beam through the turning tee is

$$F_y = \iint_{c.s.} \rho V^2 dA + \frac{\partial}{\partial t} \iiint_{c.v.} \rho V d\bar{v} - \iiint_{c.v.} \rho g d\bar{v} \quad (F.1)$$

The control volume in which the change of the vertical component of momentum flux takes place is shown

by the dotted lines inside the turning tee. Then equation (F.1) can be written as



$$F_y = \rho V^2 A_x + \frac{\partial}{\partial t} \rho V A_x L_t - \rho g A_x L_t \quad (F.2)$$

where A_x is the inlet area of the tee and equal to $\frac{\pi}{4} D^2$. Suppose the density of the two-phase flow varies sinusoidally, namely,

$$\rho = \rho_m (1 + \sin \omega_k t) \quad (F.3)$$

where ρ_m is the mean flow density and ω_k is the fluctuation frequency.

Thus, equation (F.2) becomes

$$F_y = \rho_m V^2 A_x + \rho_m V^2 A_x \sin \omega_k t + \omega_k \rho_m V A_x L_t \cos \omega_k t - \rho_m g A_x L_t - \rho_m g A_x L_t \sin \omega_k t \quad (F.4)$$

For the turning tee shown in Fig. 3.5 (a), both D and L_t are equal to 1 3/8 inches. The flow conditions are assumed to be $\beta = 80\%$ and $V = 100$ ft/sec. Having these numerical values, the term $\rho_m g A_x L_t$ in

equation (F.4) is found to be negligibly small. The vertical dynamic force acting on the beam is then

$$F_d = F_m \left(\sin \omega_k t + \frac{\omega_k L t}{V} \cos \omega_k t \right) \quad (\text{F.5})$$

or

$$F_d = \sqrt{1 + \left(\frac{\omega_k L t}{V}\right)^2} F_m \sin(\omega_k t + \phi) \quad (\text{F.6})$$

where F_m is the amplitude of the force due to the unsteady momentum fluxes in the flow.

$$F_m = \rho_m V^2 A_x \quad (\text{F.7})$$

Since the upper limit of the frequency range of interest is 50 cps, the highest value of ω_k would be 100π rad/sec. For the given values of ω_k , L_t and V , equation (F.6) becomes

$$F_d = 1.06 F_m \sin(100 \pi t + \phi) \quad (\text{F.8})$$

This shows that, under the specified conditions, in the measurement of unsteady momentum fluxes the maximum error which occurs at the highest frequency is 6%.

APPENDIX G

References

1. Semenov, N.I., "Pressure Pulsations During the Flow of Gas-Liquid Mixtures in Pipes," Heat Power Engineering Part I, USAEC, Division of Technical Information, AEC-tr-4496, December 1961, translated.
2. Hubbard, M.G. and Dukler, A.E., "The Characterization of Flow Regimes for Horizontal Two-Phase Flow," Proceedings of the 1966 Heat Transfer and Fluid Mechanics Institute.
3. Burgree, D., Byrnes, J.J. and Benforado, D.M., "Vibration of Rods Induced by Water in Parallel Flow," Trans. ASME, July 1958, 991-1003.
4. Quinn, E.P., "Vibration of Fuel Rods in Parallel Flow," GEAP-4059, USAEC, 1962.
5. Paidoussis, M.P., "The Amplitude of Fluid-Induced Vibration of Cylinders in Axial Flow," Canadian Report AECL-2225, March 1965.
6. Pavlica, R.T. and Marshall, R.C., "An Experimental Study of Fuel Assembly Vibrations Induced by Coolant Flow," Nuclear Engineering and Design, Vol, 4, 1966, 54-60.
7. Wambsganss, M.W., "Vibration of Reactor Core Components," Reactor and Fuel-Processing Technology, Vol. 10, No. 3, Summer 1967, 208-219.
8. Reavis, J.R., "WVI-Westinghouse Vibration Correlation for Maximum Fuel-Element Displacement in Parallel Turbulent Flow," Trans. ANS Vol. 10, No. 1, 1967, 369-371.
9. Bird, R.B., Stewart, W.E. and Lightfoot, E.N., Transport Phenomena, Wiley, New York, 1963.
10. Peebles, F.N. and Garber, H.J., "Studies of the Motion of Gas Bubbles in Liquids," Chem. Eng. Prog., 1953, 49, 88-97.
11. Griffith, P., "The Prediction of Low-Quality Boiling Voids," Trans. ASME, Journal of Heat Transfer, Paper No. 63-HT-20.
12. Hall - Taylor, N. and Hewitt, G.F., "The Motion and Frequency of Large Disturbance Waves in Annular Two-Phase Flow of Air-Water Mixtures," AERE-R3952, United Kingdom, 1962.

13. Andeen, G.B. and Griffith, P., "The Momentum Flux in Two-Phase Flow," Technical Report No. 4547-38, AEC CODE: Report MIT-3496-1, October 1965.
14. Griffith, P., "Two-Phase Flow in Pipes," M.I.T. Summer Session Notes, 1962.
15. Kozlov, B.K., "Regimes and Types of Flow for an Air-Water Mixture in Vertical Tubes," Hydrodynamics and Heat Transfer During Boiling in High Pressure Boiler, 7-18, AEC-tr-4490, 1954.
16. Hansen, P.D., "New Approaches to the Design of Active Filters," The Lightning Empiricist, Vol, 13, No. 1 & 2, 1965, Philbrick Researches, Inc.
17. Crandall, S.H. and Mark, W.D., Random Vibration in Mechanical Systems, Academic Press, New York, 1963.
18. Crandall, S.H. (editor), Random Vibration Volume 2, The M.I.T. Press, 1963.
19. Den Hartog, J.P., Mechanical Vibration, McGraw-Hill, New York, 1965.
20. Rose, S.C. and Griffith, P., "Some Hydrodynamic Characteristics of Bubbly Mixture Flowing Vertically Upward in Tubes," DSR Technical Report No.5003-30, M.I.T., September 1964.
21. Haberstroh, R.D. and Griffith, P., "The Transition from the Annular to the Slug Flow Regime in Two-Phase Flow," EPL Technical Report 5003-38, M.I.T., June 1964.
22. Hinkle, W.D., "A Study of Liquid Mass Transport in Annular Air-Water Flow," Sc.D. Thesis, M.I.T., 1967.